بسم الله الرحمن الرحيم

Design and Fabrication of a MIMO Antenna System for 4G Wireless Handsets

BY

Mohammad Azam Jan

A Thesis Presented to the

DEANSHIP OF GRADUATE STUDIES

KING FAHD UNIVERSITY OF PETROLEUM & MINERALS

DHAHRAN, SAUDI ARABIA

In Partial Fulfillment of the
Requirements for the Degree of

MASTER OF SCIENCE

In

TELECOMMUNICATION ENGINEERING

June 2011

KING FAHD UNIVERSITY OF PETROLEUM
DHAHRAN, SAUDI ARABIA

DEANSHIP OF GRADUATE STUDIES

This thesis written by **Mohammad Azam Jan** under the direction of his thesis advisor and approved by his thesis committee, has been presented to and accepted by the Dean of Graduate Studies, in partial fulfillment of the requirements for the degree of MASTER OF SCIENCE IN TELECOMMUNICATION ENGINEERING.

Thesis Committee

Dr. Mohammad S. Sharawi
(Thesis Advisor)

Dr. Husain M. Masoudi
(Member)

Dr. Ali A. Al Shaikhi
(Department Chairman)

Dr. Mohammad A. Alsunaidi
(Member)

Dr. Salam A. Zummo
(Dean of Graduate Studies)

20/6/11
(Date)

ACKNOWLEDGEMENTS

First of all, I am grateful to Allah Almighty, the most merciful, the most beneficent, who gave me strength, guidance and abilities to complete this thesis in a successful manner.

I would like to thank Dr. Mohammad S. Sharawi, my supervisor, for providing me the opportunity to pursue my MSc thesis with him. Without his support, constant supervision, valuable discussions and strong technical guidance it would not have been possible to achieve my goals. His valuable suggestions, countless edits, involvement in my work and friendly attitude have made this work possible. At every stage his strong encouragement has given me a lot of confidence. It has been a wonderful professional and personal experience to work with him. I would also like to thank Dr. Mohammad A. Al-Sunaidi and Dr. Husain M. Masoudi for agreeing to be members of my Thesis committee and for their valuable time and feedback which has enhanced this thesis.

Special thanks to my colleagues at work and friends for their help and encouragements throughout my graduate studies at KFUPM. I would like to give special thanks to my family, my wife Shazia and my daughter Aiman, both of whom endured my stress and absence during my research. I am eternally indebted to them for their love, understanding and unflagging support. Their constant support and prayers are ultimate success in my life.

TABLE OF CONTENTS

ACKNOWLEDGEMENTS iii

TABLE OF CONTENTS iv

LIST OF TABLES viii

LIST OF FIGURES ix

THESIS ABSTRACT xiv

THESIS ABSTRACT (Arabic) xvi

CHAPTER 1 1

INTRODUCTION 1

1.1 Wireless Systems Evolution 2

1.2 Long Term Evolution (LTE) 6

1.3 MIMO Systems 11

1.4 Work Motivation and Thesis Objectives 13

1.5 Outline of the Thesis 14

CHAPTER 2 16

ANTENNA FUNDAMENTALS 16

2.1 Radiation Pattern 17

2.2 Reflection Coefficient, Return Loss and VSWR 20

2.2.1 Reflection Coefficient 21

2.2.2 Return Loss 21

2.2.3 Voltage Standing Wave Ratio (VSWR) 21

2.3 Scattering Parameters or S-Parameters 22

2.4 Bandwidth and Quality Factor 24
2.5 Radiation Power Density 27
2.6 Radiation Intensity 28
2.7 Directivity 29
2.8 Gain and efficiency 30
2.9 Summary 32
CHAPTER 3 33
PRINTED ANTENNAS FOR MOBILE HANDSETS 33
3.1 Introduction 33
3.2 The Microstrip Patch Antenna 34
3.3 The Planar Inverted-F Antenna 38
3.4 Electrically Small Antennas (ESA) 42
3.5 Summary 48
CHAPTER 4 50
MIMO SYSTEMS 50
Single Input Single Output (SISO) 51
4.1 51
4.2 Single Input Multiple Output (SIMO) 52
4.3 Multiple Input Single Output (MISO) 53
4.4 Multiple Input Multiple Output (MIMO) 54
4.5 Antennas for MIMO Systems 56
4.6 Techniques to reduce the Mutual Coupling and to improve the Isolation between antennas 59
4.6.1 Cutting Ground Slot between antennas 61
4.6.2 Using parasitic elements between the antennas 61
4.6.3 Using Metamaterials to Improve Isolation 61

4.6.4 Use of Defected Ground Structures (DGS) 62
4.7 Literature Review of Printed Antennas for Mobile Handsets 63
4.8 Summary 71
CHAPTER 5 72
THE SHORTED 4-SHAPED ANTENNA DESIGN 72
5.1 Dual Band Shorted 4-Shaped Antenna Element 74
5.2 2x1 MIMO Antenna using 4-Shaped Element 79
5.2.1 Effect of horizontal portion (L_f) 81
5.2.2 Effect of vertical Arm 1 (L_1) 82
5.2.3 Effect of Arm 2 (L_2) 83
5.2.4 Effect of separation from the Ground Plane (h,h_1) 84
5.2.5 Effect of the Short position (X_s) 85
5.2.6 Effect of the Feed position (X_f) 85
5.3 Measurement Setup 86
5.4 2x1 MIMO Antenna: Model A 89
5.5 2x1 MIMO Antenna: Model E1 93
5.6 2x1 MIMO Antenna: Model D1 98
5.7 2x1 MIMO Antenna: Model E1T 102
5.8 2x1 MIMO Antenna: Model D1T 107
5.9 Conclusion 116
CHAPTER 6 117
2x2 MIMO ANTENNA SYSTEM DESIGN 117
6.1 2x2 MIMO Antenna: Basic Model 119
6.1.1 2x2 MIMO Antenna: Basic Model (0.8 mm substrate) 119
6.1.2 2x2 MIMO Antenna Basic Model (1.56 mm substrate) 123

6.2 2x2 MIMO Antenna: Model B 129
6.2.1 2x2 MIMO Antenna Model B1 (0.8 mm substrate) 130
6.2.2 2x2 MIMO Antenna Model: B1T (1.56 mm substrate) 134
6.3 2x2 MIMO Antenna: Model C 140
6.3.1 2x2 MIMO Antenna Model C1T (1.56 mm substrate) 140
6.4 2x2 MIMO Antenna: Model A 147
6.4.1 2x2 MIMO Antenna Model A1T (1.56 mm substrate) 149
6.5 Conclusions 165
CHAPTER 7 166
CONCLUSION AND FUTURE WORK 166
7.1 Future Work 168
Bibliography 169
Vitae 177

LIST OF TABLES

Table 1-1 Features of the different generations of wireless technologies [3]……4

Table 1-2 LTE FDD Frequency bands [14]……10

Table 1-3 LTE TDD Frequency bands [14]……11

Table 4-1 Summary Table of related work in the 700 MHz band……69

Table 5-1 Single Element Antenna Parameters……76

Table 5-2 2x1 MIMO Antenna Parameters (Model D,E)……80

Table 5-3 2x1 MIMO Antenna Model A Parameters……90

Table 5-4 Measurement results for all the 2-Element models ……112

Table 5-5 Comparison with related work in the 700 MHz band……115

Table 6-1 Parameter values for antenna element for 2x2 MIMO Antenna……119

Table 6-2 Measurement results for all 2x2 MIMO Antenna models (1.56 mm)……155

Table 6-3 Measurement results for all the 2x2 MIMO Antenna models (0.8 mm)……162

Table 6-4 : Comparison of our 2x2 MIMO Antenna models with the 2x2 MIMO antennas that appeared in Literature……164

LIST OF FIGURES

Figure 1-1 OFDM divides a broadband channel into many narrow band channels to mitigate ISI. 8
Figure 1-2 Basic concepts of OFDM and OFDMA [13] 9
Figure 1-3 A 2x2 MIMO System that can support up to two independent data streams [4] 12
Figure 2-1 Three dimensional Radiation Pattern [15] 18
Figure 2-2 The E-plane and H-plane patterns of electrically short current element [16] 20
Figure 2-3 Transmission line Thevenin equivalent of antenna in transmitting mode [18] 20
Figure 2-4 Two-port network [19] 22
Figure 3-1 A rectangular microstrip patch printed on dielectri substrate (εr) [23] 35
Figure 3-2 Field distribution under rectangular microstrip patch having resonant length L [23] . 37
Figure 3-3 Development of the planar inverted-F antenna from the monopole : (a) quarter wavelength monopole; (b) intermediate position-fed quarter wavelength monopole; (c) inverted-L antenna; (d) planar inverted-F antenna [25]. 39
Figure 3-4 Structure of Planer inverted-F antenna [26] 41
Figure 3-5 Q_{min} Comparison for TM or TE antenna enclosed in a Chu sphere of radius a [29] 46
Figure 3-6 Comparison of the maximum Gain given by Harrington and Comston et al. 48
Figure 4-1 Single Input Single Output (SISO) [34] 51
Figure 4-2 Single Input Multiple Output (SIMO) 1x2 [34] 52
Figure 4-3 Multiple Input Single Output (MISO), 2x1 [34] 54
Figure 4-4 Multiple Input Multiple Output (MIMO) 2x2 [34] 55
Figure 5-1 The different models investigated (a) Model A, (b) Models E1 and E1T and (c) Models D1 and D1T 74
Figure 5-2 The shorted 4-Shaped Antenna Element 75
Figure 5-3 Simulated Reflection Coefficient $|S_{11}|$ of the Single Element Antenna 77
Figure 5-4 Simulated Gain Pattern of Single Element Antenna at 780 MHz 78
Figure 5-5 Simulated Gain Pattern of Single Element at 2.45 GHz 79
Figure 5-6 2x1 MIMO Antenna based on the 4-shaped Antenna Element 80
Figure 5-7 Effect of L_f on the reflection coefficient $|S_{11}|$ 81
Figure 5-8 Effect of L_1 on the reflection coefficient $|S_{11}|$ 82
Figure 5-9 Effect of L2 on the reflection coefficient $|S_{11}|$ 83
Figure 5-10 Effect of h on the reflection coefficient $|S_{11}|$ 84

Figure 5-11 Effect of Xs on the reflection coefficient $|S_{11}|$ 85
Figure 5-12 Effect of X_f on the reflection coefficient $|S_{11}|$ 86
Figure 5-13 Experimental setup for Measuring S-parameters with Network Analyzer 87
Figure 5-14 Experimental Setup for measuring the gain/radiation pattern 88
Figure 5-15 Front and back side of fabricated 2x1 antenna model A 90
Figure 5-16 Simulated and Measured Reflection Coefficients (S_{11}, S_{22}) at low band 91
Figure 5-17 Simulated and Measured Reflection Coefficients (S_{11}, S_{22}) at high band 91
Figure 5-18 Simulated and Measured Isolation at low band and high band 92
Figure 5-19 Elevation (x-z) plane Gain Pattern of antenna elements 1 and 2 at 900 MHz 92
Figure 5-20 Azimuth (x-y) plane Gain pattern of antenna elements 1 and 2 at 900 MHz 93
Figure 5-21 Front and back side of fabricated 2x1 antenna model E1 94
Figure 5-22 Simulated and Measured Reflection Coefficients (S_{11}, S_{22}) at low band 95
Figure 5-23 Simulated and Measured Reflection Coefficients (S_{11}, S_{22}) at high band 95
Figure 5-24 Simulated and Measured Isolation between antennas at low band and high band .. 96
Figure 5-25 Correlation Coefficient of the antenna system at 70% and 80% efficiency 96
Figure 5-26 Elevation (x-z) plane Gain Pattern of Antenna elements 1 and 2 at 900 MHz 97
Figure 5-27 Azimuth (x-y) plane Gain pattern of antenna elements 1 and 2 at 900 MHz 97
Figure 5-28 Front and back view of fabricated 2x1 antenna model D1 99
Figure 5-29 Simulated and Measured Reflection Coefficients (S_{11}, S_{22}) at low band 99
Figure 5-30 Simulated and Measured Reflection Coefficients (S_{11}, S_{22}) at high band 100
Figure 5-31 Simulated and Measured Isolation between antennas at low band and high band 100
Figure 5-32 Correlation Coefficient for the antenna system at 70% and 80 % efficiency 101
Figure 5-33 Elevation (x-z) plane Gain Pattern of Antenna elements 1 and 2 at 900 MHz 101
Figure 5-34 Azimuth (x-y) plane Gain pattern of antenna elements 1 and 2 at 900 MHz 102
Figure 5-35 Front and back view of fabricated 2x1 antenna model E1T 103
Figure 5-36 Simulated and Measured Reflection Coefficients (S_{11}, S_{22}) at low band 104
Figure 5-37 Simulated and Measured Reflection Coefficients (S_{11}, S_{22}) at high band 104
Figure 5-38 Simulated and Measured Isolation between the antennas at low and high band .. 105
Figure 5-39 Correlation coefficient at low band and high band for 70% and 80 % efficiency 105
Figure 5-40 Elevation (x-z) plane Gain Pattern of Antenna elements 1 and 2 at 800 MHz 106
Figure 5-41 Azimuth (x-y) plane Gain pattern of antenna elements 1 and 2 at 800 MHz 106
Figure 5-42 Front and back view of fabricated antenna model D1T 108

Figure 5-43 Simulated and Measured Reflection Coefficients (S_{11}, S_{22}) at low band 108
Figure 5-44 Simulated and Measured Reflection Coefficients (S_{11}, S_{22}) at high band 109
Figure 5-45 Simulated and Measured Isolation at low and high band 109
Figure 5-46 Correlation Coefficient for the antenna system at 70% and 80 % efficiency 110
Figure 5-47 Elevation (x-z) plane Gain Pattern of Antenna elements 1 and 2 at 850 MHz 110
Figure 5-48 Azimuth (x-y) plane Gain pattern of antenna elements 1 and 2 at 850 MHz 111
Figure 6-1 Basic design of 2x2 MIMO Antenna System 118
Figure 6-2 Simulated and Measured Reflection Coefficients (S_{11}, S_{22}, S_{33}, S_{44}) at lower band 120
Figure 6-3 Simulated and Measured Isolation (S_{21}, S_{31}, S_{41}) at lower and higher bands..... 121
Figure 6-4 Simulated and Measured Reflection Coefficients (S_{11}, S_{22}, S_{33}, S_{44}) at higher band ... 121
Figure 6-5 Elevation (x-z) plane radiation pattern of antenna 1 and 2 at 800 MHz 122
Figure 6-6 Azimuth (x-y) plane radiation pattern of antenna 1 and 2 at 800 MHz 122
Figure 6-7 Simulated and Measured reflection Coefficient (S_{11}, S_{22}, S_{33}, S_{44}) for antennas at the lower band 124
Figure 6-8 Simulated and Measured reflection coefficients (S_{11}, S_{22}, S_{33}, S_{44}) for the antennas at the higher band 125
Figure 6-9 Simulated and Measured Isolation between antenna elements at low and high bands 125
Figure 6-10 Correlation Coefficient between antenna 1 and 2 and 1 and 3 at low band..... 126
Figure 6-11 Correlation coefficient for antenna 1 and 4 at low band 126
Figure 6-12 Correlation coefficient for antennas 1 and 2 and 1 and 3 at the higher band..... 127
Figure 6-13 Correlation coeffient for antenna 1 and 4 at the higher band 127
Figure 6-14 Elevation (x-z) plane Radiation pattern for antenna 1 and 2 at 800 MHz 128
Figure 6-15 Azimuth (x-y) plane radiation pattern of antenna 1 and 2 at 800 MHz 128
Figure 6-16 Model B with modified ground plane..... 129
Figure 6-17 Fabricated 2x2 MIMO Antenna Model B1T 130
Figure 6-18 Simulated and Measured reflection Coefficients (S_{11}, S_{22}, S_{33}, S_{44}) for antennas at the lower band 131
Figure 6-19 Simulated and Measured reflection Coefficient (S_{11}, S_{22}, S_{33}, S_{44}) for antennas at the higher band 132
Figure 6-20 Simulated and Measured Isolation between antenna elements at lower and high bands..... 132

Figure 6-21 Elevation (x-z) plane Radiation pattern for antenna 1 and 2 at 800 MHz 133
Figure 6-22 Azimuth (x-y) plane radiation pattern of antenna 1 and 2 at 800 MHz 133
Figure 6-23 Simulated and Measured reflection Coefficients (S_{11}, S_{22}, S_{33}, S_{44}) for antennas at the higher band 135
Figure 6-24 Simulated and Measured reflection Coefficients (S_{11}, S_{22}, S_{33}, S_{44}) for antennas at the lower band 135
Figure 6-25 Simulated and Measured Isolation between antenna elements at lower and high bands..... 136
Figure 6-26 Correlation Coefficient between antennas 1 and 2 and 1 and 3 at low band 136
Figure 6-27 Correlation Coefficient between antennas 1 and 4 at low band 137
Figure 6-28 Correlation Coefficient between antenna 1 and 2 and 1 and 3 at higher band 137
Figure 6-29 Correlation Coefficient between antenna 1 and 4 at high band..... 138
Figure 6-30 Elevation (x-z) plane Radiation pattern for antenna 1 and 2 at 770 MHz 138
Figure 6-31 Azimuth (x-y) plane radiation pattern of antenna 1 and 2 at 770 MHz 139
Figure 6-32 MIMO Antenna Model C..... 141
Figure 6-33 Fabricated 2x2 MIMO antenna model C..... 141
Figure 6-34 Simulated and Measured reflection Coefficient (S_{11}, S_{22}, S_{33}, S_{44}) for antennas at the low band..... 142
Figure 6-35 Simulated and Measured reflection Coefficient (S_{11}, S_{22}, S_{33}, S_{44}) for antennas at the high band..... 142
Figure 6-36 Simulated and Measured Isolation between antenna elements at low and high bands 143
Figure 6-37 Correlation Coefficient for antennas 1 and 2 and 1 and 3 at low band 143
Figure 6-38 Correlation Coefficient for antennas 1 and 4 at low band 144
Figure 6-39 Correlation Coefficient for antennas 1 and 2 and 1 and 3 at high band 144
Figure 6-40 Correlation Coefficient for antennas 1 and 4 at high band 145
Figure 6-41 Elevation (x-z) plane Radiation pattern for antenna 1 and 2 at 800 MHz 145
Figure 6-42 Azimuth (x-y) plane radiation pattern of antenna 1 and 2 at 800 MHz 146
Figure 6-43 2x2 MIMO Antenna Model A 148
Figure 6-44 Fabricated 2x2 MIMO Antenna Model A..... 148
Figure 6-45 Simulated and Measured reflection Coefficient (S_{11}, S_{22}, S_{33}, S_{44}) for antennas at the low band..... 150

Figure 6-46 Simulated and Measured reflection Coefficient (S_{11}, S_{22}, S_{33}, S_{44}) for antennas at the high band 150
Figure 6-47 Simulated and Measured Isolation between antenna elements at low and high bands 151
Figure 6-48 Correlation Coefficient for antennas 1 and 2 and 1 and 3 at low band 151
Figure 6-49 Correlation Coefficient for antennas 1 and 4 at low band 152
Figure 6-50 Correlation Coefficient for antennas 1 and 2 and 1 and 3 at high band 152
Figure 6-51 Correlation Coefficient for antennas 1 and 4 at high band 153
Figure 6-52 Elevation (x-z) plane Radiation pattern for antenna 1 and 2 at 760 MHz 153
Figure 6-53 Azimuth (x-y) plane radiation pattern of antenna 1 and 2 at 760 MHz 154
Figure 6-54 Comparison of low band S_{11}, S_{22} for the four fabricated models with 1.56mm substrate 157
Figure 6-55 Comparison of low band S_{33}, S_{44} for the four fabricated models with 1.56mm substrate 157
Figure 6-56 Comparison of low band S_{21}, S_{31} for the four fabricated models with 1.56mm substrate 158
Figure 6-57 Comparison of low band S_{41} for the four fabricated models with 1.56mm substrate 158
Figure 6-58 Comparison of high band S_{11}, S_{22} for the four fabricated models with 1.56mm substrate 159
Figure 6-59 Comparison of high band S_{33}, S_{44} for the four fabricated models with 1.56mm substrate 159
Figure 6-60 Comparison of high band S_{21}, S_{31} for the four fabricated models with 1.56mm substrate 160
Figure 6-61 Comparison of high band S_{41} for the four fabricated models with 1.56mm substrate 160

THESIS ABSTRACT

Name : Mohammad Azam Jan

Title : Design and Fabrication of a MIMO Antenna System for 4G Wireless Handsets

Major Field : Telecommunication Engineering

Date of Degree: June 2011

The 4th generation in the wireless evolution is called the Long Term Evolution (LTE) which will provide higher peak data rates, higher spectral efficiency and lower latency taking advantage of the latest enabling technologies such as Orthogonal Frequency Division Multiple Access (OFDMA), Adaptive modulation and coding (AMC) and Multiple-Input Multiple-Output (MIMO) technologies.

The 700 MHz band will be primarily used for LTE systems in the USA. Due to the larger wavelength, the design of multiple antennas on small handsets is a real challenge. The need for novel small size MIMO antenna systems with high isolation is of great importance to bring 4G capabilities to reality.

In this work we propose a novel 4-shaped dual band antenna geometry which is then used to design and implement 2x1 and 2x2 MIMO antenna systems. The commercial software High Frequency Structure Simulation (HFSS) was used to design, simulate and optimize the antenna models which were then fabricated through a PCB manufacturer. The available equipment and measurement setups in the Microwave Laboratory at KFUPM were used to test and characterize the fabricated antennas. MATLAB was

extensively used to analyze and plot the measurement data files and compare simulation with measurement results.

The fabricated 2x1 dual band MIMO antenna system operated at 815 MHz and 2.75 GHz providing -6dB bandwidth of 60 MHz and more than 200 MHz at the two bands, respectively. Isolation of more than 6 dB at the low band and 11 dB at the high band was achieved despite the limited spatial separation between the two antennas of only $\lambda/16$. The 2x1 dual band MIMO antenna was fabricated on an FR-4 substrate of size 50x67x1.56 mm^3 which is at least 35% smaller than some models that appeared in literature.

The fabricated 2x2 MIMO antenna system operating at the 700 MHz band was the first to appear in literature covering this low band and was fabricated on an FR-4 substrate of size 55x110x1.56 mm^3. It covered the 734-790 MHz band and the 2307-2475 MHz band, enabling its use in MIMO systems for the LTE 700 MHz band and other wireless standards in the 2400 MHz band such as WLAN, WiMAX, as well as higher LTE frequency bands. Isolation of more than 7 dB was achieved for most of the antenna elements indicating acceptable MIMO performance. Several isolation enhancement techniques were implemented and evaluated. It was found that improving isolation between such closely spaced antenna elements presents a challenge and conventional techniques may not prove very useful. The performance of the designed antennas was compared against their counterparts that appeared in literature.

THESIS ABSTRACT (Arabic)

ملخص الرسالة

الاسم : محمد أعظم جان

عنوان الرسالة : تصميم وتصنيع نظام هوائي الإدخال والإخراج المتعدد (MIMO)لهواتف اللاسلكية الجيل الرابع

التخصص : هندسة الاتصالات

تاريخ التخرج : حزيران 2011

سوف يقوم الجيل الرابع من الاتصالات اللاسلكية والمسمى التطورطويل الأمد بتزويد المستخدم بمعدل ارسال واستقبال بيانات أعلى، فاعلية اكبرومعدل تباطىء اقل عن طريق استخدام التكنولوجياالجديدة والمتمثلة فى الاستخدام المتعدد للترددات المتعامدة والشفروالتحميل المتغيروثالثا عن طريق استخدام تكنولوجيا تعدد المدخلات والمخرجات .

باقة ٧٠٠ ميغاهرتزسوف يتم استخدامها لأنظمة التطور طويل الأمد بالولايات المتحدة. هناك تحدى حقيقى فى تصميم عدة هوائيات فى أجهزة المحمول لهذه الباقة من الترددات نظرًا لطول موجتها. ان الحاجة لتصميم هوائيات جديدة لأنظمة تعدد المدخلات والمخرجات مع عزل كافى هوالذى سوف يعطى الجيل الرابع قدرته الحقيقية.

في هذه الرسالة، نقدم هوائى مطبوع فريد من نوعة على شكل ٤ بالانجليزية و يغطى حزمتان من الترددات الراديوية. هذا الهوائى سوف يستخدم على شكل مصفوفة ٢×١ و ٢×٢ لأجهزة متعددة المدخلات والمخرجات. البرنامج المستخدم فى نمذجة هذا الهوائى هو HFSS وقد تم تصميم الهوائى وتعديله ومن ثم طباعته و فحصه فى

المختبر المايكروويف فى قسم الهندسة الكهربائية فى الجامعة الملك فهد. برنامج آخر تم استخدامه MATLAB لتحليل النتائج ورسمها بيانيا.

ان الهوائى المصمم المصفوفة ٢×١ يعمل بحزمة الترددات ٨١٥ ميغاهرتز و ٢٧٥٠ ميغاهرتز و بسعة dB 6- مقدار ٦٠ ميغاهرتز و ٢٠٠ ميغاهرتز على التوالي. العزل بين الهوائيين كان أكثر من 6 dB و 11 dB للحزمتى التردد على التوالي. يجب الاخذ بعين الاعتبار ان المسافة مابين الهوائيين كانت اقل من ١/١٦ الطول الموجى. لقد تم تصنيع مصفوفة الهوائيات على لوح من ماركة FR-4 بحجم ١,٥٦ × ٦٧ × ٥٠ ملم ^{٣}. هذا الحجم أقل ب٣٥٪ من معظم الهوائيات الواردة فى الاعمال السابقة.

أما المصفوفة ٢×٢ لنظام تعدد المدخلات والمخرجات والعاملة بحزمة ترددات ٧٠٠ ميغاهرتز فإنها الأول من نوعها فى الاعمال المنشورة عالميا. لقد تم تصنيعها على لوح من ماركة FR-4 بحجم ١,٥٦ × ١١٠ × ٥٥ ملم ^{٣}. تغطى هذه الهوائيات الترددات ٧٣٤ – ٧٩٠ ميغاهرتز و ٢٣٠٧ – ٢٤٧٥ ميغاهرتز. هذه الحزم هى معمول فيها فى الجيل الرابع للهواتف النقالة والانترنت المتحركة. لقد تم الحصول على عزل بمقدار 7 dB لمعظم الهوائيات. عدة طرق لتحسين العزل تم دراستها و تطبيقها لتحسين أداء المصفوفة. لقد تم التوصل ان تحسين أداء العزل محدود لمصفوفة بهذه التقارب مابين عناصرها له حده لا يمكن تجاوزه بالطرق المعهودة. مع ذالك، فقد تم مقارنة أداء المصفوفة مع مثيلاتها ممن تم نشرها، والأداء فى حزمة التردد ٧٠٠ ميغاهرتز للمصفوفة المطروحة فى هذا العمل لا يوجد لها مقارن.

CHAPTER 1

INTRODUCTION

There has been tremendous advancements in communication technologies and services over the past century. The invention of the telephone by Alexander Graham Bell can be considered as the starting point for the communication revolution. The initial basic voice communication service has evolved over time into the mobile broad-band multimedia services available today. The invention of wireless radio by Marconi and the introduction of other new technologies such as satellite and cellular networks contributed greatly to this revolution as well.

In this chapter, we will review the wireless system evolution and highlight the enabling technologies of the fourth generation in wireless systems. Then, the work motivation and thesis objectives are presented followed by the thesis outline and contribution.

1.1 Wireless Systems Evolution

The development of wireless communication technologies and services has been divided into different stages called generations. The initial voice-only systems such as the Advanced Mobile Phone System (AMPS), Total Access Communication System (TACS) and Nordic Mobile Telephone (NMT) used analog modulation techniques and were termed as the first generation (1G). These systems were soon replaced by the second generation (2G) wireless systems which used digital modulation and offered higher capacity and services such as roaming, Short Message Service (SMS) and Circuit Switched Data (CSD). Popular 2G systems included GSM (Global System for Mobile Communications) in Europe, IS-95 (cdmaOne), IS-136 (also known as US-TDMA and Digital AMPS) in the United States (U.S.), and PDC (Personal Digital Communications) in Japan. GSM is the most widely deployed wireless system in the world, with deployments in Europe, Asia, Australia, South America, and some parts of the U.S.

Second generation mobile systems provided only limited data rates that were insufficient for internet and multimedia applications. 2.5G systems were introduced by minimal hardware/software upgrades to 2G systems in order to support higher data rates and provide features like web browsing, e-mail and mobile commerce. Popular 2.5G systems that are currently deployed are the High Speed Circuit Switched Data (HSCSD), General Packet Radio Service (GPRS) and Enhanced Data Rate for GSM Evolution (EDGE). The EDGE system allows a maximum data rate of 384 kb/s.

Nowadays, third generation (3G) mobile communication technologies provide digital voice, video telephony, internet access, multimedia messaging (MMS) and video/music download services. 3G technology provides 144kbps or higher data rates for higher mobility traffic. 3G wireless standards include Universal Mobile Telecommunication System (UMTS also known as W-CDMA) which has evolved from GSM and IS-136 and CDMA-2000 which has evolved from IS-95 [1, 2]. To meet the challenge of continuously improving the speed and capacity of these systems, operators introduced the High Speed Packet Access (HSPA) which refers to improvements in both the downlink (D) and uplink (U) of the radio access network that are called HSDPA and HSUPA respectively. HSPA allows a downlink speed of up to 14 Mbps and uplink of 5.7 Mbps. Table 1-1 shows different wireless technologies and their performance characteristics [3].

Wireless Local Area Network (WLAN) technology has also progressed rapidly alongside mobile communication technology by introducing WiFi (Wireless Fidelity). WiFi consists of a set of LAN technology standards based on the IEEE 802.11 specifications. It enables a person with a wireless-enabled computer, laptop or personal digital assistant (PDA) to connect to the internet through an access point (Hot-Spot) at a maximum data rate of 54Mbps. In addition to internet connectivity, WiFi is also used to broadcast quality multimedia content throughout the entire coverage area. Another new wireless technology is the Worldwide Interoperability for Microwave Access (WiMAX) which is designed for Metropolitan Area Networks (MAN) based on the IEEE 802.16

specifications. Its aim is to provide high speed wireless internet connections over long distances [4].

Table 1-1 : Features of the different Generations of wireless technologies [3]

Generation	Technology	Carrier BW	UL Peak Data Rate	DL Peak Data Rate	Latency (ms)	Spectrum (MHz)	Peak Spectral Eff. (Bit/s/Hz)
2G	GSM / GPRS EDGE (MCS-9)	200 kHz	56 Kbps 118 Kbps	114 Kbps 236 Kbps	500 300	900/1800	0.17 0.33 EDGE
3G	W-CDMA	5 MHz	384 Kbps	384 Kbps (2 Mbps)	250	900/1800/ 2100/2600	0.51
	HSPA	5 MHz	5.7 Mbps	14 Mbps	~70	DD/900/ 2100/2600	2.88
	HSPA+ (16 QAM) (64 QAM + Dual)	5 MHz	11.5 Mbps	~28 Mbps (42 Mbps)	~30	DD/900/ 2100/2600	12.5
4G	LTE (Rel.8) (2x2 MIMO)	var. up to 20 MHz	~75 Mbps	~150 Mbps @20 MHz	~10	DD/900/1800 2100/2600	16.32
	WiMax IEEE 802.16e	10 MHz	70 Mbps	70 Mbps 134 Mbps	~50	2600/3500	3.7
	LTEAdvanced	var. up to 100 MHz	>500 Mbps	>1 Gbps	<5	IMT	DL: >30 UL: >15
	IMTAdvanced	var. up to 100 MHz	270 Mbps 675 Mbps	600 Mbps 1.5 Gbps	<10	IMT	DL: >15 UL: >6.75

Successive wireless generations have improved the performance of the air-link which enabled operators to introduce new and improved services. The resulting growth in consumer's demands has tremendously increased the need for reliable, power efficient and cheaper wireless services with high data rates. The radio spectrum available for new wireless systems is expensive and limited; therefore, the need to increase the channel capacity and reliability of current wireless systems without using additional spectrum is of great importance [1, 5]. This has always fueled research for more efficient utilization of the available bandwidth and the introduction of new technologies.

In order to achieve maximum channel utilization, new technologies have to be found to approach the physical limits of the radio channels as much as possible. A well known upper bound on the maximum achievable data rate for the ideal band-limited additive white Gaussian noise (AWGN) channel is the Shannon-Nyquist criterion. For an available channel bandwidth W and signal-to-noise ratio (γ) over this bandwidth, the maximum transmit data rate is given by

$$C = W\ log_2(1+\gamma) \quad bits/\text{s} \qquad 1.1$$

From equation (1.1), higher data rates can be achieved by increasing the bandwidth utilized or the SNR using a higher transmit power. However, spectrum is very expensive and there is a limit to its usage. Also, the signal power cannot be increased as the communication system is interference limited. During the past few years, these limits have been expanded by introducing the spatial domain to mobile communication antennas.

By introducing an array of antenna elements at both the receiver and the transmitter, the channel capacity of that system can grow linearly with the number of antennas under ideal conditions. This system with multiple antennas at both link-ends is termed a multiple-input multiple-output (MIMO) system. Winters in 1987 was the first to explore the capacity of multi-antenna fading channels applying antenna arrays at both link-ends [6]. However, the potential of these systems was realized more than a decade later when they were re-invented by Foschini and Gans [7,8] and Telatar [9]. Since then, MIMO systems have received tremendous attention in research and industry [4].

1.2 Long Term Evolution (LTE)

Long Term Evolution (LTE) is the next generation of cellular technology and will evolve from the current Universal Mobile Telecommunication System/High Speed Packet Access (UMTS/HSPA). The LTE standard will provide higher peak data rates, higher spectral efficiency, lower latency, flexible channel bandwidths and lower system cost. LTE is considered the fourth generation (4G) in mobile communications. It is referred to as MAGIC; Mobile Multimedia, Anywhere anytime, with Global mobility support, Integrated wireless solution and Customized personal service. LTE will be based on internet-protocol (IP) and provide higher throughput, broader bandwidth and better handoff to realize seamless services across covered areas [10].

The service targets promised by LTE will be made possible by utilizing the latest advances in adaptive modulation and coding (AMC), multiple-input-multiple-output systems (MIMO) and adaptive antenna arrays. The target for the spectral efficiency (max. data rate/max. channel BW) of LTE is 300Mbps/20MHz = 15bits/Hz (with the use of MIMO capability) which is 6 times higher compared with the current 3G based networks. Orthogonal frequency division multiple access (OFDMA) will be used in the new air interface for LTE radio access network (RAN). OFDM converts a frequency selective fading channel into multiple flat fading sub-channels facilitating easy equalization while MIMO helps in increasing the throughput. It has been shown that the capacity of MIMO systems increases linearly with number of transmit or receive antennas under the assumption that the number of transmit antennas and receive antennas are identical. If M_T is the number of transmitting antennas, N_R is the number of receiving antennas, W is the channel bandwidth in Hz an γ is the average signal to noise ratio at the receiver, then the channel capacity is given by equation (1.2) [11].

$$C = W\ log_2\ (1 + M_T \text{ x } N_R \text{ x } \gamma) \quad bits/\text{s} \qquad 1.2$$

This can be considered as an M_T x N_R times increase in the SNR which results in an increase in channel capacity. For the same bandwidth this capacity scaling feature of MIMO systems facilitates spatial multiplexing systems to transmit more data with the help of multiple antennas in comparison to a single antenna system. MIMO systems can also be used for providing better error-rate performance. This improvement is quantified as

diversity advantage, which essentially implies a better bit-error-rate (BER) performance for a given SNR. It helps in providing a more reliable transmission with multiple antennas compared to a single antenna system.

Orthogonal Frequency Division Multiplexing (OFDM) is a multi-carrier block modulation scheme suitable for wireless communications. With increasing data rate requirements, the technology challenges of the physical layer are moving towards wide-band wireless communications. One of the key issues to be addressed in such systems is the frequency selectivity of the wireless channel caused by multi-path delay spread. The performance degradation due to frequency selective fading increases with an increase in signal bandwidth and/or bit rate. OFDM is primarily used in high bit rate systems to mitigate inter-symbol interference (ISI) caused by delay spread. OFDM transforms a frequency selective fading channel into multiple narrow flat fading parallel sub-channels as shown in Fig. 1-1. This increases the symbol duration and mitigates ISI caused due to multi-path [12]. Orthogonal Frequency-Division Multiple Access (OFDMA) is a multi-user version of the OFDM scheme.

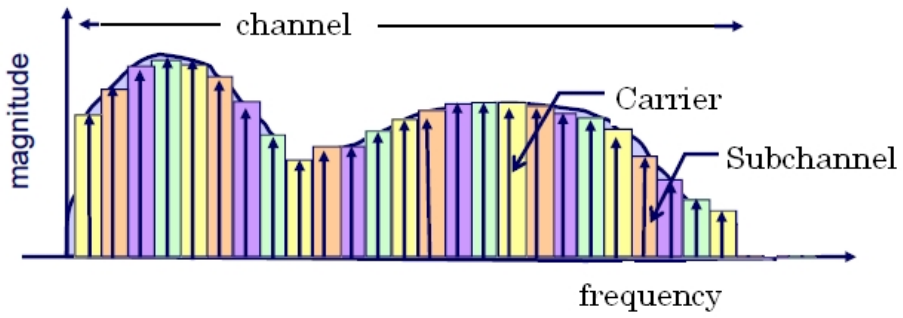

Figure 1-1 OFDM divides a broadband channel into many narrow band channels to mitigate ISI

Multiple access is achieved in OFDMA by assigning subsets of subcarriers to individual data streams as illustrated in Fig. 1-2 [13]. This allows simultaneous transmission of several individual data streams for different users.

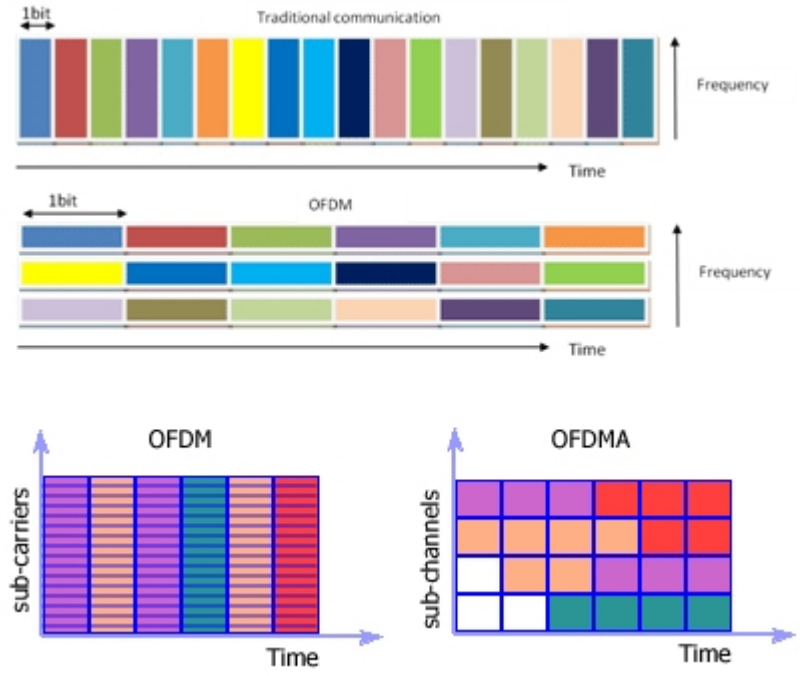

Figure 1-2 Basic concepts of OFDM and OFDMA [13]

One of the important features of LTE is flexible spectrum usage which enables it to operate in different frequency bands using paired as well as unpaired bands by employing either frequency division duplex (FDD) or time division duplex (TDD) operation. Tables 1-2 and 1-3 show the different paired and unpaired frequency bands allocated to LTE.

The new band at 700 MHz to be used in the USA can provide better in-building penetration and support larger cell sizes to provide cost effective network coverage.

Table 1-2 : LTE FDD Frequency Bands [14]

Operating Band	3GPP Name	Total Spectrum	Uplink (MHz)	Downlink (MHz)
Band 1	2100	2x60 MHz	1920-1980	2110-2170
Band 2	1900	2x60 MHz	1850-1910	1930-1990
Band 3	1800	2x75 MHz	1710-1785	1805-1880
Band 4	1700/2100	2x45 MHz	1710-1755	2110-2155
Band 5	850	2x25 MHz	824-849	869-894
Band 6	800	2x10 MHz	830-840	875-885
Band 7	2600	2x70 MHz	2500-2570	2620-2690
Band 8	900	2x35 MHz	880-915	925-960
Band 9	1700	2x35 MHz	1750-1785	1845-1880
Band 10	1700/2100	2x60 MHz	1710-1770	2110-2170
Band 11	1500	2x25 MHz	1427.9-1452.9	1475.9-1500.9
Band 12	US700	2x18 MHz	698-716	728-746
Band 13	US700	2x10 MHz	777-787	746-756
Band 14	US700	2x10 MHz	788-798	758-768
Band 17	US700	2x10 MHz	704-716	734-746
Band 18	Japan800	2x30 MHz	815-830	860-875
Band 19	Japan800	2x30 MHz	830-845	875-890

Table 1-3 : LTE TDD Frequency Bands[14]

Operating Band	3GPP Name	Total Spectrum	Uplink & Downlink (MHz)
Band 33	UMTS TDD1	1x20 MHz	1900-1920
Band 34	UMTS TDD2	1x15 MHz	2010-2025
Band 35	US1900 UL	1x60 MHz	1850-1910
Band 36	US1900 DL	1x60 MHz	1930-1990
Band 37	US1900	1x20 MHz	1910-1930
Band 38	2600	1x50 MHz	2570-2620
Band 39	UMTS TDD	1x40 MHz	1880-1920
Band 40	2300	1x50 MHz	2300-2400

1.3 MIMO Systems

MIMO systems use multiple antennas at both the transmitter and receiver sides of the communication link as shown in Fig. 1-3 to increase the capacity of the channel according to equation (1.2). Multiple antennas can easily be deployed at a base station because there is no strict limitation on the size. However, implementing multiple antennas on a small mobile terminal is challenging as there is not much space available for multiple antennas on a small mobile terminal such as a handset or PDA. Therefore, a multiple-element

antenna system should be small in order to be embedded into the small mobile terminal. It also should meet some additional requirements, such as low cost, reliability, good isolation and diversity performance for multiple antennas in addition to being compact, light weight, low profile and robust [1].

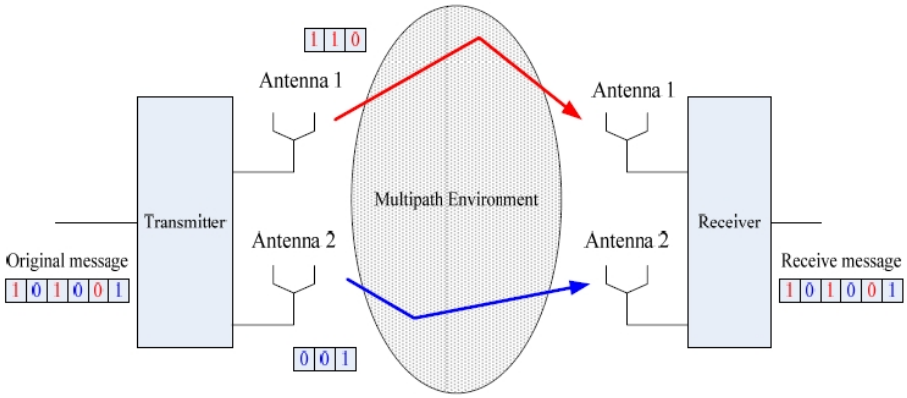

Figure 1-3 A 2x2 MIMO System that can support up to two independent data streams [4]

Currently, there are some MIMO products readily available in the market for WLAN applications (IEEE 802.11a/b/g standards). Using MIMO technology and the OFDM modulation scheme, WLAN provides high speed broadband internet connections, bandwidth intensive applications such as video streaming and reliable coverage throughout a business or residence.

Airgo has reported providing MIMO systems delivering a peak data rate of 108Mbps compared to 54 Mbps provided by SISO systems. However MIMO technology is still not

being implemented on small mobile terminals (e.g. PDAs and handsets). The next generation of WLAN will use the new IEEE 802.11n standard aimed at delivering a peak data rate of 600Mbps using MIMO technology and other advanced technologies such as beamforming [4].

1.4 Work Motivation and Thesis Objectives

The 700 MHz band will be primarily used for LTE systems in the USA. Operation at these frequencies provides good in-building penetration and allows the use of larger cells, thus reducing the cost of network rollout. However, due to the larger wavelength, the design of multiple antennas with high isolation on small handsets is a real challenge. When antennas are located close to each other, the isolation is very low and no diversity gain can be achieved. The need for novel small size MIMO antenna systems with high isolation is of great importance to bring 4G capabilities to reality. The purpose of this work is to design, analyze and fabricate a novel 4-element MIMO antenna system for the 700MHz band with good diversity performance and low mutual coupling between the elements in addition to acceptable gain, bandwidth and radiation characteristics. The objectives of this work are:

A. To design a novel dual element, compact size, dual band MIMO antenna system covering the 700 MHz bands and investigate its performance

B. To design a novel four element dual band MIMO antenna system covering the 700 MHz bands and apply different isolation techniques to achieve the desired performance metrics

C. To optimize the performance of the dual and four element MIMO antenna systems by enhancing their isolation characteristics

D. Fabricate the dual and 4-element MIMO antenna designed and measure its performance against LTE specifications and other antennas that appeared in literature.

1.5 Outline of the Thesis

This thesis presents the design and fabrication of novel dual band MIMO antenna systems covering the 700 MHz LTE band. The performance of the MIMO antenna system is investigated through several design models and extensive simulations and measurements of the fabricated structures. *Chapter 2* presents some basic concepts and properties of antennas and their performance parameters. The need to accommodate multiple antennas on a small terminal requires that the antenna type should be low profile and compact. *Chapter 3* introduces low profile printed antennas suitable for handheld devices and discusses the characteristics of two most common antenna types i.e. Microstrip and Planar Inverted-F Antennas which are potential candidates for MIMO antennas for LTE mobile terminals. Multiple antennas on handheld terminals are essentially

electrically small antennas (ESAs), for lower operating bands that have their own limitations. *Chapter 3* also examines the fundamental limits of ESAs and discusses the effect of size reduction on antenna performance. *Chapter 4* presents MIMO antenna systems and the challenges faced in their design and the techniques to improve their isolation performance. It also gives a survey of the literature available regarding MIMO antennas for LTE. *Chapter 5* presents the proposed novel dual band 4-shaped antenna element design. This basic antenna element is used in a 2x1 (dual element) MIMO antenna system and its simulated and measured performance results are presented and discussed. *Chapter 6* presents the models designed for the 4-element MIMO antenna system and their measured and simulated performance parameters as well as the different isolation techniques investigated. *Chapter 7* gives the conclusions and suggestions for future work.

CHAPTER 2

ANTENNA FUNDAMENTALS

Antennas and antenna systems are the eyes and ears of wireless communication systems which have experienced an unprecedented rapid expansion over the past few decades [15]. These wireless systems, whether simple or complex, cannot operate efficiently without transmitting and receiving elements/antennas that efficiently radiate and receive the electromagnetic waves that carry the information. By definition, an antenna is the part of a transmitting or receiving system that is designed to radiate or receive electromagnetic waves in an efficient and desired manner. The antenna is actually a transducer that transforms electrical signals (voltages and currents from a transmission line) into electromagnetic waves (electric and magnetic fields), or vice versa. It is normally made of metal but other materials may also be used e.g. ceramic materials are used to make dielectric resonator antennas (DRAs) [16]. There are many kinds of antennas used for various applications which include wire antennas, reflector antennas, aperture antennas and printed or microstrip antennas.

Generally an antenna needs to have high gain, small physical size, broad bandwidth, versatility and the ability to be embedded in the device. Particularly, the radiation patterns, bandwidth and gain are the most important factors that affect the application of antennas in contemporary and future wireless communication systems. This chapter will provide an introduction to the important parameters that describe antenna performance.

2.1 Radiation Pattern

The radiation pattern is defined as the spatial distribution of a quantity that characterizes the electromagnetic field generated by an antenna [17]. The distribution can be expressed as a mathematical function or as a graphical representation. The quantities that are most often used to characterize the radiation from an antenna are the electric field strength, power flux density, radiation intensity, directivity, phase or polarization. Simply stated, the radiation pattern of an antenna is a plot of the radiated field/power as a function of the angle at a fixed distance, which should be large enough to be considered far field. When the amplitude or relative amplitude of a specified component of the electric field vector is plotted graphically, it is called an amplitude pattern, field pattern, or voltage pattern. When the square of the amplitude or relative amplitude is plotted, it is called a power pattern. Often the field and power patterns are normalized with respect to their maximum value, yielding normalized field and power patterns [15].

An isotropic radiator is defined as “a hypothetical lossless antenna having equal radiation in all directions.” Although it is ideal and not physically realizable, it is often taken as a reference for expressing the directive properties of actual antennas. A directional antenna is one “having the property of radiating or receiving electromagnetic waves more effectively in some directions than in others” [15].

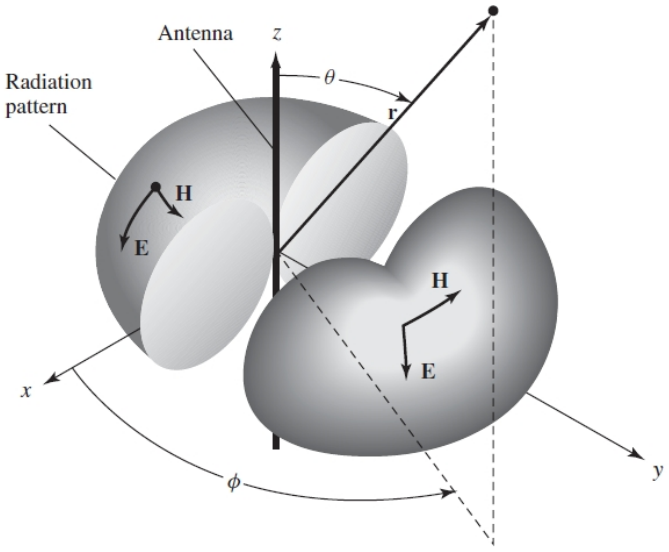

Figure 2-1 Three dimensional Radiation Pattern [15]

The 3D pattern shown in Fig. 2-1 is an excellent illustration of the radiated field distribution as a function of the spatial spherical co-ordinates θ and φ. However, it is difficult and also very time-consuming to measure the 3D pattern of an antenna in practice. Most antennas have certain symmetrical features and the most important patterns are the

radiation patterns in the two main planes: the E-plane and the H-plane. The E-plane is defined as the plane containing the electric field vector ***E*** and the direction of maximum radiation while the H-plane as the plane containing magnetic field vector ***H*** and the direction of maximum radiation. Usually the antenna is oriented so that at least one of the principal plane patterns coincides with one of the geometrical principal planes. For the radiation pattern shown in Fig. 2-1, the x-z plane (elevation plane $\varphi=0$) is the principal E-plane and the x-y plane (the azimuthal plane θ =90°) is the principal H-plane. The electric field is E_θ and the magnetic field is H_φ, thus the E-plane pattern is the field E_θ measured as a function of θ when the angle φ and the distance are fixed, while the H-plane pattern is the field E_θ measured as a function of φ when the angle θ and the distance are fixed. The E-plane (at φ =0) and H-plane (at θ =90°) patterns of the short current element (dipole antenna) are shown in Fig. 2-2. As can be seen the pattern is non directional in the H-plane and directional in the E-plane. This type of a pattern is designated as omnidirectional, and it is defined as one "having an essentially nondirectional pattern in a given plane (in this case in azimuth) and a directional pattern in any orthogonal plane (in this case in elevation)" [15]. The omni-directional pattern of Fig. 2-1 has an infinite number of principal *E*-planes (elevation planes; $\varphi = \varphi_c$) and one principal *H*-plane (azimuthal plane; θ =90°).

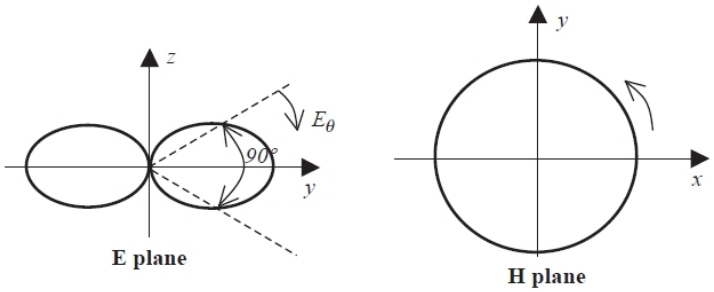

Figure 2-2 The E-plane and H-plane patterns of electrically short current element [16]

2.2 Reflection Coefficient, Return Loss and VSWR

Antenna is like a load connected to a transmission line as shown in the equivalent circuit in Fig. 2-3 and impedance matching between them is extremely important for maximum efficiency of the antenna system. We can use the reflection coefficient, return loss and voltage standing wave ratio (VSWR) as performance parameters to estimate degree of matching and quantify the percentage of power that will be reflected at the input to the antenna. All these three parameters are interlinked.

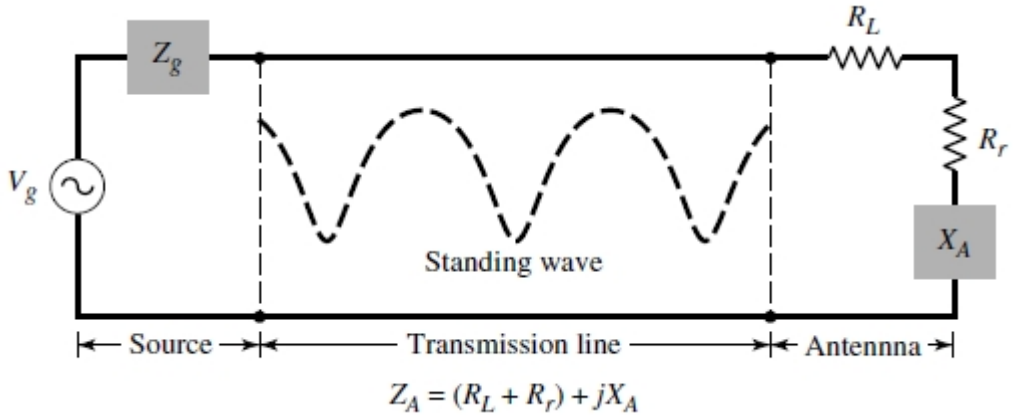

Figure 2-3 Transmission line Thevenin equivalent of antenna in transmitting mode [18]

2.2.1 Reflection Coefficient

Reflection coefficient Γ (a complex number) is a measure of the reflected signal at the feed point of the antenna. It is defined in terms of the input impedance Z_{in} of the antenna and the characteristic impedance Z_o of the feed line as given by

$$\Gamma = \frac{Z_{in} - Z_0}{Z_{in} + Z_0} \qquad (2.1)$$

2.2.2 Return Loss

When an antenna is mismatched in a system, the power from the source is not fully transferred to the antenna and the loss is called return loss RL which is defined in dB as

$$RL = -20 \log |\Gamma| \qquad (2.2)$$

where Γ is the reflection coefficient as defined in equation (2.1). For perfect matching between the transmitter and the antenna, Γ=0 and $RL = \infty$ which means no power would be reflected back, whereas a Γ=1 $(RL = 0\ dB)$ implies that all the incident power is reflected.

2.2.3 Voltage Standing Wave Ratio (VSWR)

When the condition for matching is not satisfied, some of the power may be reflected back and this results in the creation of standing waves. This can be characterized by the Voltage Standing Wave Ratio (VSWR) defined in terms of the reflection coefficient Γ as

$$VSWR = \frac{1 + |\Gamma|}{1 - |\Gamma|} \qquad (2.3)$$

The VSWR is basically a measure of the mismatch between the transmitter and the antenna. The higher the VSWR, the greater is the mismatch. The minimum VSWR which corresponds to a perfect match is unity. The bandwidth is usually specified frequency range over which VSWR is less than 2. This corresponds to a return loss of 9.5 dB or 11% reflected power [19]. Sometimes for stringent applications, the VSWR requirement is specified to be less than 1.5 which corresponds to a return loss of 14 dB or 4% reflected power. For mobile phone antennas, a VSWR<3 corresponding to a return loss of 6 dB is also commonly specified which results in 25% reflected power [16].

2.3 Scattering Parameters or S-Parameters

Linear two-port (and multi-port) networks shown in Fig. 2-4 are represented and analyzed by a number of equivalent circuit parameters such as their impedance matrix, admittance matrix and scattering matrix. The scattering or S-parameters are a set of parameters that relates to the travelling waves that are scattered or reflected when a multi-port network is inserted into a transmission line.

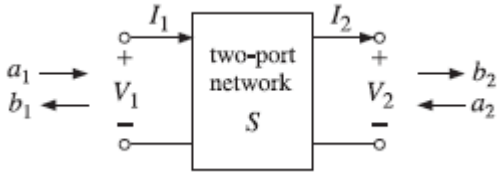

Figure 2-4 Two-port network [19]

The scattering matrix relates the outgoing voltage waves b_1, b_2 to the incoming waves a_1, a_2 that are incident on the two ports [20].

$$\begin{bmatrix} b_1 \\ b_2 \end{bmatrix} = \begin{bmatrix} S_{11}\, S_{12} \\ S_{21}\, S_{22} \end{bmatrix} \begin{bmatrix} a_1 \\ a_2 \end{bmatrix}, \quad S = \begin{bmatrix} S_{11}\, S_{12} \\ S_{21}\, S_{22} \end{bmatrix} \ (scattering\ matrix) \qquad (2.4)$$

The matrix elements S_{11}, S_{12}, S_{21}, S_{22} are referred to as the scattering parameters or S-parameters. The parameters S_{11}, S_{22} have the meaning of reflection coefficients, and S_{21}, S_{12}, the meaning of transmission coefficients.

The travelling wave variables a_1, b_1 at port 1 and a_2, b_2 at port 2 are defined in terms V_1, I_1 and V_2, I_2 and a reference impedance Z_0 as follows [20]

$$a_1 = \frac{V_1 + Z_0 I_1}{2\sqrt{Z_0}} \qquad (2.5)$$

$$b_1 = \frac{V_1 - Z_0 I_1}{2\sqrt{Z_0}} \qquad (2.6)$$

$$a_2 = \frac{V_2 - Z_0 I_2}{2\sqrt{Z_0}} \qquad (2.7)$$

$$b_2 = \frac{V_2 + Z_0 I_2}{2\sqrt{Z_0}} \qquad (2.8)$$

The S-parameters can be easily measured by inserting the two-port network (the device under test or DUT) in a transmission line whose ends are connected to a network analyzer. A typical network analyzer can measure the S-parameters over a large frequency range.

2.4 Bandwidth and Quality Factor

The bandwidth of an antenna is defined as "the range of frequencies within which the performance of the antenna, with respect to some characteristic, conforms to a specified standard" [17]. The bandwidth can be considered to be the range of frequencies, on either side of a center frequency (usually the resonance frequency for a dipole), where the antenna characteristics (such as input impedance, pattern, beamwidth, polarization, side lobe level, gain, beam direction, radiation efficiency) are within an acceptable value of those at the center frequency. The bandwidth of an antenna can, therefore, be defined as impedance, radiation pattern and polarization bandwidth. An antenna needs to have a satisfactory impedance bandwidth to allow most of the energy to be transmitted to the antenna from a feed or a transmission system at a transmitter, and from the antenna to its load at a receiver in a wireless communication system. Also, a designated radiation pattern ensures that maximum or minimum energy is radiated in a specific direction. Finally, a defined polarization of an antenna minimizes possible losses due to polarization mismatch within its operating bandwidth.

In general, an antenna is a resonant device and its input impedance varies greatly with frequency of the input signal [21]. If the antenna is matched to its feed across a certain frequency range, that frequency range is defined as its impedance bandwidth. The impedance bandwidth can be specified in terms of return loss (S parameter: $|S_{11}|$) or a voltage standing-wave ratio (VSWR) over a frequency range. The well-matched impedance bandwidth must totally cover the required operating frequency range for some specified level, such as VSWR = 2 or 1.5 or a reflection coefficient $|S_{11}|$ of less than −10 dB or −15 dB. Impedance bandwidth is closely linked to the quality factor, *Q*, which is a measure of how much lossless reactive energy is stored in a circuit compared to the average power dissipated. The quality factor is quoted as being either loaded or unloaded. For the loaded case, the losses of the external circuit such as the source / matching network are included, whereas for the unloaded Q they are not included. The unloaded quality factor, Q, is defined as [16]

$$Q = \omega \frac{(total\ energy\ stored)}{(average\ power\ loss\ in\ the\ load)} = \omega \frac{W_E + W_M}{P_L} \qquad (2.9)$$

where W_E is the energy stored in the electric field, W_M is the energy stored in the magnetic field and P_L is the average power delivered to the load. The loaded quality

factor, Q_L, can also be given by the above equation but with P_L replaced by the total power P_T , which is dissipated in both the external circuit and the load.

At resonance, the electric and magnetic field energies have the same magnitudes and the formulas simplify such that the unloaded quality factor at resonance Q_0 is given by [16]

$$Q_0 = \frac{2\omega_0 W_E}{P_L} = \frac{2\omega_0 W_M}{P_L} \tag{2.10}$$

where ω_0 is the angular resonant frequency (equal to $2\pi f_0$, where f_0 is the resonant frequency).

The impedance bandwidth is inversely proportional to the *quality factor* (Q) of an antenna and the relationship is given by [21]

$$BW = \frac{VSWR - 1}{Q\sqrt{VSWR}} \tag{2.11}$$

Another simple relationship between the bandwidth and Quality factor is given by [16]

$$Q_0 = \frac{f_0}{f_2 - f_1} = \frac{1}{B_F} \tag{2.12}$$

where $f_1$and $f_2$are the frequencies at which the power reduces to half of its maximum value at the resonant frequency, f_0, and B_F is the *fractional bandwidth*. This equation

provides a good approximation that accurately applies to simple, single resonant circuits and should therefore be used with some care. We can see that antenna bandwidth is maximized when the Q is low or the power dissipation is comparatively high. Thus, a low *Q* is required for wide bandwidths. In turn, the extent to which this energy is associated with radiation (rather than conductor or dielectric losses) determines the antenna efficiency. For a circuit component such as an inductor or capacitor, we require the resistive losses to be low; hence *Q* is required to be high. It is often the case that antennas and circuit components have seemingly contradictory requirements: *antennas are designed to have a low Q, whereas circuit components are designed for a high Q* [16].

The antenna Q factor is related to its physical size as will be discussed in Chapter 3. Extensive research has been conducted on the minimum Q (and hence the maximum BW) that can be achieved by an electrically small antenna that can be enclosed in a sphere of a certain radius.

2.5 Radiation Power Density

The quantity used to describe the power associated with an electromagnetic wave is the instantaneous Poynting vector defined as [15]

$$\mathcal{W} = \boldsymbol{\mathcal{E}} \times \mathcal{H} \tag{2.13}$$

where

$\mathcal{W}$ = instantaneous Poynting vector (W/m^2)

$\mathcal{E}$ = instantaneous electric-field intensity (V/m)`

$\mathcal{H}$ = instantaneous magnetic-field intensity (A/m)

The time average Poynting vector is called the Radiation Power Density W_{rad} and can be written as

$$W_{rad} = \frac{1}{2} Re[\mathbf{E} \times \mathbf{H}^*] \qquad \left(\frac{W}{m^2}\right) \tag{2.14}$$

The $1/2$ factor appears above because the **E** and **H** fields represent peak values, and it should be omitted for RMS values [15].

2.6 Radiation Intensity

Radiation intensity in a given direction is defined as "the power radiated from an antenna per unit solid angle." The solid angle is measured in steradians and one steradian is defined as a solid angle subtended by an area of r^2 at the center of a sphere of radius r. Since the total area of sphere is 4π r^2, the total solid angle for the sphere is 4π. If W_{rad} is the radiation density (W/m^2), then the radiation intensity U is given by [15]

$$U = r^2 W_{rad} \tag{2.15}$$

2.7 Directivity

Directivity of an antenna is defined as "the ratio of the radiation intensity in a given direction from the antenna to the radiation intensity averaged over all directions. The average radiation intensity is equal to the total power radiated by the antenna P_{rad} divided by 4π. If the direction is not specified, the direction of maximum radiation intensity is implied" [15]. Stated more simply, the directivity of a nonisotropic source is equal to the ratio of its radiation intensity in a given direction over that of an isotropic source. In mathematical form, it can be written

$$D = \frac{U}{U_0} = \frac{U}{P_{rad}/4\pi} = \frac{4\pi\, U}{P_{rad}} \tag{2.16}$$

If the direction is not specified, it implies the direction of maximum radiation intensity (maximum directivity) expressed as

$$D_{max} = D_0 = \frac{U_{max}}{U_0} = \frac{4\pi\, U_{max}}{P_{rad}} \tag{2.17}$$

where

D = directivity (dimensionless)

D_0 = maximum directivity (dimensionless)

U = radiation intensity (W/unit solid angle)

U_{max} = maximum radiation intensity (W/unit solid angle)

U_0 = radiation intensity of isotropic source (W/unit solid angle)

P_{rad}= total radiated power (W)

For an isotropic source, it is very obvious that the directivity is unity since U, U_{max}, and U_0 are all equal to each other.

2.8 Gain and efficiency

Gain of an antenna (in a given direction) is defined as "the ratio of the intensity, in a given direction, to the radiation intensity that would be obtained if the power accepted by the antenna were radiated isotropically. The radiation intensity corresponding to the isotropically radiated power is equal to the power accepted (input) by the antenna divided by 4π [15]." Therefore, the gain G can be expressed as

$$G = \frac{U}{P_{in}/4\pi} = \frac{4\pi\, U}{P_{in}} \qquad (2.18)$$

where U is the radiation intensity in W/S_r and P_{in} is the total input power accepted by the antenna in W. From the definition of Directivity, we can see that the Gain and directivity are related by [16]

$$G = \frac{P_{rad}}{P_{in}}\, D = \eta_{rad} D \qquad (2.19)$$

where η_{rad} is the radiation efficiency of the antenna and is the ratio of the radiated power to the input power accepted by the antenna. This efficiency factor has taken both the conductor loss and dielectric loss into account, but not the impedance mismatch between the feed line and the antenna. When the feed line is not matched with the antenna, some power is reflected back and there is reflection or mismatch loss and the input power supplied is different from the input power accepted by the antenna. This is characterized by the matching or reflection efficiency which is defined as the ratio of the input power accepted by the antenna to the source supplied power (P_s) [16]

$$\eta_m = \frac{P_{in}}{P_s} = 1 - |\Gamma|^2 \qquad (2.20)$$

where Γ is the voltage reflection coefficient at the input terminals of the antenna and is given by [16]

$$\Gamma = \frac{Z_{in} - Z_0}{Z_{in} + Z_0} \qquad (2.21)$$

where Z_{in} is the antenna input impedance and Z_0 is the characteristic impedance of the transmission line. Basically, if the feed line is matched with the antenna, Γ = 0 and the matching efficiency is 100%.

The total or overall efficiency of the antenna system (feed and antenna) is the product of the two efficiencies [16].

$$\eta_t = \frac{P_{rad}}{P_s} = \eta_{rad}\eta_m \qquad (2.22)$$

2.9 Summary

The fundamental antenna parameters that describe its features have been presented and discussed in this chapter. The concepts of radiation pattern, antenna bandwidth, S-parameters as well as gain and efficiency were discussed and their governing equations have been presented.

CHAPTER 3

PRINTED ANTENNAS FOR MOBILE HANDSETS

Microstrip and printed antennas have been increasingly used for personal wireless applications. Due to their low-profile, compatibility with Integrated Circuit technology and conformability to shaped surfaces, they are suitable for use as embedded antennas in handheld wireless devices. Theoretical and experimental research on microstrip and printed antennas has continued since 1970s and has resulted in a remarkable change in antenna design and in producing multifunction configurations with simple construction and low manufacturing cost [22]. This chapter describes these two antenna types as well as their characteristics, construction and features. Also, the characteristics of electrically small antennas (ESA) are presented and discussed.

3.1 Introduction

'Printed antennas is a generic term that includes the ever-increasing constructional variations that printed technology makes possible. The basic microstrip or printed

antenna configuration resembles a printed circuit board (PCB) consisting of a thin substrate with both sides coated with copper film. Printed transmission lines, patches etc., are produced on one side of the board and the other copper-clad surface is used as the ground plane. An electromagnetic wave is launched and allowed to spread in between the printed structure and the ground plane. Such a structure has great advantages such as low profile, low cost, light weight, ease of fabrication and suitability to conform on curved surfaces. All these have made microstrip technology attractive since the early phase of its development [22, 23]. Despite the previously mentioned features, microstrip patch antennas suffer from several inherent disadvantages of this technology in its pure form, namely, they have small bandwidth and relatively poor radiation efficiency resulting from surface wave excitation and conductor and dielectric losses. Also, to accurately predict the performance of this form of radiator, in particular, its input impedance nature, typically a full-wave computationally intensive numerical analysis is required [24].

3.2 The Microstrip Patch Antenna

The geometry of a typical microstrip patch antenna is illustrated in Fig. 3-1 and consists of :

a. A very thin metallic region called a patch
b. A dielectric substrate
c. A ground plane which is usually much larger than the patch

d. A feed to supply power to the patch (from bottom through a pin in this case)

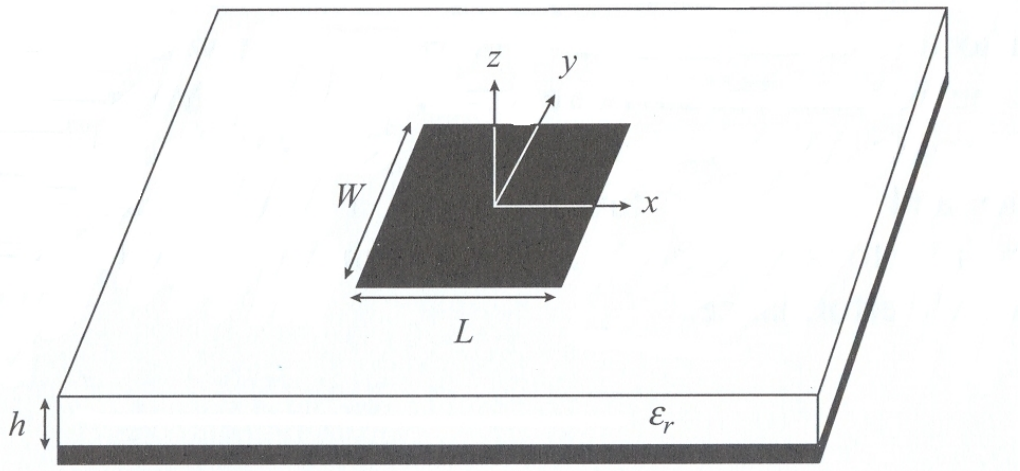

Figure 3-1 A rectangular microstrip patch printed on dielectri substrate (εr) [23]

The length of the patch (L) is typically about a third to a half of a free-space wavelength (λ_0), while the dielectric thickness is in the range of 0.003 λ_0 to 0.05 λ_0. A commonly used dielectric for such antennas is polytetrafluoral ethylene (PTFE), which has a relative dielectric constant of about 2.5. There are other substrates with dielectric constants in the range $2.2 \leq \varepsilon_r \leq 12$ that can be used for the design of microstrip antennas. Thick substrates with lower dielectric constanats are most desirable for antenna performance as they provide better efficiency, larger bandwidth, loosely bound fields for radiation into space but at the expense of larger element size. Substrate materials with high dielectric constants can also be used. Such substrates result in elements that are

electrically small in terms of free-space wavelengths and consequently have relatively small bandwidth and low efficiency [15].

There are many ways in which the microstrip antenna can be fed [23]. The most popular are through a microstrip line, coaxial probe, aperture coupling and proximity coupling. The microstrip feed line is a conducting strip of small width and is easy to fabricate and provides simple impedance matching. However, surface waves and spurious feed radiation are significant as the substrate thickness increases and limits the bandwidth. In Coaxial feeding, the inner conductor of the coax is connected to the patch while the outer conductor is connected to the ground plane. The coaxial probe is easy to fabricate and match and has low spurious radiation. However, it has narrow bandwidth. The microstrip feed line and the probe generate higher order modes due to asymmetries which produce cross-polarized radiation. The aperture coupling feed is used to overcome this problem. However, this is difficult to fabricate and it also has narrow bandwidth although it has moderate spurious radiation. The aperture coupling uses two substrates separated by a ground plane. The energy from a microstrip feed line on the bottom of the lower substrate is coupled through a slot on the ground plane to the patch. Typically, a high dielectric material is used for the bottom substrate and thick low dielectric constant material for the top substrate. The ground plane between the substrates isolates the feed from the radiating element and minimizes interference of spurious radiation. Impedance matching is performed by controlling the width of the feed line and the length of the slot.

There are different models presented for the analysis of microstrip antennas. The most popular models are the transmission-line, cavity and full-wave [23]. The transmission-line model is the easiest of all, it gives good physical insight but is less accurate. The cavity model is comparatively more accurate and gives good physical insight but also more complex. The full-wave analysis models are very accurate and versatile but are the most complex and usually give less physical insight. We will refer to the cavity model here to understand the radiation mechanism only.

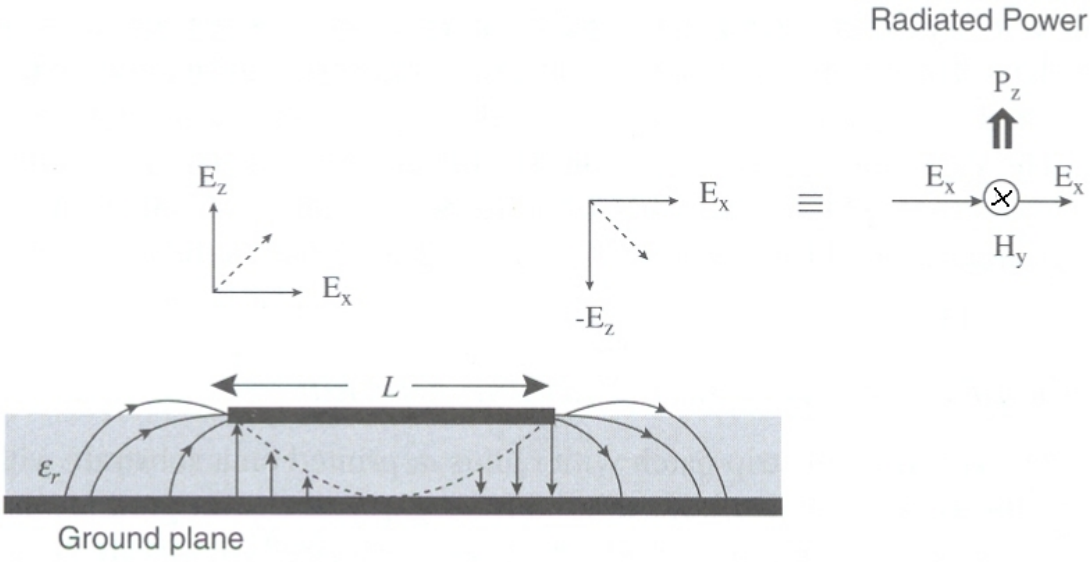

Figure 3-2 Field distribution under rectangular microstrip patch having resonant length L [23]

The rectangular path can be considered as a partially open cavity having electric walls at the top and bottom and magnetic walls surrounding its boundary. This cavity will resonate under the condition of $L \approx \lambda/2$. The open boundary imposes a condition on

the electric field ideally to be zero near the patch center and maximum near the patch edges with mutually opposite polarity as shown in Fig. 3-2. Once it starts resonating, the vertical electric fields near the open edges fringe around over the ground plane and the field vectors no longer remain purely vertical. The inclined electric field vectors around the edges can be split into horizontal and vertical components as shown in Fig. 3-2. We can see that there is only the horizontally polarized electric field E_x as the z-polarized electric fields cancel out due to opposite polarity. So the resultant field leaking from the open microstrip resonator is E_x which is associated with orthogonal magnetic field H_y and thus radiates vertically upwards following the "Poynting vector" P_z. Over the years there have been many conductor shapes proposed and investigated for a microstrip patch antenna including square, rectangular, circular, elliptical triangular among other shapes.

3.3 The Planar Inverted-F Antenna

Planar inverted-F antennas (PIFAs) are compact antennas that are compatible with printed circuit technology and are widely used in mobile phones and laptops. Their operation can be understood by considering their development from two well known antennas i.e. the quarter-wavelength monopole and rectangular microstrip patch antenna [25]. Fig. 3-3 shows the development from the monopole. The conventional monopole Fig. 3-3(a) is fed at the base and has an input impedance of 37.5 Ω for the thin wire type at resonance. As this is a resonant structure, the current distribution is

sinusoidal, with a peak at the feed point and zero at the monopole tip. This means that the impedance varies along the wire length and it is possible to find a position with an impedance of 50 Ω suitable for connection to standard connectors and cables as shown in Fig. 3-3(b).

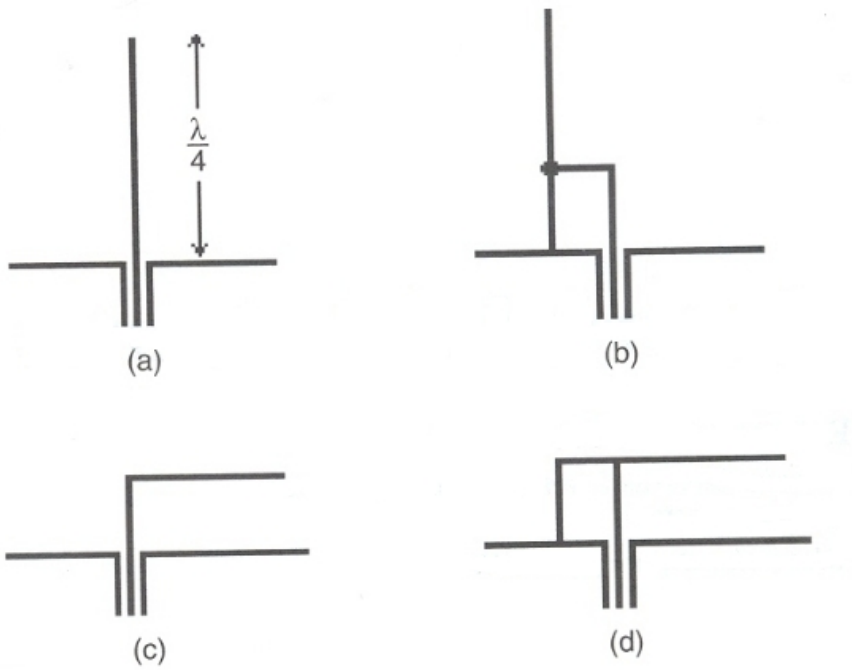

Figure 3-3 Development of the planar inverted-F antenna from the monopole : (a) quarter wavelength monopole; (b) intermediate position-fed quarter wavelength monopole; (c) inverted-L antenna; (d) planar inverted-F antenna [25].

It is also possible to reduce the height of the base-fed monopole by the wire as shown in Fig. 3-3(c) to form an L-shaped antenna. This is done to reduce the height of the antenna, while maintaining a resonant trace length. This parallel section introduces

capacitance to the input impedance of the antenna, which is compensated by implementing a short-circuit stub. The stub's end is connected to the ground plane through a via. To a first order the current distribution is the same as the straight monopole so that the horizontal section introduces some cross-polarized components into the radiation pattern. If these two concepts are combined, the inverted-F antenna of Fig. 3-3(d) is obtained. This form has been widely used in hand-held terminals and is well suited for coplanar mounting on top of a printed circuit board. The planar inverted-F antenna can be obtained from the wire inverted-F antenna by replacing the top wire by a rectangular conducting plate and operating it over a ground plane normal to the feed pin [25] as shown in Fig. 3-4.

The resonant frequency of the PIFA is proportional to the effective length of the current distribution. There are two cases in which it is easy to formulate an expression of the resonant frequency with respect to the size of the PIFA. The first case is when the width of the short-circuit plate W is equal to the length of the planar element L1. This corresponds to the case of the short-circuited microstrip antenna which is a quarter-wavelength antenna. The effective length of the microstrip antenna is L2+h where h is the height of the short-circuit plate. The resonance condition then is expressed by [26]

$$L_2 + h = \frac{\lambda_0}{4} \qquad (3.1)$$

where λ_0 is the wavelength.

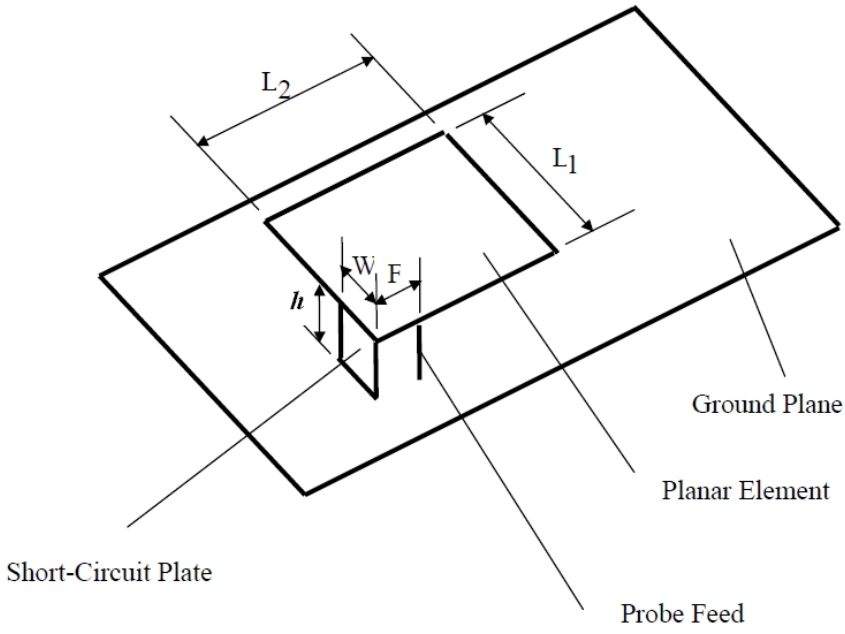

Figure 3-4 Structure of Planer inverted-F antenna [26]

The resonant frequency associated with W=L_1 calculated from (3.1) is

$$f_1 = \frac{c}{4(L_2 + h)} \tag{3.2}$$

where c is the speed of light. The other case is for *W*=0. A short-circuit plate with a width of zero can be physically represented by a thin short-circuit pin. The effective length of the current flow is then L_1+L_2+h. For this case, the resonance condition is expressed by

$$L_1 + L_2 + h = \lambda_0/4 \tag{3.3}$$

For the case when $0 < W/L_1 < 1$, the resonant frequency f_r can be expressed by the following equation [26]:

$$f_r = r.f_1 + (1-r).f_2 \qquad for\frac{L1}{L2} \leq 1 \qquad (3.4)$$

$$f_r = r^k.f_1 + \left(1-r^k\right).f_2 \qquad for\frac{L1}{L2} > 1 \qquad (3.5)$$

where $r = W/L_1$ and $k = L_1/L_2$ and the frequency f_1 is given by equation (3.2) and f_2 is given by

$$f_2 = \frac{\mathrm{c}}{4(\mathrm{L_1} + \mathrm{L_2} + \mathrm{h} - \mathrm{W})} \qquad (3.6)$$

3.4 Electrically Small Antennas (ESA)

As the miniaturization of mobile communication equipment and handsets continues, antennas are expected to follow the same trend. Today's multifunctional portable equipment further drives the need for small antennas. However, antenna size reduction results in gain, bandwidth and efficiency performance reduction. The antenna acts as a transducer which converts the free space electromagnetic wave into received power or vice versa. This cannot be done efficiently when the size of the antenna is much smaller than the wavelength. When the antenna size is reduced, although the resulting loss of gain can

be compensated for by amplification, the loss of bandwidth cannot be compensated for [27].

Electrically Small Antennas (ESA) are generally defined as antennas which fit inside a sphere of radius a=1/k, where k is the wave number ($2\pi/\lambda$) associated with the electromagnetic field at the frequency of operation [28]. Thus we can say that for ESAs, the condition to be satisfied is ka<1. The sphere of radius "a" is referred to as the "radiansphere" which contains the stored energy in the antenna's electric or magnetic field and represents the boundary between the near- and far-field radiation for a Hertzian dipole. The radius a=$\lambda/2\pi$ is referred to as the "radianlength" [26].

In the study of small antennas, the Q factor is an important quantity because it is related to the antenna bandwidth and is defined as [29]

$$Q = \frac{2\,\omega_0 \max(W_E, W_M)}{P_A} \qquad (3.7)$$

W_E and W_M are the time averaged stored electric and magnetic energies, and P_A is the antenna received power. The radiated power is related to the received power through $P_{rad} = \eta\, P_A$, where $\boldsymbol{\eta}$ is the antenna efficiency. It is assumed that the small antenna is tuned to resonance at ω_0, either through self-resonance or by using a lossless reactive tuning element. Antenna Q is inversely proportional to the antenna bandwidth (approximately) and can be evaluated using equivalent circuit representation of the

antenna. A commonly used approximation between Q and the 3dB fractional bandwidth B of the antenna is [29]

$$Q \cong \frac{1}{B} \qquad for\ Q \gg 1 \tag{3.8}$$

Wheeler was the first to investigate small antennas in 1947 and discussed the fundamental limitations of small antennas using a simple model that represents the small antenna with lumped capacitor or inductor and a radiation resistance. Using the concept of radiation power factor – a ratio of radiated power to reactive power – he discovered that the Q of a small antenna is inversely proportional to its physical volume and thus the antenna size imposes a fundamental limitation on bandwidth. Wheeler derived the lowest Q for a constant pitch spherical coil antenna with infinite permeability core. With TE_{10} type as the mode radiated by this structure and no energy is stored inside the sphere, the limiting value for the Q was found to be given by

$$Q_{min} = \frac{1}{(ka)^3} \tag{3.9}$$

Wheeler also considered a self-resonant coil supporting TE_{10} and TM_{10} modes, with zero stored internal energy and found the limiting value for Q as

$$Q_{min} = \frac{1}{2(ka)^3} \tag{3.10}$$

Wheeler's work was only approximate and accurate only for extremely small antenna sizes as it did not take into account the radiated spherical modes as the antenna size increased.

In 1948, Chu derived the minimum possible Q for an omnidirectional antenna enclosed in a radianshpere (also called Chu sphere) by expressing the radiated field as a sum of spherical modes. Each mode was represented by an equivalent circuit and the Q of each mode was found by lumped circuit analysis. According to Chu's criterion, the minimum quality factor Q_{min} of an antenna of a given size is given approximately by [21]

$$Q_{min} = \frac{1 + 3(ka)^2}{(ka)^3[1 + (ka)^2]} \tag{3.11}$$

Harrington [30] followed much of Chu's analysis and was the first to consider the antenna radiating both TE and TM modes. As a result, his work led to lower minimum Q values. He also attempted to quantify antenna losses as a function of antenna size and the number of modes excited and concluded that as antenna size decreases, its efficiency also decreases [29]. Collin and Rothschild [29] found that the Q associated with TM_1m or TE_1m modes represents the absolute lower bound on the Q for a small antenna radiating only TE or TM modes, and is given by

$$Q_{min} = \frac{1}{(ka)^3} + \frac{1}{(ka)} \tag{3.12}$$

Compared to Wheeler's result, this equation has an extra term 1/ka. However, both the results are very close for $ka \ll 1$. Mc Lean [28] also derived the same result for an antenna exciting only TE modes or TM modes. When both TE and TM modes are excited, the fundamental limit is given by

$$Qmin = \frac{1}{2}\left(\frac{1}{(ka)^3} + \frac{1}{(ka)}\right) \qquad (3.13)$$

Fig. 3-5 compares the approximate results derived by Wheeler (equation 3.9) and Chu (equation 3.11) with the exact relation given by Collin and Rothschild (equation 3.12). All the results agree very closely for small values of ka.

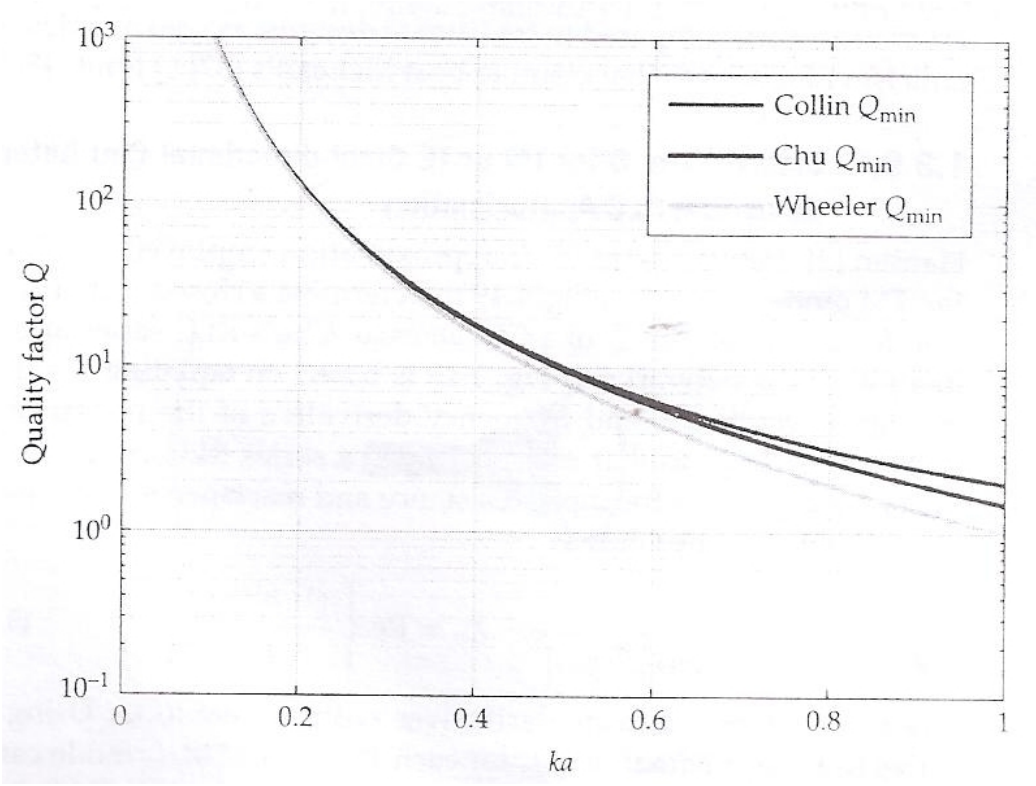

Figure 3-5 Q_{min} Comparison for TM or TE antenna enclosed in a Chu sphere of radius a [29]

The antenna should be designed so that it occupies the maximum size possible in the space provided. As is clear from the above discussion, there are physical laws that govern the relationship between the antenna dimensions and its performance factors (gain, bandwidth, efficiency). For an antenna of a certain size, its gain can be increased at the expense of its bandwidth. Similarly, its bandwidth can be increased reducing its gain and efficiency. The upper limits on the gain and bandwidth of ESAs were provided in literature and given by [27,31].

$$G_{max} < (ka)^2 + 2(\text{ka}) \tag{3.14}$$

$$B_{max} < \left(\frac{1}{1+3\left(\frac{a}{\lambda}\right)^2}\right)\left(\frac{a}{\lambda}\right)\left(1+\left(\frac{a}{\lambda}\right)^2\right) \tag{3.15}$$

Andrew J. Compston et.al. [32] have also given an upper bound for the gain of ESAs which can be expressed as

$$G_{max} < (2ka)^3\sqrt{\frac{2}{1+(2ka)^2}} \tag{3.16}$$

Fig. 3-6 shows the maximum gain obtained from an ESA as a function of ka based on the Harrington (Equation 3.14) and Compton (Equation 3.16) expressions. It is clear that for ka values less than 0.7, the difference between the two is small.

The challenge of antenna miniaturization is to find the best compromise between gain and bandwidth for the antenna volume available in a particular case. For many applications, low-profile planar antennas are the best solution since they are miniaturized by using different techniques such as using a high permittivity dielectric, modifying their shape and the use of well placed short-circuits [27].

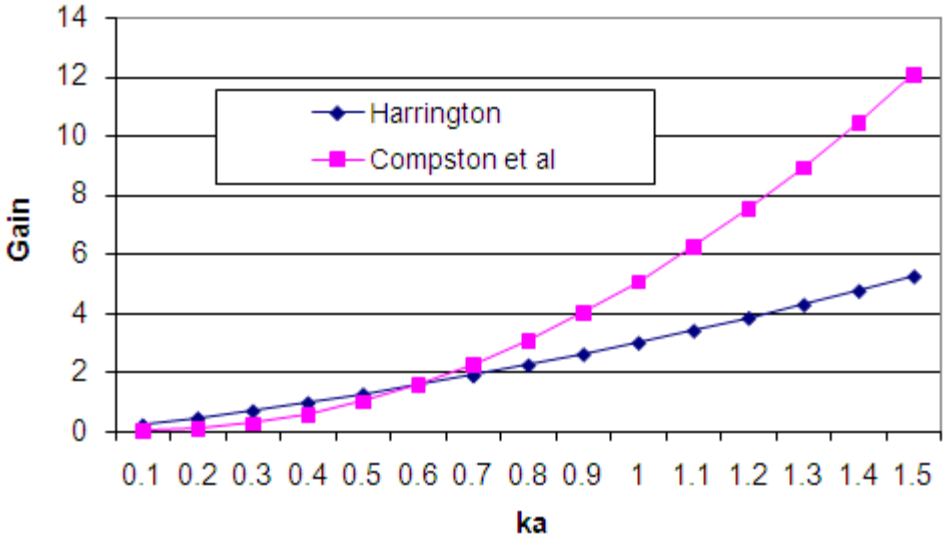

Figure 3-6 Comparison of the maximum Gain given by Harrington and Comston et al.

3.5 Summary

Printed antennas are widely used in consumer electronics nowadays due to their low profile, low cost, ease of fabrication and integration. In this chapter, two of most widely

used printed antenna geometries have been discussed. In addition, the concept of ESA was introduced along with its governing gain and bandwidth bounds.

CHAPTER 4

MIMO SYSTEMS

Modern wireless systems have to provide higher and higher data rates as required by new applications. Since increasing the bandwidth is expensive and there is limit to using higher order modulation types, new methods for utilizing the transmission channel have to be used. Multiple antenna systems (Multiple Input, Multiple Output – MIMO) give a significant enhancement to data rate and channel capacity. A key feature of MIMO systems is that it turns multipath propagation, which is a pitfall of wireless transmission, into a benefit for the user. MIMO effectively takes advantage of random fading and multipath delay spread for enhancing the data rate. The possibility of many orders of magnitude improvement in wireless communication performance at no cost of extra spectrum (only hardware and complexity are added) has turned MIMO into an active topic for new research [33]. This chapter gives an introduction to basic MIMO concepts and terminology and presents MIMO antenna systems and the challenges faced in their design. It also gives a survey of the literature available regarding MIMO antennas for LTE.

4.1 Single Input Single Output (SISO)

Conventional systems use one antenna at the transmitter and one antenna at the receiver as shown in Fig. 4-1. In MIMO terminology, this is called Single Input, Single Output (SISO). Both the transmitter and the receiver have one RF chain. SISO is relatively simple and cheap to implement and it has been used age long since the birth of radio technology. It is used in radio and TV broadcast and our personal wireless technologies (e.g. Wi-Fi and Bluetooth). The capacity C of SISO is given by [33]

$$C = log_2 (1 + \gamma |p_c|^2) \quad bits/s/Hz \qquad 4.1$$

where p_c is the normalized complex gain of a fixed wireless channel or that of a particular realization of a random channel and γ is the SNR at the RX antenna. The capacity given by the above equation is normalized by the bandwidth.

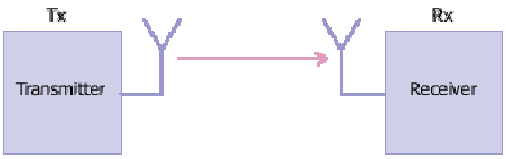

Figure 4-1 Single Input Single Output (SISO) [34]

4.2 Single Input Multiple Output (SIMO)

To improve performance, a multiple antenna technique has been developed. A system which uses a single antenna at the transmitter and multiple antennas at the receiver is named Single Input Multiple Output (SIMO). This configuration is known as receive diversity. Because of the different transmission paths, the receiver sees two differently faded signals. By using the appropriate method in the receiver, the signal-to-noise ratio can now be increased. The receiver can either choose the best antenna to receive a stronger signal or combine signals from all antennas in such a way that maximizes SNR (Signal to Noise Ratio). The first technique is known as switched diversity or selection diversity. The latter is known as maximal ratio combining (MRC). A SIMO system is shown in Fig. 4-2.

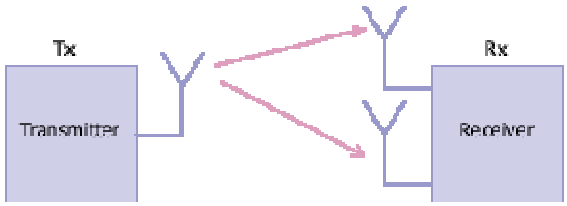

Figure 4-2 Single Input Multiple Output (SIMO) 1x2 [34]

With M R_X antennas, we have a SIMO system with capacity given by [33]

$$C = log_2\left(1 + \gamma \sum_{i=1}^{M} |p_{c_i}|^2\right) \qquad bits/s/Hz \qquad 4.2$$

where p_{c_i} is the gain for receive antenna i. It is to be noted that increasing the value of M only results in a logarithmic increase in average capacity.

4.3 Multiple Input Single Output (MISO)

A system which uses multiple antennas at the transmitter and a single antenna at the receiver is named Multiple Input Single Output (MISO). In this case, the same data is transmitted redundantly over two or more antennas. This method has the advantage that the multiple antennas and redundancy coding is moved from the mobile handset to the base station, where these technologies are simpler and cheaper to implement. To generate a redundant signal, space-time codes are used. Alamouti developed the first codes for two antennas [35]. Space-time codes additionally improve the performance and make spatial diversity usable. The signal copy is transmitted not only from a different antenna but also at a different time. This delayed transmission is called delayed diversity.

Multiple antennas (each with an RF chain) of either SIMO or MISO are usually placed at a base station (BS). This way, the cost of providing either a receive diversity (in SIMO) or transmit diversity (in MISO) can be shared by all subscriber stations served by the BS. This is shown in Fig. 4-3.

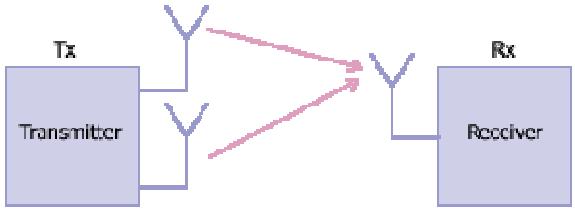

Figure 4-3 Multiple Input Single Output (MISO), 2x1 [34]

Considering a MISO system with *N* transmit antennas where the transmitter does not have channel knowledge, the capacity of the system is given by

$$C = log_2\left(1 + \frac{\gamma}{N}\sum_{i=1}^{N}|p_{c_i}|^2\right) \qquad bits/\text{s/Hz} \qquad 4.3$$

where the normalization by *N* ensures a fixed total transmitter power. Similar to the SIMO case, the capacity has a logarithmic relationship with *N*.

4.4 Multiple Input Multiple Output (MIMO)

To increase the throughput of a radio link, multiple antennas (and multiple RF chains accordingly) are employed at both the transmitter and the receiver as shown in Fig. 4-4. This system is referred to as Multiple Input Multiple Output (MIMO). In order to be able to benefit from MIMO fully it is necessary to be able to utilize coding on the channels to separate the data from the different paths. This requires extra processing, but provides additional channel robustness / data throughput capacity. MIMO radios get more out of

the RF bandwidth they occupy than their single channel equivalents by exploiting differences in the paths between the transmitter and the receiver inputs. If a conventional single-channel radio system creates one data "pipe" between the transmitter and the receiver, the object of a MIMO radio system is to create multiple such pipes. It does this by creating a mathematical model of the paths from transmitters to receivers and solving the resulting equations, and has to do so as fast as the channel is changing. If the data pipes can be completely separated, the channel capacity increases linearly as more transmitter-receiver antenna pairs are added.

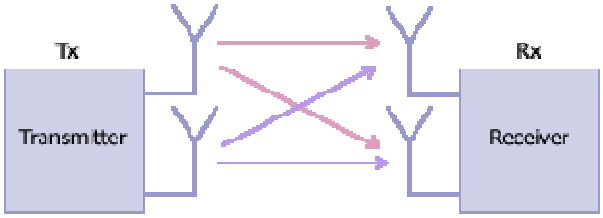

Figure 4-4 Multiple Input Multiple Output (MIMO) 2x2 [34]

For a MIMO system with N antennas at the transmitter and M antennas at the receiver, the capacity is given by [33]

$$C = log_2\left[\det\left(\boldsymbol{I}_M + \frac{\gamma}{N}\boldsymbol{P_c}\boldsymbol{P_c}^*\right)\right] \qquad bits/s/Hz \qquad 4.4$$

where $(*)$ means transpose-conjugate and $\boldsymbol{P_c}$ is the *MxN* channel matrix. It has been demonstrated that the capacity in 4.4 grows linearly with m=min (M,N) rather than logarithmically as in case of SIMO/MISO [33]. A MIMO system with similar count of

antennas at both the transmitter and the receiver in a point-to-point (PTP) link is able to multiply the system throughput linearly with every additional antenna. For example, a 2x2 MIMO will double the throughput.

4.5 Antennas for MIMO Systems

The size and weight of mobile terminals have been dramatically reduced over the last few years. This reduction in the terminal's size has sparked a rapid evolution of the antennas used for mobile terminals. Also, the antenna requirements for a handset have evolved from a single main antenna to multi-antenna solutions as the demand for higher data rate and multiple band communication has increased. Hence, the design of antennas for small mobile terminals is becoming more challenging. The antennas are required to be small while their performances have to be maintained. However, usually a degradation of the gain and bandwidth are observed when the antenna's size is reduced. In MIMO systems, more than one antenna will be implemented in a mobile terminal to take advantage of the diversity that these systems provide. As a result, the design of two or more antennas in a small mobile terminal for the MIMO systems is more challenging compared to the design of a single conventional antenna in the mobile terminal. The main problem in MIMO systems for mobile handsets is the short distance between the antennas because when two or more antennas are located in close proximity, mutual coupling can occur between them. This lowers the isolation between the antennas and no diversity gain

can be achieved. The coupling between antennas also decreases their efficiencies as part of the power that would normally be radiated is captured by the other antenna. Sufficient isolation between antennas is important in diversity and MIMO systems. Different techniques have to be utilized to reduce the mutual coupling and improve the isolation between the antennas.

Usually, reduced coupling can be achieved by separating two antennas at a distance of a half wavelength or more at the operating frequency, but this method is not suitable for practical portable devices. This may be feasible if higher bands such as 2.6 GHz are the ones targeted for reception; however 700 MHz designs are going to be problematic. A new approach is needed to support multiple antennas in the lower frequency ranges in small form factors. Antenna complexity increases as the frequency band decreases. It is easier to implement multiple antenna systems on high frequency bands (> 1 GHz) than on low bands (< 1GHz) in small, handheld form factor devices. The 850 and 900 MHz bands used in the US and globally (respectively) present definite challenges, while the 700 MHz band introduces the greatest challenge of all [36].

Antenna size is also a major consideration. The dimensions of an antenna are inversely proportional to its frequency of operation. It is easy to calculate that the length of a quarter of wavelength monopole antenna operating at 750 MHz to be approximately 10 cm. This will be longer than many handhelds available in the market.

As shown in previous chapters, the theoretical capacity of the MIMO system increases linearly with the number of antenna elements. However, practical considerations indicate that the corresponding capacity of the system may be reduced if the received signals in any of the different antenna elements are highly correlated. A practical approach to characterize and evaluate the diversity capabilities of a MIMO antenna system is finding its envelope correlation coefficient. The envelope correlation coefficient acts as an important parameter for MIMO antennas, and diversity gain is obtained in the antenna system when its value is less than 0.5 [37]. The lower the correlation coefficient, the better is the MIMO system performance.

The envelope correlation coefficient can be measured directly in a representative scattering environment, or calculated from the full-sphere radiation patterns. Both methods require special measurement equipment and are time-consuming. Several papers [38, 39] give expressions for the envelope correlation coefficient in terms of scattering S-parameters of the antennas, i.e., the port reflection coefficients S_{11} and S_{22} of the two antennas, and the coupling $S_{21}=S_{12}$ assuming lossless antennas and uniform distributed incoming waves. From the measurement point of view S-parameter approach involves simple measurement with the network analyzer. A more comprehensive expression for the envelope correlation coefficient that takes antenna efficiencies into account was derived in [40] and also given in [41], it is given by :

$$|\rho_{i,j}|_{max} = \left| \frac{-S_{ii}^{*}S_{ij} - S_{ji}^{*}S_{jj}}{\sqrt{(1-|S_{ii}|^2-|S_{ji}|^2)(1-|S_{jj}|^2-|S_{ij}|^2)\eta_i\eta_j}} \right| + \sqrt{\left(\frac{1}{\eta_i}-1\right)\left(\frac{1}{\eta_j}-1\right)} \qquad 4.5$$

where $|\rho_{i,j}|_{max}$ is the upper bound on the envelope correlation coefficient between antennas *i* and *j*, η_i and η_j are the efficiencies of antennas *i* and *j*, respectively, and S_{ij} are the S-parameter measurement values.

4.6 Techniques to reduce the Mutual Coupling and to improve the Isolation between antennas

The space available on mobile handsets is very limited and accommodating two or more antennas for MIMO applications is very challenging, especially at the low 700 MHz band. The close spacing of the antenna elements is an important issue in MIMO systems for mobile handsets because when two or more antennas are located in close proximity, mutual coupling can occur between them. However, high isolation among antenna elements is required for MIMO systems to guarantee the reception of uncorrelated signals when the antennas are closely spaced. Several techniques to reduce the mutual coupling and improve the isolation are discussed in this section.

Factors that affect the isolation between antennas include antenna separation, polarization, surface wave propagation and ground plane currents. Knowledge of the polarization can be used to design the antenna with maximum isolation. Two linear polarized waves, one rotated 90 degrees from the other are orthogonally polarized. Waves of orthogonal polarizations do not interact and, therefore, antennas transmitting orthogonal polarizations will be well isolated. Building antennas that produce only one polarization is not trivial. Although the polarization of the antenna will be mixed (i.e. not pure) parts of the pattern of an antenna can be found where the polarization is quite strongly biased. By integrating multiple antennas in such a way that the directions where the polarization is highly biased are orthogonal should improve the isolation between the antennas.

Many antennas such as monopoles and PIFAs are driven directly from the ground plane. They excite currents in the ground plane which are common to all antennas attached to it and therefore are important in terms of coupling. A common disadvantage of microstrip antennas is surface waves, which are excited whenever the substrate has dielectric permittivity greater than one [42]. Surface waves lead to mutual coupling between antenna elements. One way to ensure that the surface wave coupling remains low is to use a technology which confines the surface wave flow such as electromagnetic band gap (EBG) structures and defected ground structures (DGS) or by including baluns at the antenna input feeds.

Numerous studies have been conducted to discuss techniques that reduce the mutual coupling and increase the isolation between antennas [43, 44]. The commonly used

techniques include split/slits in the ground plane between the antennas [41, 45], hybrid coupler [46], placing a neutralization line between antennas [47], use of decoupling network [48] and use of defected ground structures (DGS) [42].

4.6.1 Cutting Ground Slot between antennas

An effective way of improving isolation between the antennas is the disturbance of the ground current distribution. Thus, a rectangular slot on the ground plane was cut for improving the isolation between closely spaced antennas [41, 43, 45, 49].

4.6.2 Using parasitic elements between the antennas

In [50], several resonant parasitic microstrip elements were employed to reduce the mutual coupling between antenna elements. These parasitic elements are shown to improve the antenna efficiency as well.

4.6.3 Using Metamaterials to Improve Isolation

A Metamaterial is an artificial structure, whose properties may not be found in nature. When its geometrical structure is much smaller than its operating wavelength, some special properties, such as negative permittivity and negative permeability, can be obtained. The authors of [51] have proposed the use of metamaterial isolator arrays in between two antenna elements to reduce the coupling effect.

4.6.4 Use of Defected Ground Structures (DGS)

The concept of Defected Ground Structures (DGS) evolved from Photonic Bandgap Structures (PBG) in electromagnetics. The PBGs employed in electromagnetic applications are referred to as Electromagnetic Bandgap (EBG). These are artificial periodic structures that prevent electromagnetic waves from propagating through them over a range of frequencies called the "stopband" and allow electromagnetic waves to propagate through them over a range of frequencies called the "passband". DGS refers to certain geometries, called unit cell, etched out as a single defect or in periodic configurations on the ground plane of a PCB to stop wave propagation through the substrate over a certain frequency range. The DGS slots are resonant in nature. They have different shapes and sizes with different frequency responses. The presence of DGS under the printed transmission line actually perturbs the current distribution in the ground plane and thus modifies the equivalent line parameters over the defected region. Thus it influences the guided wave characteristics and exhibits bandgap properties and a slow wave effect (which helps in compacting the printed circuits).

Although DGS has been widely used for microstrip feeds to control the individual elements, a DGS can be placed in between two microstrip antennas to reduce mutual coupling between them. Indeed the surface waves propagating through the grounded substrate result in undesirable coupling between adjacent printed antennas. The bandstop feature of a DGS can be used to reduce the intensity of surface waves propagating across it over certain frequency bands [23].

4.7 Literature Review of Printed Antennas for Mobile Handsets

There is large number of allocated radio spectrum reserved for LTE use. This includes the 700 MHz band which was previously used for analog TV broadcasting in the USA and will now be used for LTE. At these low frequencies, implementing multiple antennas in a handheld device with maximum dimensions of 50x100 mm^2 poses significant challenges in terms of high antenna radiation efficiency on small ground plane, high isolation, and low far-field envelope correlation between antennas. Antennas for mobile handsets in the Global System for Mobile communications (GSM; 880-960 MHz), Digital Communication System (DCS; 1710-1880MHz), Personal Communication System (PCS; 1880-1900 MHz), Universal Mobile Telecommunication System (UMTS; 1920-2170 MHz) and Wireless Local Area Network (WLAN; 2.4 GHz, 5 GHz) frequency bands have been extensively discussed in literature [52-57]. Planar inverted-F antennas (PIFAs), Meander line, slot and a variety of other antenna types have been considered as well. However, there is limited literature available regarding MIMO LTE antennas as this technology is under extensive investigation as we speak. Antennas suitable for LTE have been presented in literature which cover the higher frequency bands (1.8-2.6 GHz) [52, 58, 59] and the lower (700-800) MHz band [60, 53, 46, 61, 62, 63, 64, 65]. Some of antennas described are multi-band [53, 54, 62, 63, 66, 67] covering LTE and other GSM/UMTS/WLAN bands. Although PIFA is by far the most popular antenna type,

other antennas such as meander line [41, 46, 55, 60], folded monopole [48, 65] and inverted folded-h [52] have also been presented and discussed in literature.

Electrically small antennas (ESAs) have been discussed in literature emphasizing the relationship between the antenna size, gain and bandwidth and providing theoretical upper limits on the gain and bandwidth [28-32, 68-69]. An ESA for the 800 MHz band of LTE is proposed in [60] using a meander antenna structure. The antenna has a measured center frequency of 897 MHz, bandwidth of 185 MHz and total size of 23.5x43 mm^2 making it suitable for operation in the 800-900 MHz band. Although a single element antenna is presented, its small size allows its use in a MIMO system as four such antenna elements can be accommodated in the standard phone size.

Reference [54] presents a multiband PIFA antenna that covers 8 bands LTE700, GSM850/900, GSM1800/1900, and UMTS/LTE2300/2500. It has a simple structure and mainly comprises a radiating strip, an inductive shorting strip and a coupling feed. It can be seen that two wide operating bands centered at about 850 and 2200 MHz can be generated successfully. The lower band has a wide bandwidth (3:1 VSWR) covering the desired 698~960 MHz band. The upper band has an even wider bandwidth of larger than 1.2 GHz (3:1 VSWR) covering the desired 1710~2690 MHz band. Over the LTE700/ GSM850/900 bands, the radiation efficiency is about 46~76%, and the antenna gain is about −1.2~1.0 dBi. Over the GSM1800/1900/ UMTS/LTE2300/2500 bands, the radiation efficiency varies from about 57 to 86%, and the antenna gain is about 2.2~4.3

dBi. The size of the antenna is 4x36x5mm^3 and two ground planes of size 40x80mm^2 and 40x70mm^2 are used for a folding type mobile terminal. This is a single element antenna.

The work in [59] introduced a compact dual-port MIMO antenna that merges two PIFAs into a single unit, thus getting rid of the need to place the individual antenna elements far apart from each other to obtain high isolation. The isolation between the two antenna elements is improved by using orthogonal polarization diversity. The implemented prototype operates in the 2.6-GHz LTE bands (2.5–2.7 GHz) with return loss of better than 10 dB. This satisfies the required bandwidth for LTE 2.6-GHz band applications. The isolation between the two ports is better than 10 dB in the bandwidth of interest with values as low as −15 dB at some frequencies. These values indicate that the two ports are highly isolated, although they are only separated by a distance of 0.08 λ_0 (at 2.6 GHz, measured in free-space wavelengths).

In [46] a dual-element antenna operating at 710 MHz has been presented which consists of two meander-line monopoles printed on FR-4 substrate measuring 50x110mm^2. The two elements in this configuration are highly coupled which is undesirable for MIMO application. An LC-based branch-line hybrid coupler has been used to decouple the ports but it greatly reduced the -10dB impedance BW of the antennas to about 15 MHz. Measured reflection coefficient of the antenna at 0.71 GHz is better than -28 dB, and the isolation between the ports is better than 25 dB with peak directivity of 2.4 dBi. This antenna will partially cover LTE band 12.

In [48], the proposed MIMO antenna consists of two parallel folded monopole antennas and a decoupling network to improve the isolation between the antennas. The overall size of the proposed MIMO antenna is 48×12× 6mm^3. Two similar elements are placed at the two corners of top edge of a FR4 substrate measuring 48x108×0.8 mm^3. From the measured results, the 6-dB return loss impedance bandwidth is 4.15% (from 755 MHz to 787 MHz) for LTE band 13 and the isolation at LTE band is about 15 dB. The measured peak gains of two antenna elements are -0.12 dBi and -0.32 dBi while measured antenna efficiencies are 37.2 % and 31.4% at 770 MHz**.**

In [61], the authors propose a 2-element metamaterial MIMO array consisting of dual resonance antennas at center frequency 771MHz of the LTE bands (13, 14). The antenna element occupies an area of 38x9.5mm^2, thus two of these antennas can be easily placed on a 50mm x 120mm board. Two different placements for the antenna elements were explored. The fabricated antenna achieved a -6dB return loss bandwidth of about 100 MHz and isolation better than 10dB. If we consider the 2:1 VSWR, the antenna bandwidth is only about 25MHz (730-755MHz).

In [64] the authors present a dual monopole multiband antenna which covers the LTE band 13 (746-787 MHz) in addition to GPS (1565-1585MHz), PCS (1810-1990MHz) and UMTS (1920-2170MHz) bands. The two monopoles are connected by suspended line to improve the isolation. The antenna size is 40x20x5mm^3 and two elements are implemented on a substrate of size 40x80x1mm^3. Considering the LTE band covered,

the -6dB impedance bandwidth of the antenna is 70 MHz (735-810MHz) with average gain of -3.42 dBi and isolation of 15dB.

In [65] an internal MIMO antenna consisting of two folded monopole antenna elements and a hybrid coupler is presented. The proposed antenna covers the LTE bands (13, 14) satisfying the 10dB return loss requirement. A hybrid coupler is used to improve the isolation between the antenna elements. The two elements of size 30x10x5mm^3 are installed on FR4 substrate of size 120x45x1 mm^3. The antenna achieved an isolation of more than 30dB and the gain varied from 1.52 to 3.51dBi.

In [66] the authors present a multiband antenna consisting of a driven strip monopole and parasitic shorted strip. The antenna has two wide operating bands. The lower band has a 6-dB return loss bandwidth of about 305 MHz to cover the LTE700, GSM850/900 bands. The upper band has a higher bandwidth of 1210MHz and covers the GSM1800/1900/UMTS/LTE2300/2500 bands. Over the lower band (698-960), the antenna gain is -0.4 – 1.1 dBi while a higher gain of 2.7 - 4.4 dBi is achieved at the higher band.

In [70], the authors present the simulation results for a dual band antenna for LTE handsets. The antenna consists of a meandered monopole operating in the 700MHz band and a parasitic element which radiates in the 2.5-2.7GHz band. Two such antennas are placed on a 120x50 mm^2 PCB and a neutralization technique is used to reduce the coupling between them. In the lower band, the antenna gives a -6dB bandwidth of 40MHz while a

higher bandwidth of 250 MHz in the higher band. The isolation value is found to be higher that 6dB in both the bands. According to the authors, these values are state-of-the-art performance for dual band LTE antennas so closely packed in a small communication device.

Table 4.1 provides a summary of the related MIMO designs that appeared in the literature and compares their features for later benchmarking against our design. It is clear that most of the antennas considered are either single or 2x1 MIMO and have a narrow -10dB impedance bandwidth and large size. The single antenna elements presented are not suitable to be employed in a 2x2 MIMO configuration on the regular size PCB for a mobile terminal. In this work we propose an antenna element that has a wide bandwidth, dual resonance frequencies and can be easily fabricated on a mobile terminal sized PCB in 2x2 MIMO configuration. The proposed design will utilize several isolation enhancement techniques to improve its diversity performance.

Table 4.1 Summary Table of Related Work in 700 MHz band

Reference / Parameter	[54]	[46]	[48]	[61]
Frequency band (MHz)	698-960 LTE700/ GSM	705-720 (LTE band 12)	755-787 (LTE band 13)	746-796 (LTE band 13,14)
Single/ Multiband	Multiband	Single	Single	Single
SISO / MIMO	SISO	2x1	2x1	2x1
Isolation (dB)	-	-25	-15	-10
-10 dB Bandwidth (MHz)	262*	15	32*	100*
Gain (dBi)	-1.2~1	2.4	<0	<0
Single Element Size (mm)	15x45x0.8	22x50	48x12x6	38x9.5x1
Substrate Size (mm)	45x100x0.8	50x110 x1	48x108x0.8	50x120x1

* -6 dB Bandwidth

Table 4.1 Summary Table of Related Work in 700 MHz band (continued)

Reference / Parameter	[64]	[65]	[66]
Frequency band (MHz)	735-810 GPS/PCS/ UMTS	746-794 (LTE band 13)	LTE(698-960) GSM/ UMTS/ LTE2300
Single/ Multiband	Multiband	Single	Multiband
SISO / MIMO	2x1	2x1	SISO
Isolation (dB)	-15	-35	-
-10 dB Bandwidth (MHz)	70*	100	305*
Gain (dBi)	-3.42	-1.5∼-3.5	<1dB
Single Element Size (mm)	40x20x5	30x10x5	15x60x0.8
Substrate Size (mm)	40x80x1	45x120	60x115x0.8

* -6 dB Bandwidth

4.8 Summary

This chapter summarized the differences between SISO, MISO, SIMO and MIMO communication systems. It highlighted the parameters that affect the performance of a MIMO system such as the number of antenna elements and the correlation coefficient. Several techniques for enhancing the isolation between closely spaced antennas on a practical handset have been presented, and some of these techniques will be used within our proposed design models in later chapters.

A comprehensive literature review was presented and a performance comparison table was created for ease of performance benchmarking against our proposed design in later chapters.

CHAPTER 5

THE SHORTED 4-SHAPED ANTENNA DESIGN

This chapter describes the design and modeling of the single antenna element that will be used later in a multi-element MIMO antenna system. The design is based on a miniaturized printed antenna which was chosen due to its low cost, low profile and ease of fabrication. The novel antenna designed is derived and optimized starting from an inverted-F antenna. The proposed antenna is denoted as a shorted 4-shaped antenna.

The single antenna element designed is then used in a 2x1 MIMO antenna system configuration. The Full Wave Finite Element Method (FEM) computer aided design (CAD) tool Ansoft High Frequency Structure Simulator (HFSS) is used to optimize the antenna parameters to meet the required characteristics for LTE. A parameteric investigation of the effect of different geometrical antenna parameters on its performance

is also presented. A total of five models are investigated and simulation and measurement results are provided and discussed.

The models investigated are shown in Fig. 5-1 and have the following names and features :

1. Model A-2-2: A 2-Element model of total size 50x50x0.8 mm^3 which is based on two 4-Shaped antennas separated by a very thin Ground plane as shown in Fig. 5-1(a).
2. Model E1: This 2x1 MIMO antenna model uses a wider Ground plane between the two 4-shaped antenna elements and its total size is 67x50x0.8 mm^3 shown in Fig. 5-1(b)
3. Model D1: This model uses capacitively loaded loops (CLL) between the two 4-shaped antennas to improve the isolation between them as shown in Fig. 5-1 (c). The total size is the same as model E1 i.e. 67x50x0.8 mm^3.
4. Model E1T: This model is similar to model E1 shown in Fig. 5-1(b) but the substrate thickness was doubled, so the size of this model is 67x50x1.56 mm^3.
5. Model D1T: This model is similar to model D1 shown in Fig. 5-1(c) but the substrate thickness was doubled, so the total size of this model is 67x50x1.56 mm^3.

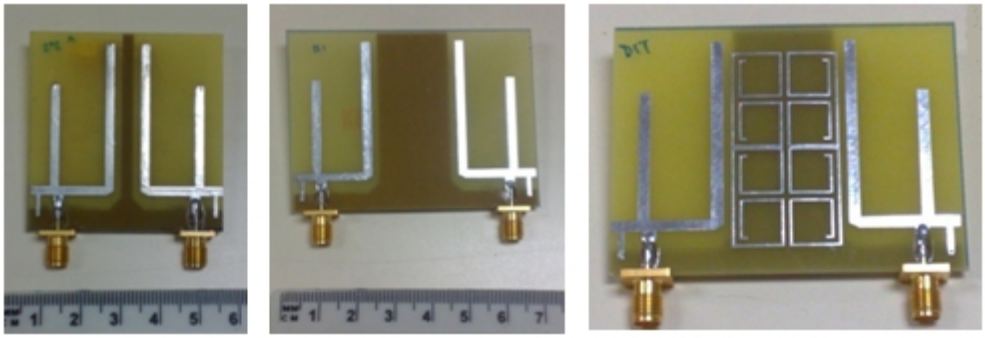

Figure 5-1 The different models investigated (a) Model A, (b) Models E1 and E1T and (c) Models D1 and D1T

5.1 Dual Band Shorted 4-Shaped Antenna Element

A new antenna geometry that has never been investigated in literature before has been modeled as shown in Fig. 5-2. It is a two layer printed antenna based on the inverted-F antenna (IFA). The antenna geometry was altered and optimized for the MIMO antenna application at hand. Since up to 4 of these antenna elements will have to be placed on a substrate of size 50x100mm^2, to get a 2x2 MIMO antenna, the size of the individual antenna element has to fit within 25x50 mm^2. The inductive and capacitive arms for the printed inverted-F antenna add up as the total length of the antenna [71]. However, for the low frequency (750MHz) that is considered, it is necessary to use some techniques to increase the electrical length of the antenna to allow it to resonate at the

desired frequency. This was achieved by using an L-shaped ground plane and bending the IFA along it as shown in the Fig. 5-2.

With 400mm wavelength at 750 MHz, we have ka=0.44 and thus the single antenna element indeed represents an ESA. The maximum gain expected from this ESA as given by equation (1.1) will be about 0.3dB. The geometry of the designed dual band antenna element (called from now on as shorted 4-shaped antenna) is shown in Fig. 5-2.

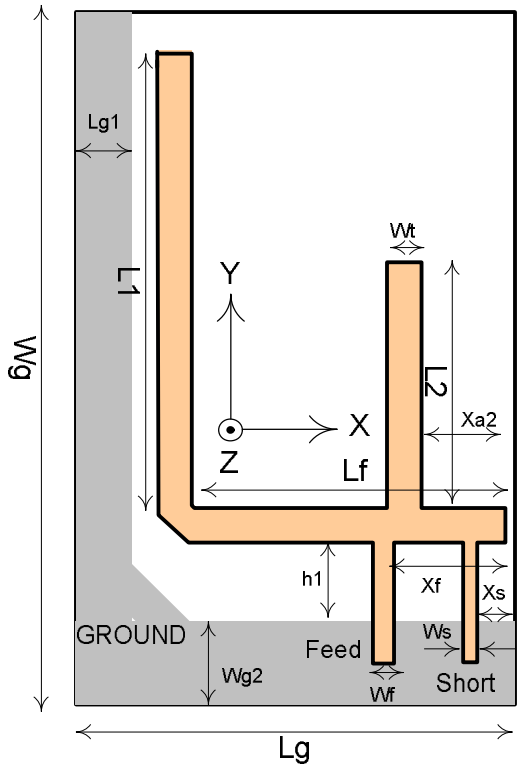

Figure 5-2 The shorted 4-Shaped Antenna Element

The antenna structure consists of an antenna printed on the top layer and a ground plane printed on the bottom layer. The antenna has a number 4-shape (hence the name). The horizontal arm is of length L_f and the vertical arms are of lengths L_1 and L_2. L_1 , L_2 and L_f control the resonant frequencies of the antenna element in the two bands covered. The antenna geometry has been optimized to fit a 25x50x0.8 mm^3 size and operate in the LTE 700 MHz and WLAN 2.4 GHz bands. Table 5.1 shows the values of the different antenna dimensions used for the single element design.

Table 5-1 Single Element Antenna Parameters

Parameter	Value	Parameter	Value
Wg	50 mm	Xs	0 mm
Lg	25 mm	h=h1	2 mm
Lg1	5 mm	Wt	2mm
Wg2	10 mm	D	0.8 mm
L1	35 mm	Lf	16 mm
L2	16 mm	Wf	1.5 mm
Xa2	2 mm	Ws	1.5 mm
Xf	3.5 mm		

The commercially available software Ansoft HFSS is used to model, design and analyze the new proposed antenna. Fig. 5-3 shows the simulated reflection coefficient $|S_{11}|$ for the single element on an FR-4 substrate. The single element resonates at two

center frequencies (770MHz and 2.45GHz) with somewhat small -10dB bandwidth of 11 MHz and -6dB bandwidth of 21 MHz at the lower resonance frequency. The bandwidth of the higher band was around 230 MHz @ -6 dB and 115 MHz @ -10dB reflection coefficient.

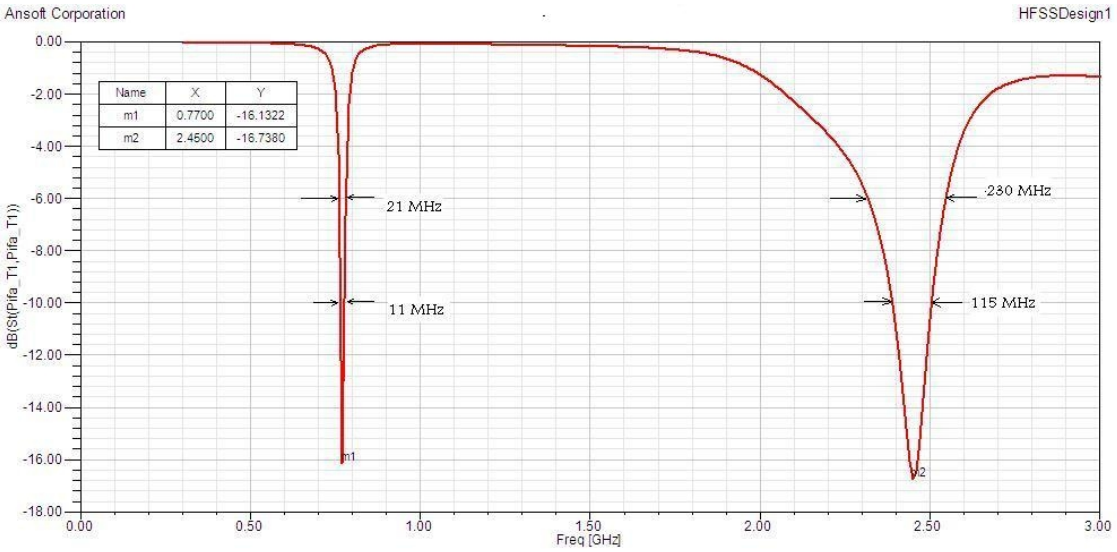

Figure 5-3 Simulated Reflection Coefficient $|S_{11}|$ of the Single Element Antenna

The gain obtained from the simulation was very low (-8dB) at the 700 MHz band as shown in the radiation pattern shown in Fig. 5-4. The gain pattern for the 2.45GHz band is shown in Fig. 5-5. A maximum gain of about 7 dB is shown with radiation pattern maximum normal to the antenna plane. The poor gain at the lower frequency band is due

to the small ground plane used with respect to the frequency of operation. Antenna performances such as gain and bandwidth are reduced when a small size ground plane is used [72]. Also the volume occupied by the antenna is only a small fraction of the sphere of radius ka.

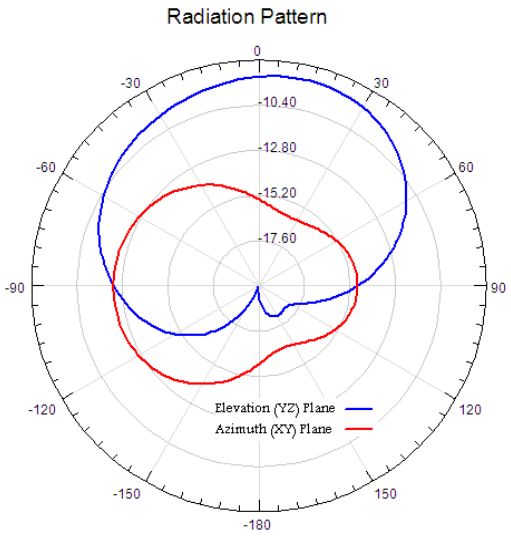

Figure 5-4 Simulated Gain Pattern of Single Element Antenna at 780 MHz

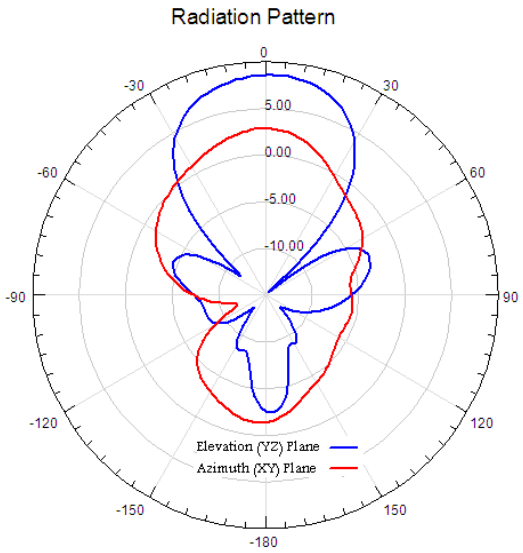

Figure 5-5 Simulated Gain Pattern of Single Element at 2.45 GHz

5.2 2x1 MIMO Antenna using 4-Shaped Element

The 4-shaped antenna element discussed in Section 5.1 is used to construct a 2x1 MIMO antenna as shown in Fig. 5-6. The antenna elements are mirror image of each other and have the same dimensions. The effect of the various parameters of the antenna such as the length of the vertical arms (L_1, L_2) and horizontal portion (L_f), the height above the ground plane (h1,h), the position of the short (X_s) and the position of the feed point (X_f) are investigated in the following sections. Changing the value of any parameter will change it for both the antenna elements.

Table 5.2 shows the values of the geometrical parameters used in the 2x1 MIMO antenna geometry of the dual band 4-shaped antenna in Fig. 5-6.

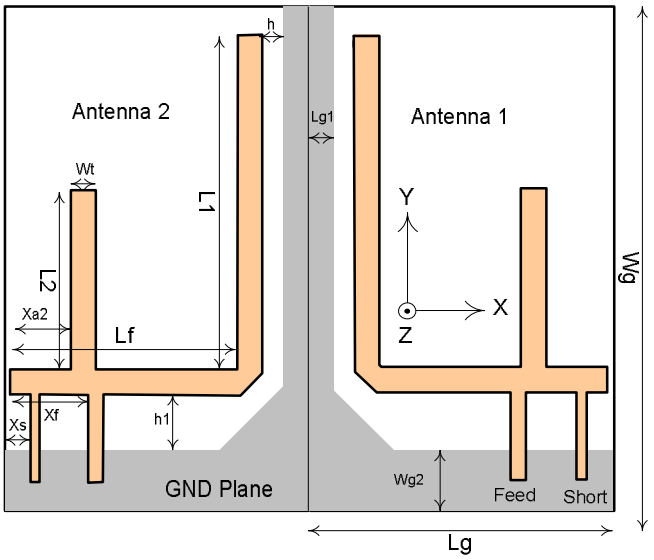

Figure 5-6 2x1 MIMO Antenna based on the 4-shaped Antenna Element

Table 5-2 2x1 MIMO Antenna Parameters (Model D, E)

Parameter	Value	Parameter	Value
Wg	50 mm	Xf	6 mm
Lg	33.5 mm	H	2 mm
Lg1	10 mm	Wt	2.2 mm
Wg2	5 mm	D	1.56 mm
L1	38 mm	Lf	19.5 mm
L2	26 mm	Wf	2.5 mm
Ws	1 mm	Xs	1.5 mm
Xa2	5 mm	h1	3.5 mm

5.2.1 Effect of horizontal portion (L_f)

Fig. 5-7 shows the effect of L_f on the resonance frequency of the dual element antenna. As L_f is increased, the lower and higher resonance frequencies are lowered. As the length L_f is increased from 17.5mm to 20.5mm in 1mm increments, the lower frequency band decreased from about 810 MHz to 770 MHz. The same effect is observed in the higher frequency band, where the center frequency changed from 2.86 GHz to 2.75 GHz. There was little change in the BW, while $|S_{11}|$ got improved.

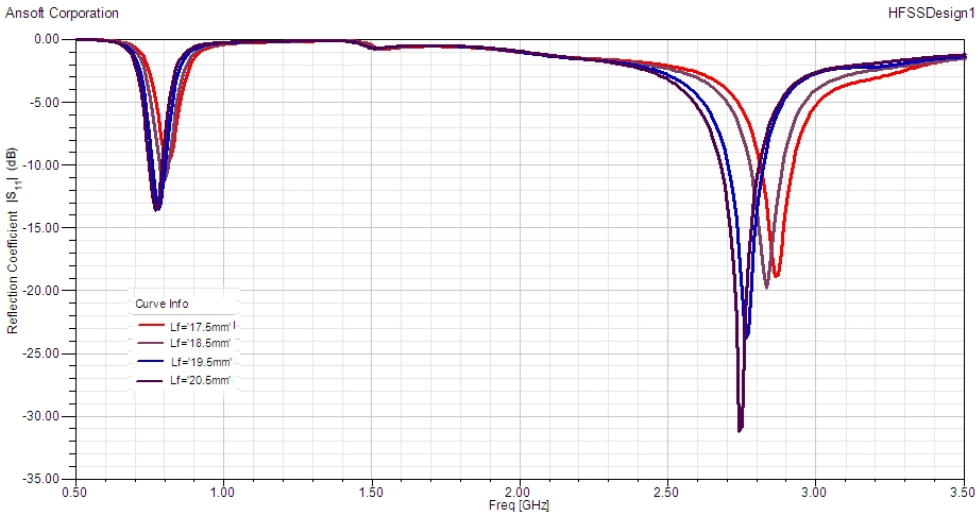

Figure 5-7 Effect of L_f on the reflection coefficient $|S_{11}|$

5.2.2 Effect of vertical Arm 1 (L_1)

Fig. 5-8 shows the effect of L_1 on the resonance frequency of the 2-element antenna. Increasing L_1 decreases the lower and the higher band resonance frequencies. As the length L_1 is increased from 30 mm to 40 mm in 2 mm increments, the lower frequency band decreased from about 860 MHz to 770 MHz. The same effect is observed in the higher frequency band, where the center frequency changed from 3.18 GHz to 2.71 GHz. With increasing L_1, $|S_{11}|$ is improved at the lower frequency band. At the higher band $|S_{11}|$ is improved upto L_1 = 34 mm beyond which $|S_{11}|$ deteriorated. The bandwidth is decreased with increasing L_1, with the effect more pronounced at the higher band.

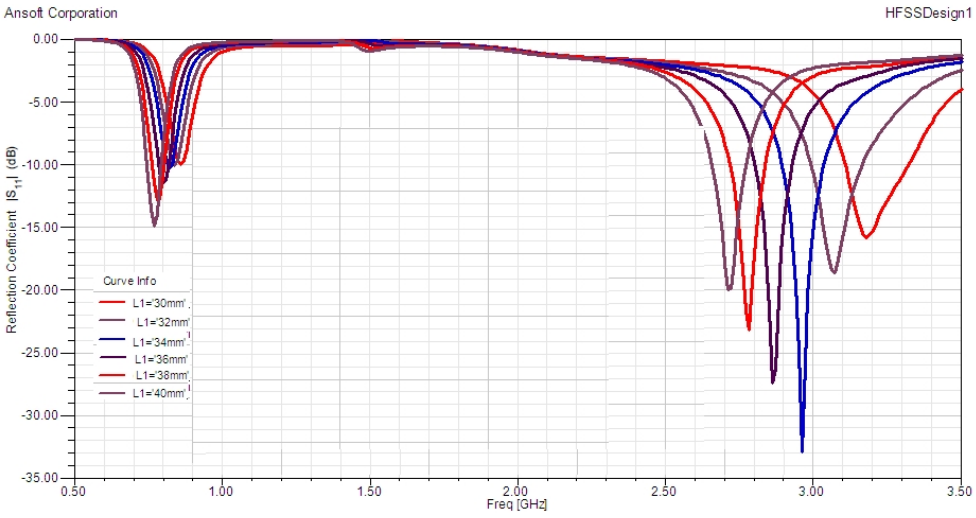

Figure 5-8 Effect of L_1 on the reflection coefficient $|S_{11}|$

5.2.3 Effect of Arm 2 (L_2)

The length of the vertical Arm 2 (L_2) does not affect the resonance frequency or the BW. However, it has an effect on the value of the reflection coefficient as shown in Fig. 5-9. Increasing L_2 improves the value of the reflection coefficient (and thus the impedance matching) at the lower band while deteriorates it at the higher band. Its value has to be chosen to get a balance between the reflection coefficient (amount of impedance matching) at the two bands. Fig. 5-9 shows the $|S_{11}|$ curves when changing the length L_2 from 24 – 32 mm in 4 mm increments.

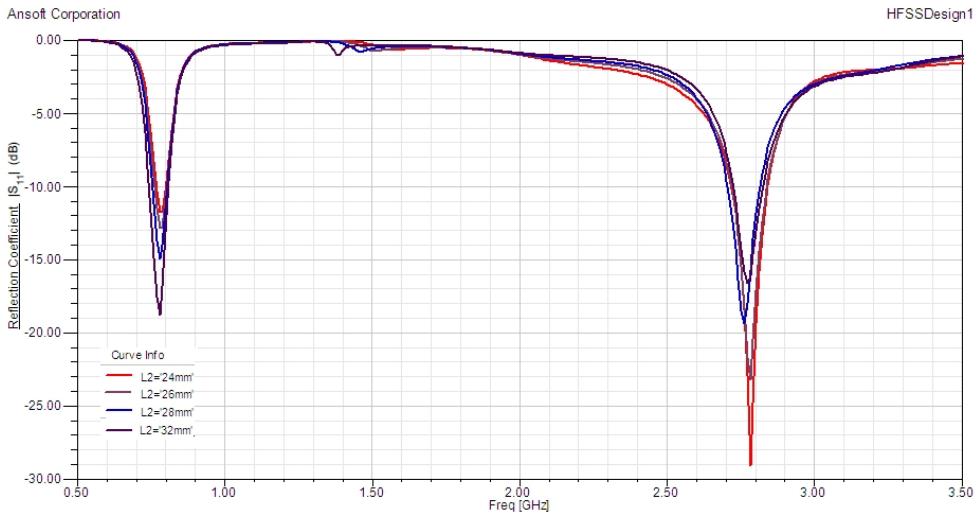

Figure 5-9 Effect of L2 on the reflection coefficient $|S_{11}|$

5.2.4 Effect of separation from the Ground Plane (h,h_1)

As shown in Fig. 5-10, increasing the separation from the ground plane improves the $|S_{11}|$ but also increases the resonant frequency. As the value of h is increased from 0.5 mm to 2.5 mm in steps of 1 mm, the center frequency at the lower band increases from 765 MHz to 825 MHz while the center frequency at the higher band increases from 2.48 GHz to 2.81 GHz. The $|S_{11}|$ changes from -13.5 dB to -17.5 dB at the lower band while from -9 dB to -13 dB at the higher band. For this parametric study, we have made $h=h_1$. In the actual models, we are using different separation (h_1) from the horizontal and (h) from the vertical grounds because we cannot use larger values for h which will not allow enough space for the required length (L_f) of the antenna horizontal portion.

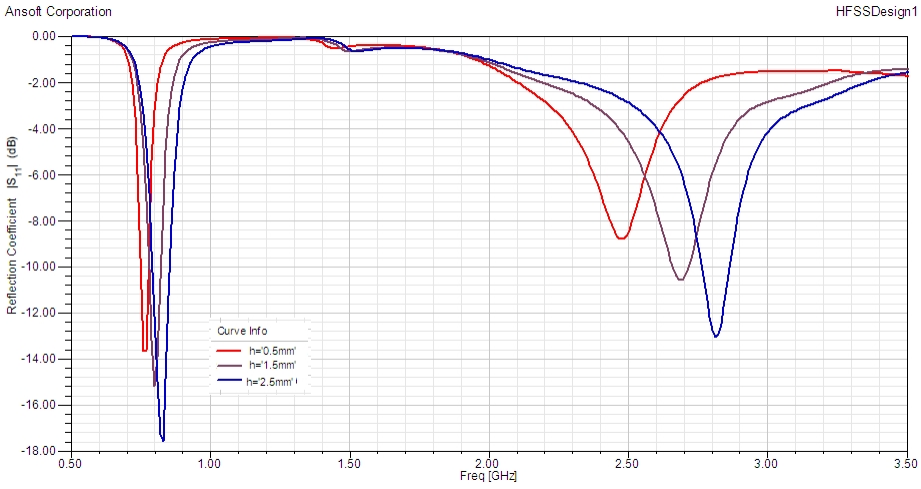

Figure 5-10 Effect of h on the reflection coefficient $|S_{11}|$

5.2.5 Effect of the Short position (X_s)

As shown in Fig. 5-11, the position of the short (X_s) was varied from 1.5 mm to 4.5 mm in steps of 1.5mm. At the lower band, the reflection coefficient is improved as X_s is changed from 1.5 mm to 3mm. However, when X_s is changed to 4.5mm, dual resonance takes place with a higher reflection coefficient. At the higher band, the resonance frequency is reduced slightly with increasing values of X_s.

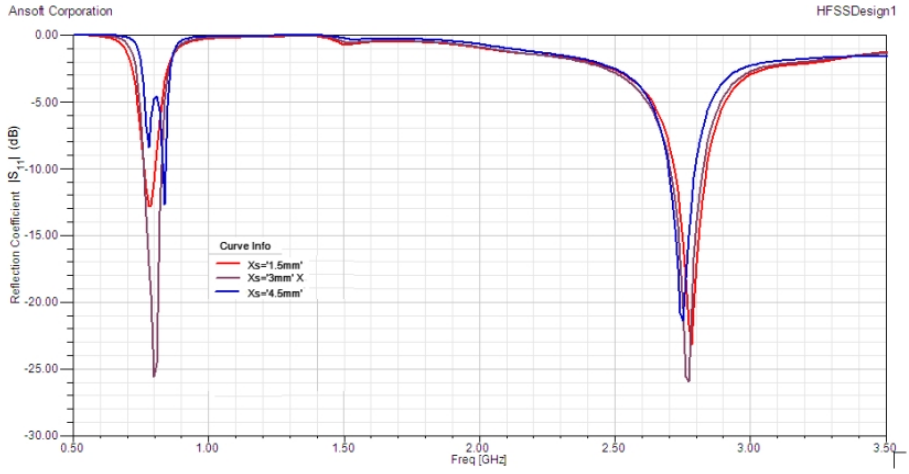

Figure 5-11 Effect of Xs on the reflection coefficient $|S_{11}|$

5.2.6 Effect of the Feed position (X_f)

Fig. 5-12 shows the effect of X_f (and hence the separation between the short and the feed points) on the resonance frequency. As the value of X_f is increased from 4 – 8 mm in 2 mm increments, the lower resonance frequency increases from 770 MHz to 800 MHz

while the higher resonance frequency increases from 2.68 GHz to 2.87 GHz. The reflection coefficient deteriorates as the value of X_f is increased.

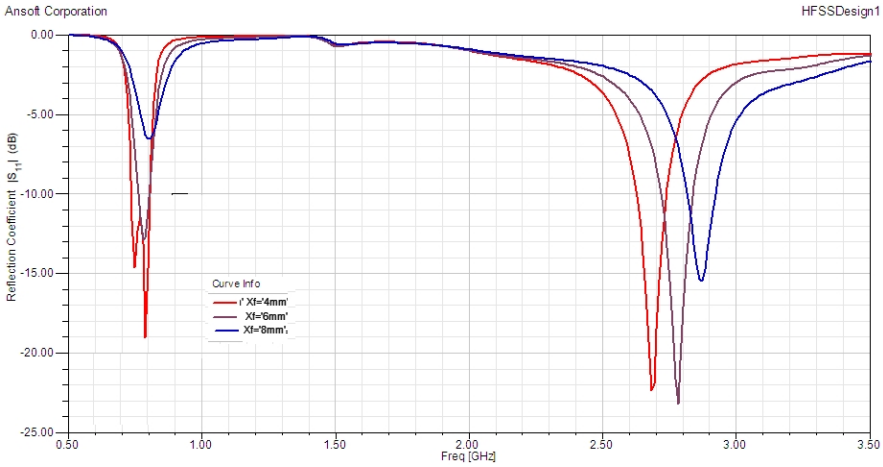

Figure 5-12 Effect of X_f on the reflection coefficient $|S_{11}|$

5.3 Measurement Setup

A vector network analyzer (VNA) as shown in Fig. 5-13 is used to measure the S-parameters of the fabricated antenna models. The frequency sweep used was from 0.5 GHz to 3.5 GHz. MATLAB was extensively used to process the measurement files and plot the S-parameters and calculate the Correlation coefficients $|\rho|_{max}$.

The Lab Volt Antenna Measurement System available in the Microwave and Antenna measurement laboratory at KFUPM was used to obtain the gain/radiation patterns for the fabricated antennas. As shown in Fig. 5-14, this system uses a Yagi antenna as the

transmitting antenna which is connected to an RF generator whose frequency can be tuned by external DC voltage from 700 MHz to 1.2 GHz. The gain/radiation patterns of the antennas could not be investigated at the higher band (2-3GHz) due to unavailability of an RF generator compatible with the Lab Volt setup at this frequency. The comparison or gain substitution method was used to measure the gain of the antennas. This is a simple method which depends on comparing the power received by a reference antenna P_{ref} to the power received by the antenna under test P_{test}. The gain G_{test} of the unknown antenna is given by

$$G_{test} = \frac{P_{test}}{P_{ref}} G_{ref} \qquad 5.1$$

where G_{ref} is the gain of the reference antenna. This can be expressed in dB as

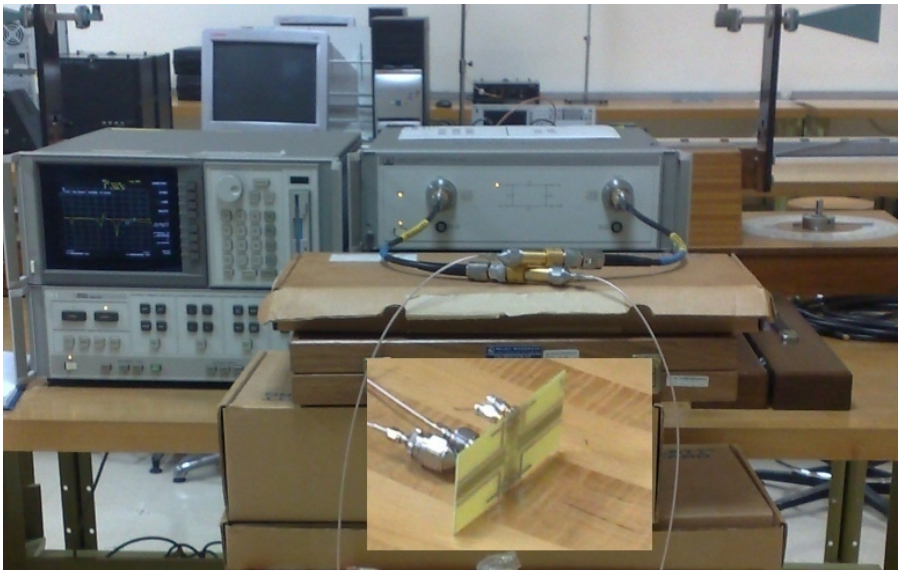

Figure 5-13 Experimental setup for Measuring S-parameters with Network Analyzer

$$G_{test}(dB) = P_{test}(dB) - P_{ref}(dB) + G_{ref}(dB) \qquad 5.2$$

Figure 5-14 Experimental Setup for measuring the gain/radiation pattern

A λ/2 dipole antenna resonating at 915 MHz was used as a reference antenna for the gain measurement and its gain was assumed to be 1.9 dBi (according to the manufacturer specification sheet). For the antennas operating at other frequencies, we plotted only the radiation patterns. The transmitting and receiving antennas were separated by a distance of about 1.7 m. The antenna under test was mounted on the antenna positioner and rotated 360° to obtain the radiation patterns in the principal planes. The power levels versus rotation angles were saved as text files and then the gain substitution method was used with several MATLAB scripts that were created.

5.4 2x1 MIMO Antenna: Model A

This antenna model occupies a volume of 50x50x0.8 mm^3 and the fabricated model is shown in Fig. 5-15. The geometrical dimensions of the model are shown in Table 5-3. Fig. 5-16 to Fig. 5-18 show the Reflection coefficients and isolation for the two antennas in the lower band and the higher band of resonance. As can be seen, both of the antennas show acceptable reflection coefficient at the lower as well as the higher band. A -10 dB reflection coefficient bandwidth of 62 MHz (6.88%) at the lower band (900MHz) and 193 MHz (6.23%) at the higher band (3.1 GHZ) is obtained. However, the measured isolation between the two antenna elements is only -2 dB at the lower band and -3.5 dB at the higher band which is very low and we need to use isolation improvement techniques to enhance the isolation and reduce coupling between the antenna elements. The slight shift in the center frequencies between the simulations and measurements is due to the dielectric constant variation in the fabricated susbtrates.

The measured radiation patterns at 900 MHz are shown in Fig. 5-19 and Fig. 5-20 and show some omni-directional behavior in both the elevation and azimuth planes with some dips close to the ground plane. This is in contrast to the simulations which predict a directional pattern along the z-axis in the elevation plane. This is possibly due to the

environment in which the gain measurement is performed which contains a lot of reflective objects. Due to the unavailability of accurate radiation measurement facilities, the gain patterns could not be measured at the higher band.

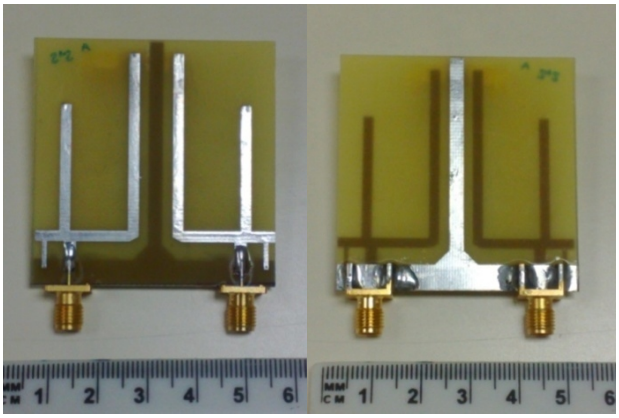

Figure 5-15 Front and back side of fabricated 2x1 antenna model A

Table 5-3 2x1 MIMO Antenna Model A Parameters

Parameter	Value	Parameter	Value
Wg	50 mm	Xf	6 mm
Lg	25 mm	h	2 mm
Lg1	1.5 mm	Wt	2.2 mm
Wg2	5 mm	d	0.8 mm
L1	38 mm	Lf	19.5 mm
L2	26 mm	Wf	2.5 mm
Ws	1 mm	Xs	1.5 mm
Xa2	5 mm	h1	3.5 mm

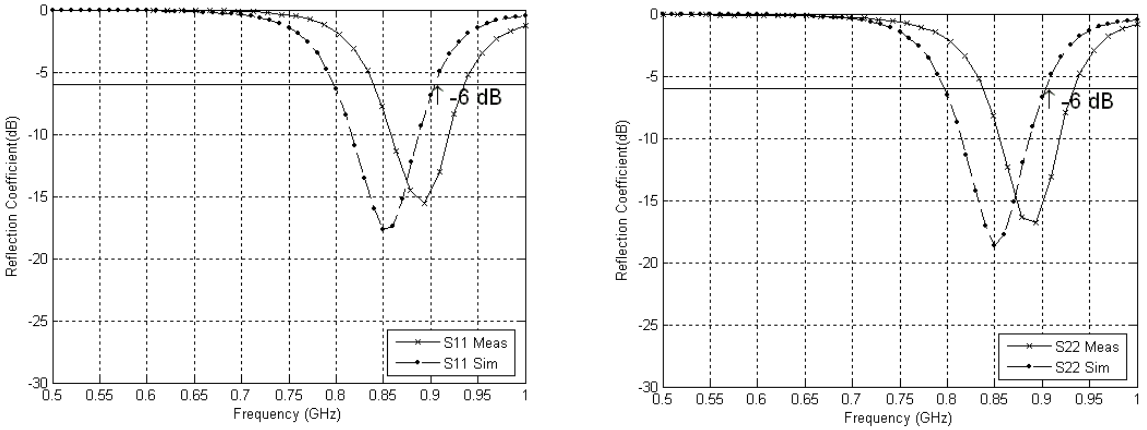

Figure 5-16 Simulated and Measured Reflection Coefficients (S_{11}, S_{22}) at low band

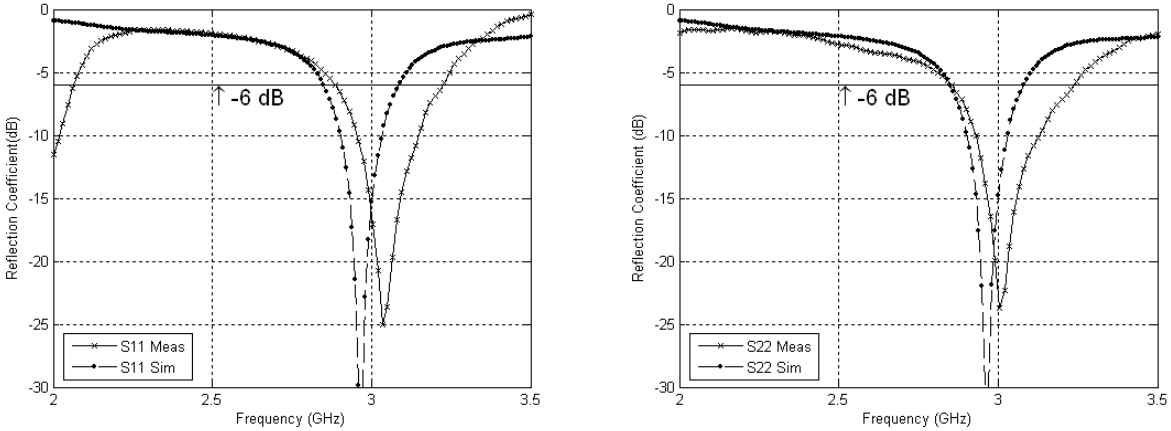

Figure 5-17 Simulated and Measured Reflection Coefficients (S_{11}, S_{22}) at high band

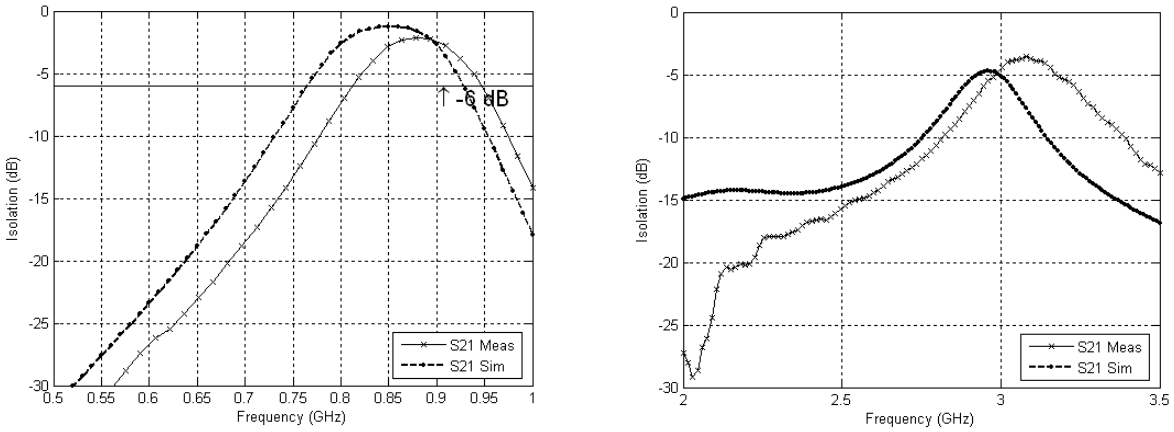

Figure 5-18 Simulated and Measured Isolation at low band and high band

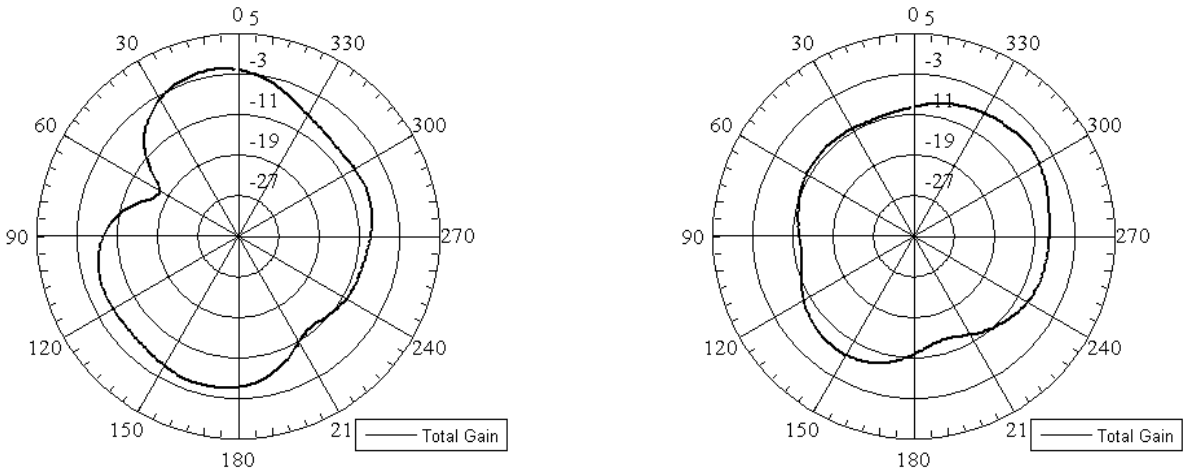

Figure 5-19 Elevation (x-z) plane Gain Pattern of antenna elements 1 and 2 at 900 MHz

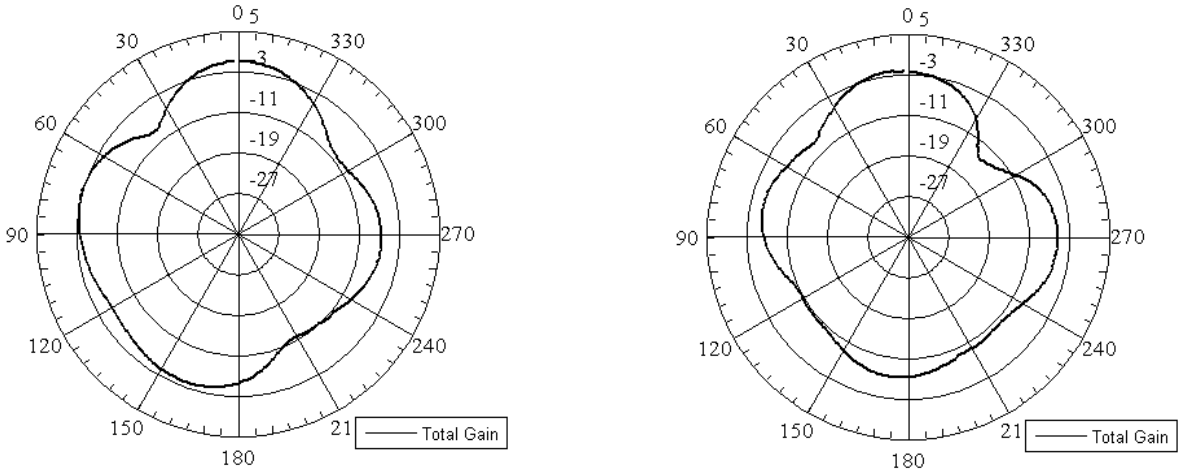

Figure 5-20 Azimuth (x-y) plane Gain pattern of antenna elements 1 and 2 at 900 MHz

5.5 2x1 MIMO Antenna: Model E1

Model E1 is also printed on 0.8 mm thick FR-4 substrate and the fabricated model is shown in Fig. 5-21. As a first attempt to improve the isolation between the two antenna elements, the separation between them has been increased by widening the vertical ground plane between them from 3mm to 20mm. This resulted in a total size of 67x50x0.8 mm^3 for model E1. The simulated and measured reflection coefficients for this model are shown in Fig. 5-22 and Fig. 5-23. The antenna measurements at the lower band did not give results comparable with simulations. The higher band

measured performance is comparable with simulations. The isolation improved to -12.5 dB at the higher band as shown in the isolation curves of Fig. 5-24.

The correlation coefficient is plotted in Figure 5-25 for both the low and the high bands and clearly indicate the poor performance at the lower band. The gain patterns at 900 MHz are shown in figures 5-26 and 5-27. A maximum gain of -3 dB in the elevation plane and -2 dB in the azimuth plane can be observed in the radiation patterns.

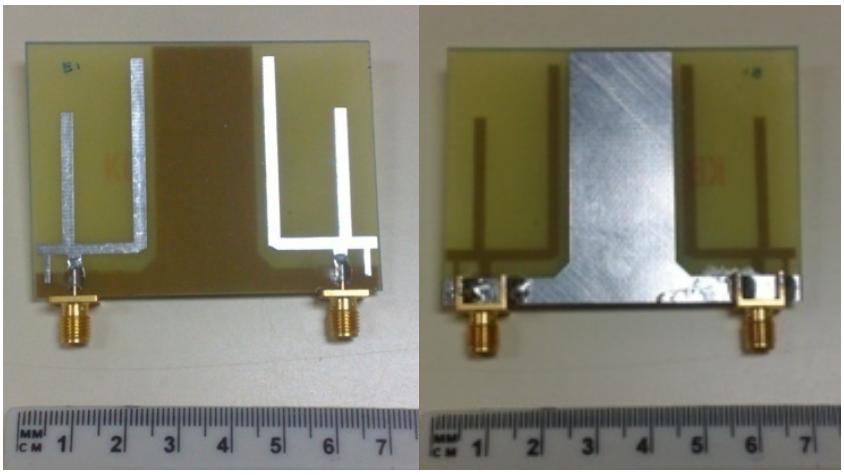

Figure 5-21 Front and back side of fabricated 2x1 antenna model E1

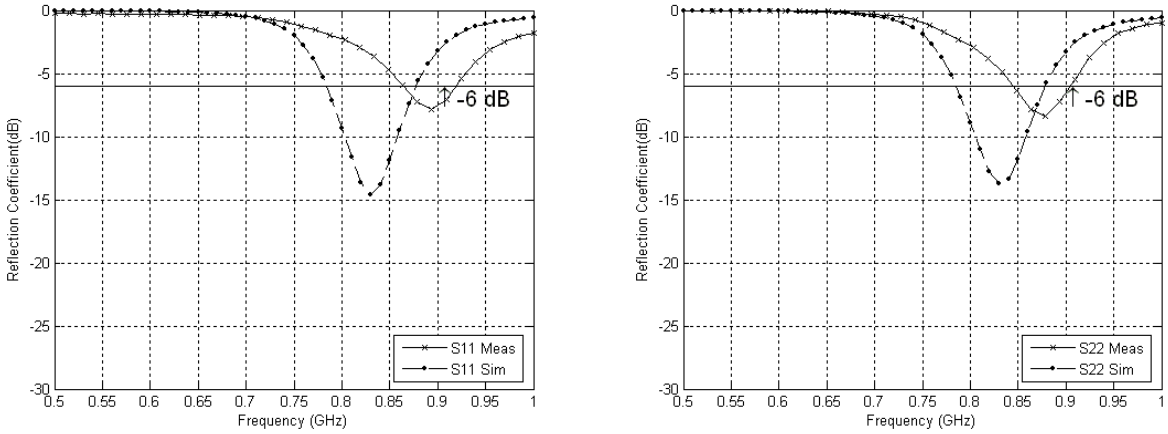

Figure 5-22 Simulated and Measured Reflection Coefficients (S_{11}, S_{22}) at low band

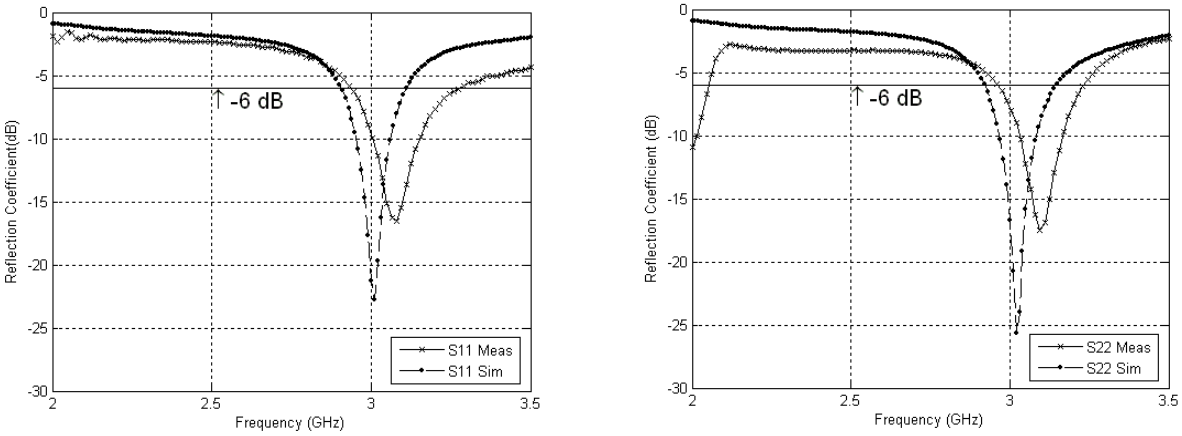

Figure 5-23 Simulated and Measured Reflection Coefficients (S_{11}, S_{22}) at high band

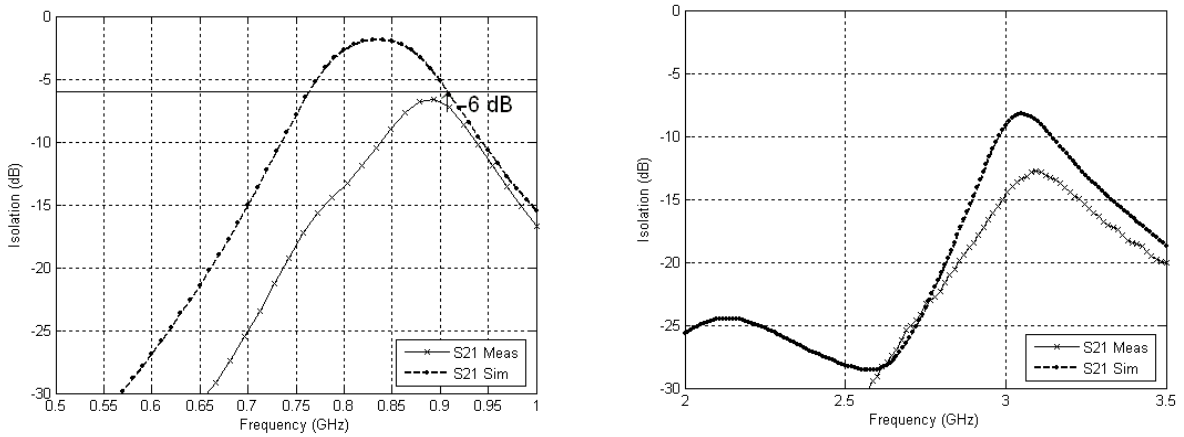

Figure 5-24 Simulated and Measured Isolation between antennas at low band and high band

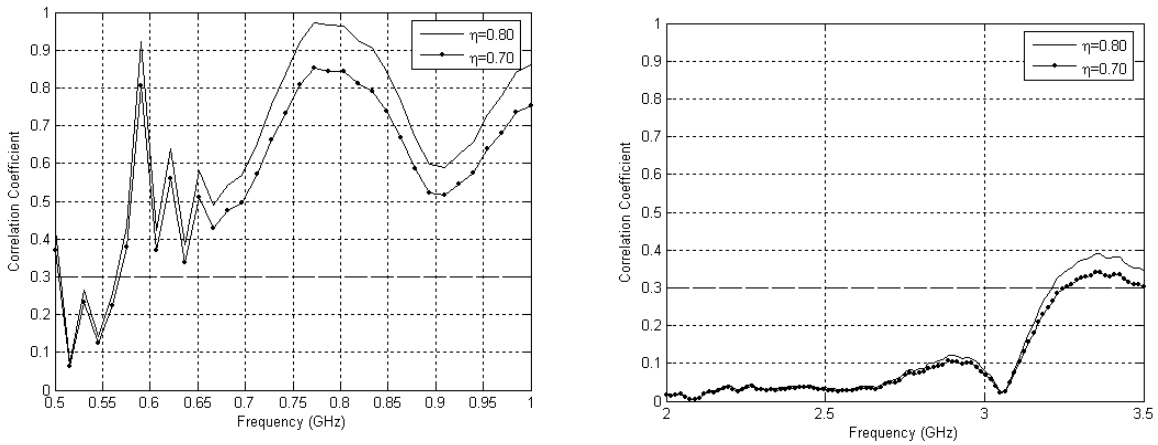

Figure 5-25 Correlation Coefficient of the antenna system at 70% and 80% efficiency

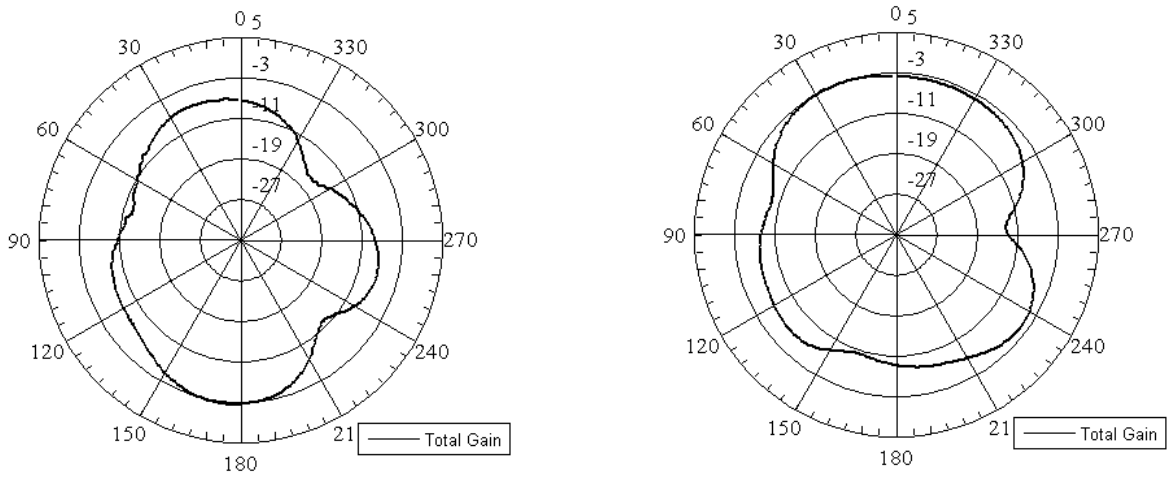

Figure 5-26 Elevation (x-z) plane Gain Pattern of Antenna elements 1 and 2 at 900 MHz

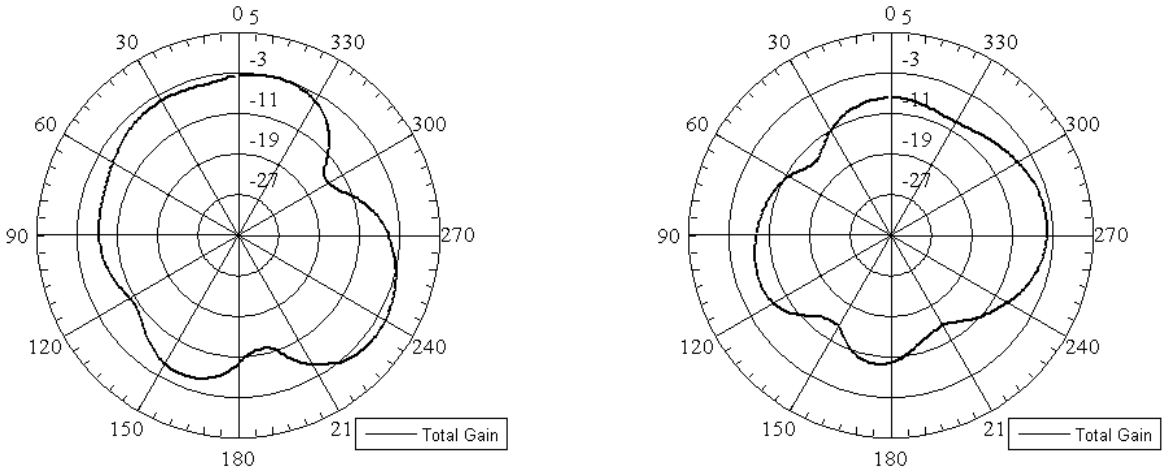

Figure 5-27 Azimuth (x-y) plane Gain pattern of antenna elements 1 and 2 at 900 MHz

5.6 2x1 MIMO Antenna: Model D1

Model D1 uses capacitively loaded loops (CLL) between the two antennas for improving the isolation as shown in the fabricated model photograph in Fig 5-28. A single CLL measures 10x20 mm^2. These loops act as resonant structures providing additional resonances and prevent energy coupling from one antenna to the other. However, this structure has an adverse effect on the efficiency of the antenna, especially at the lower band. The reflection coefficient for the antennas at lower and higher bands are shown in Fig. 5-29 and Fig. 5-30 respectively and show that, compared with model E1, the loops improve the reflection coefficient at the lower band. Although the BW is very narrow at 750 MHz, another wider band appears between 850-930 MHz. The isolation curves in Fig. 5-31 show values of -17 dB and -10 dB at 750 MHz and 900 MHz, respectively. The correlation coefficients in Fig. 5-32 show that this antenna satisfies the 0.3 requirement with good margin. The gain patterns at 900 MHz are shown in figures 5-33 and 5-34. A maximum gain of -4 dB in the elevation plane and -2 dB in the azimuth plane can be observed in the radiation patterns.

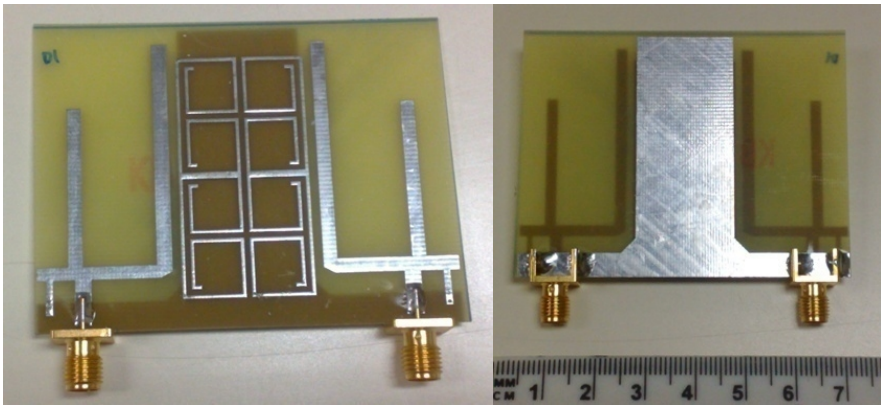

Figure 5-28 Front and back view of fabricated 2x1 antenna model D1

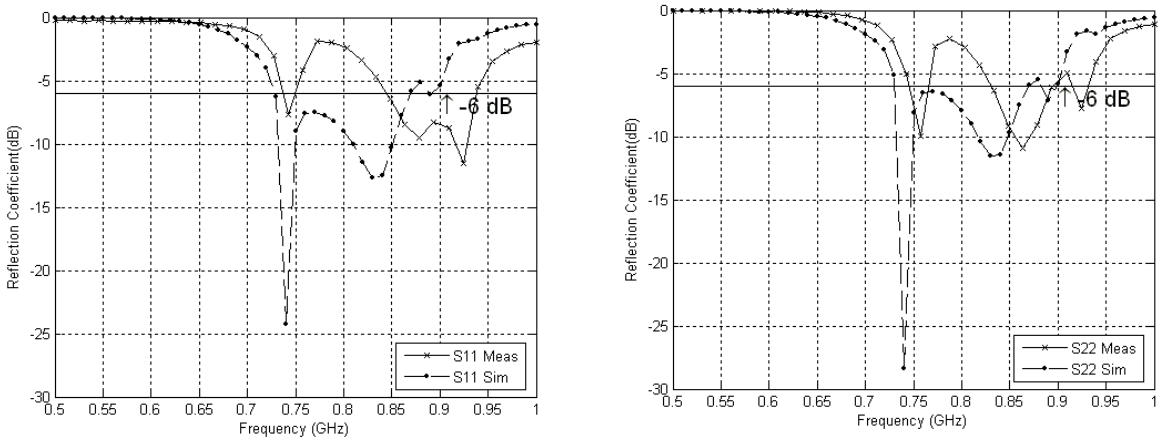

Figure 5-29 Simulated and Measured Reflection Coefficients (S_{11}, S_{22}) at low band

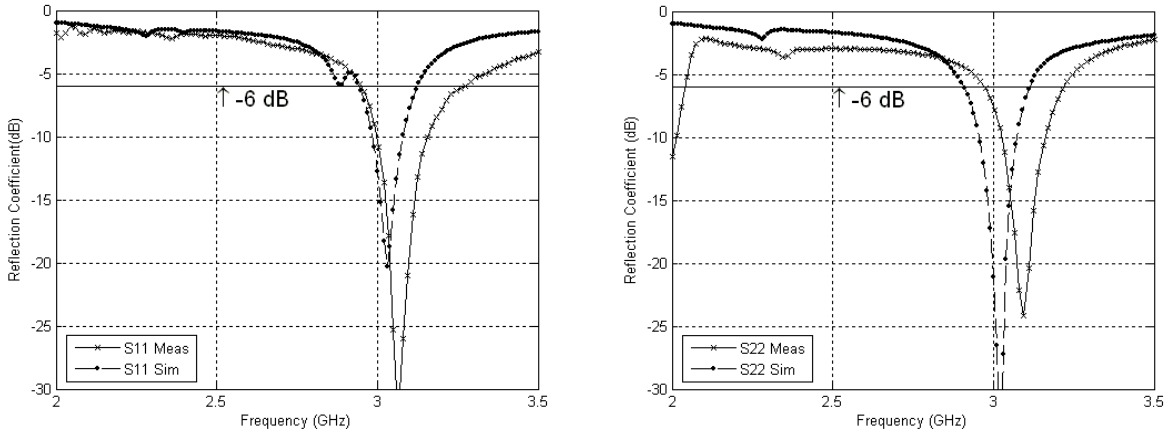

Figure 5-30 Simulated and Measured Reflection Coefficients (S_{11}, S_{22}) at high band

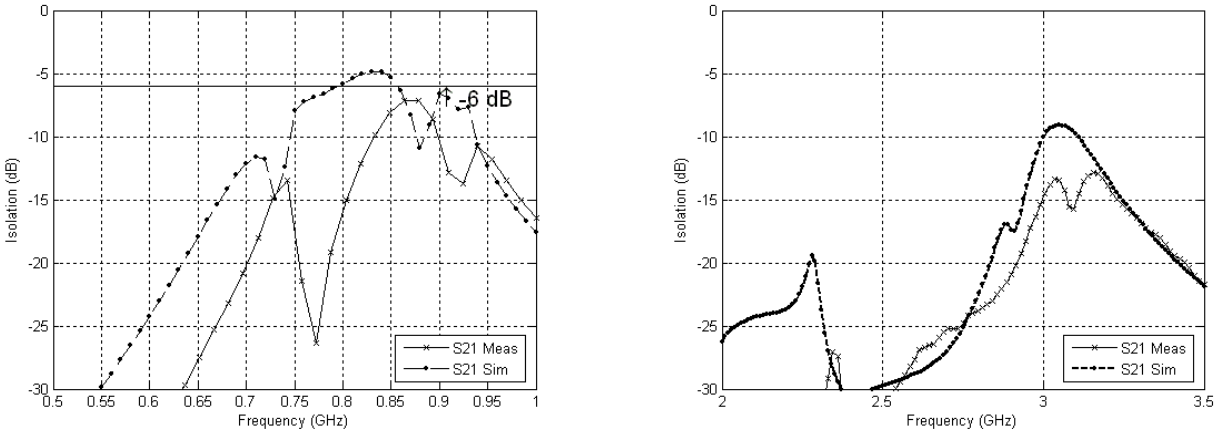

Figure 5-31 Simulated and Measured Isolation between antennas at low band and high band

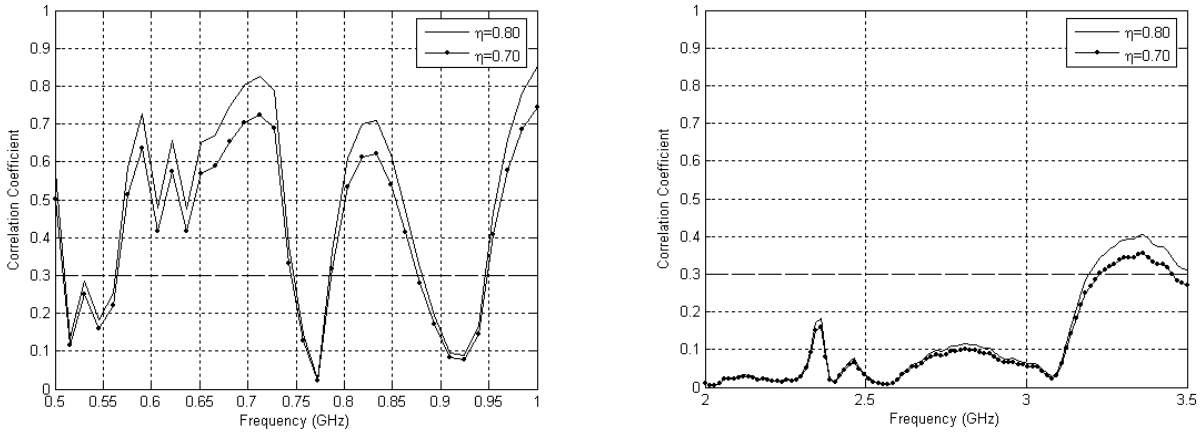

Figure 5-32 Correlation Coefficient for the antenna system at 70% and 80 % efficiency

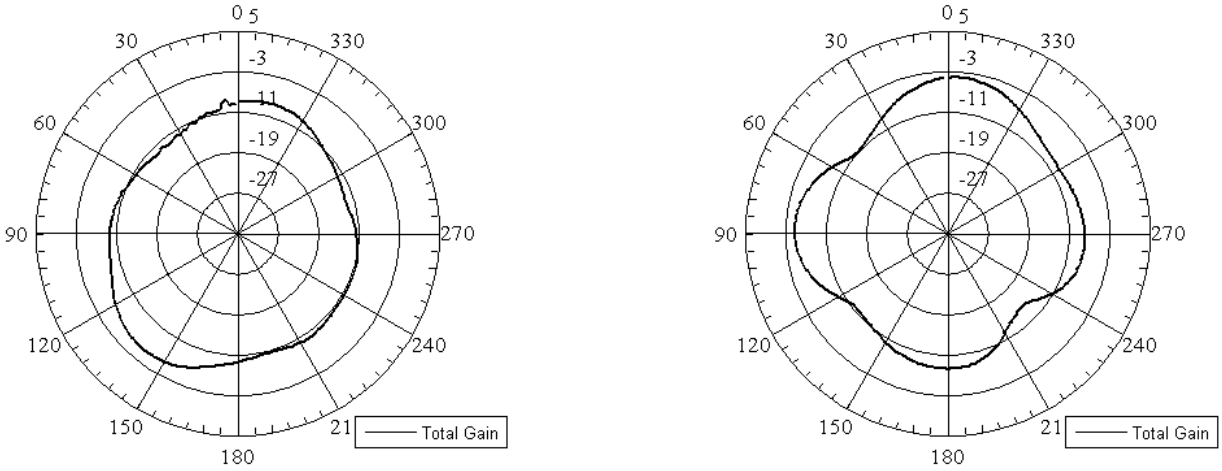

Figure 5-33 Elevation (x-z) plane Gain Pattern of Antenna elements 1 and 2 at 900 MHz

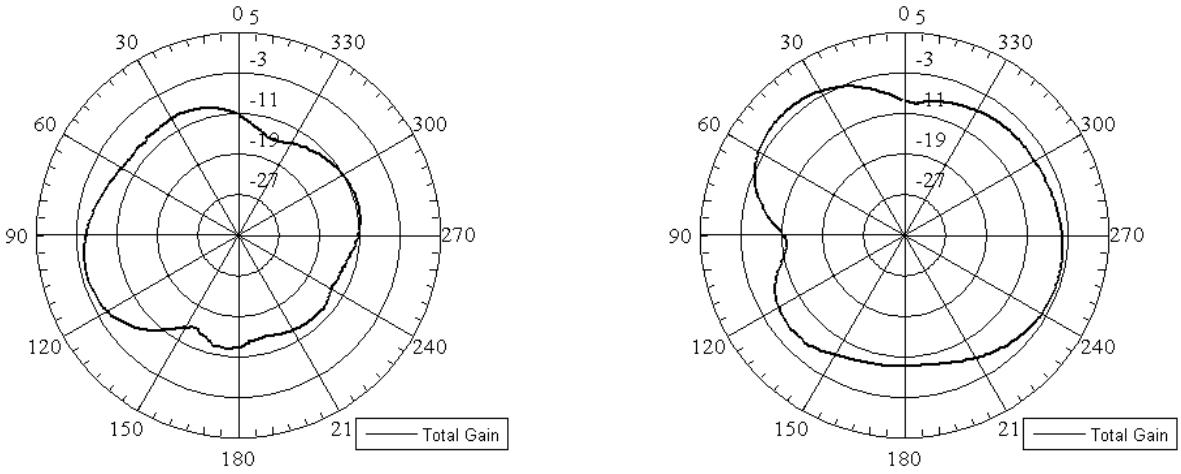

Figure 5-34 Azimuth (x-y) plane Gain pattern of antenna elements 1 and 2 at 900 MHz

5.7 2x1 MIMO Antenna: Model E1T

The fabricated Model E1T shown in Fig. 5-35 is the same as model E1 but the substrate thickness has been increased from 0.8 mm to 1.56 mm. This has the effect of reducing the resonance frequency as shown in the reflection coefficient plots shown in Fig. 5-36 and Fig. 5-37 for the low and high frequency bands, respectively. The -6 dB BW with a center frequency of 815 MHz was about 60 MHz while in the high band centered at 2.75 GHz, it was about 200 MHz. As shown in Fig. 5-38, the isolation remained the same with a value of about -6.5 dB at the lower band while it is deteriorated

at the high band to about -11 dB from -13 dB for model E1. The correlation coefficient remained less than 0.7 at the low band and less than 0.3 at the high band as shown in Fig. 5-39. The gain patterns are shown in Figs. 5-40 and 5-41 for the elevation and azimuth planes, respectively. The maximum measured gain was about -4 dB in elevation and -5 dB in azimuth.

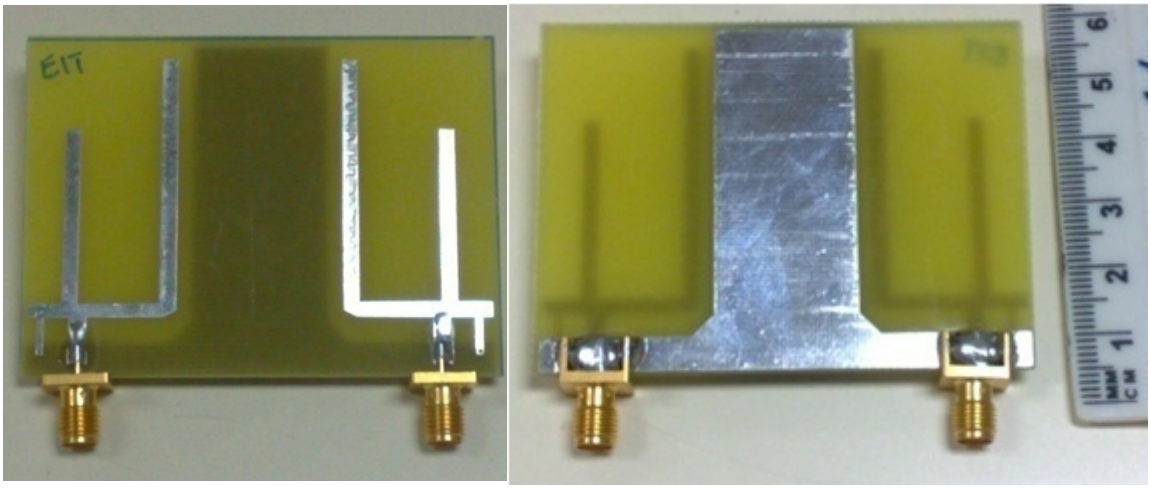

Figure 5-35 Front and back view of fabricated 2x1 antenna model E1T

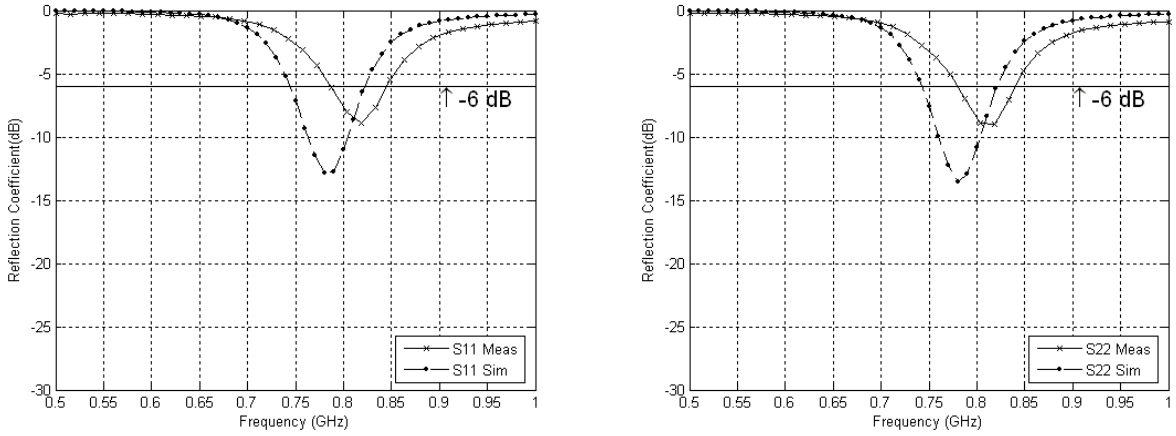

Figure 5-36 Simulated and Measured Reflection Coefficients (S_{11}, S_{22}) at low band

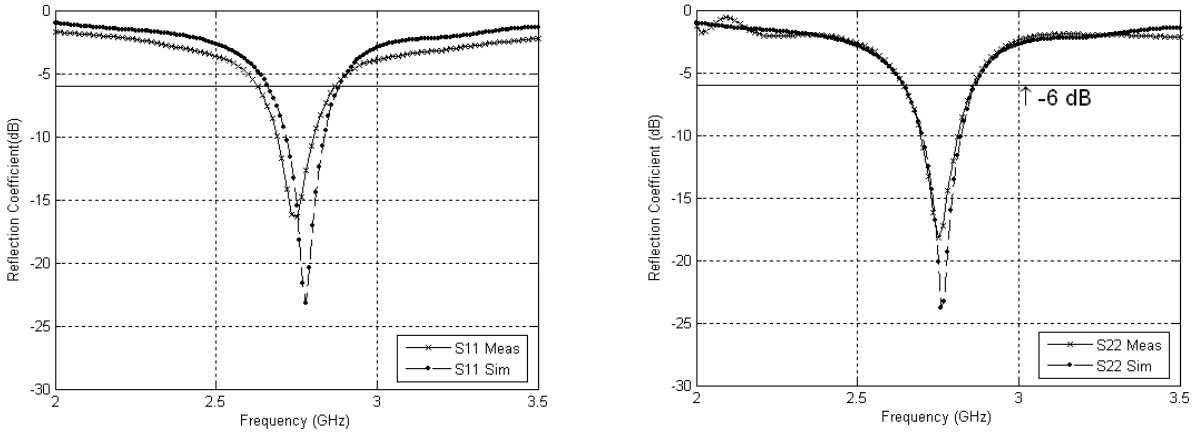

Figure 5-37 Simulated and Measured Reflection Coefficients (S_{11}, S_{22}) at high band

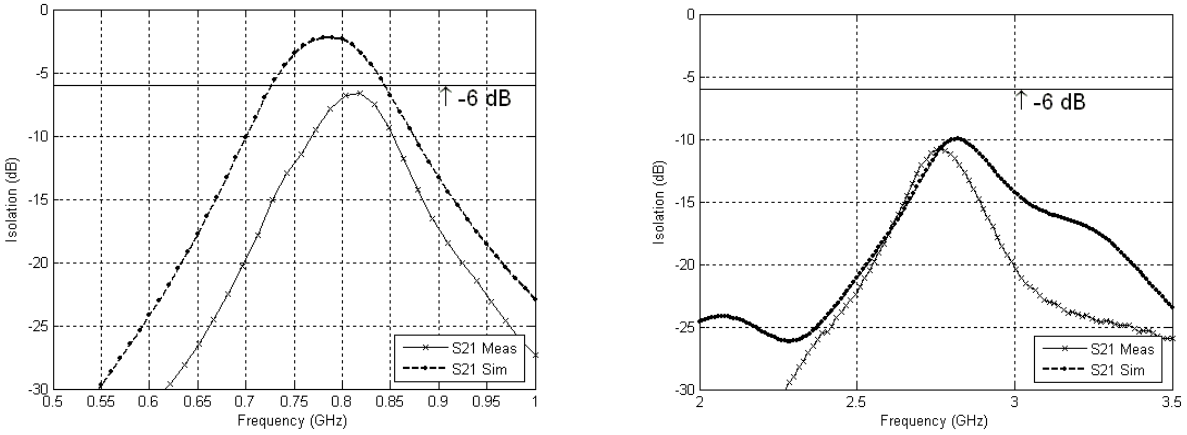

Figure 5-38 Simulated and Measured Isolation between the antennas at low and high band

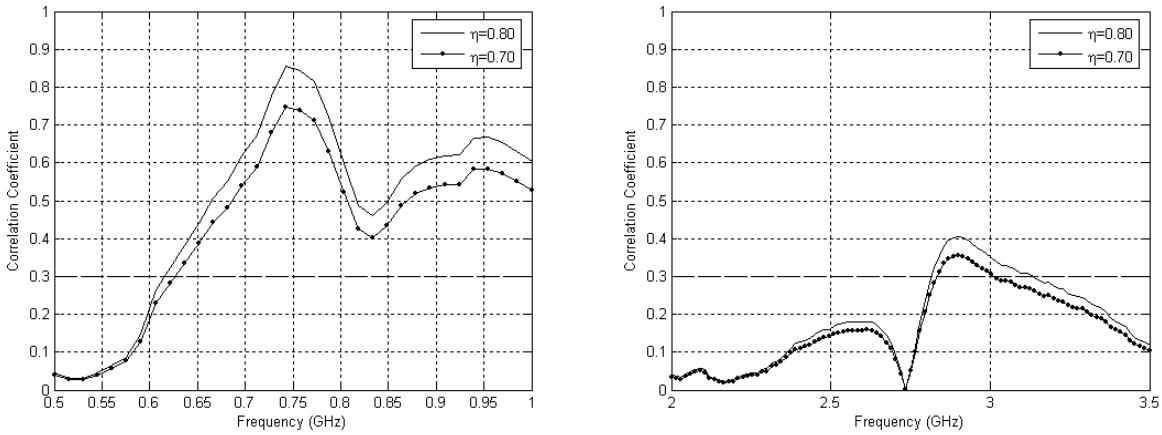

Figure 5-39 Correlation coefficient at low band and high band for 70% and 80 % efficiency

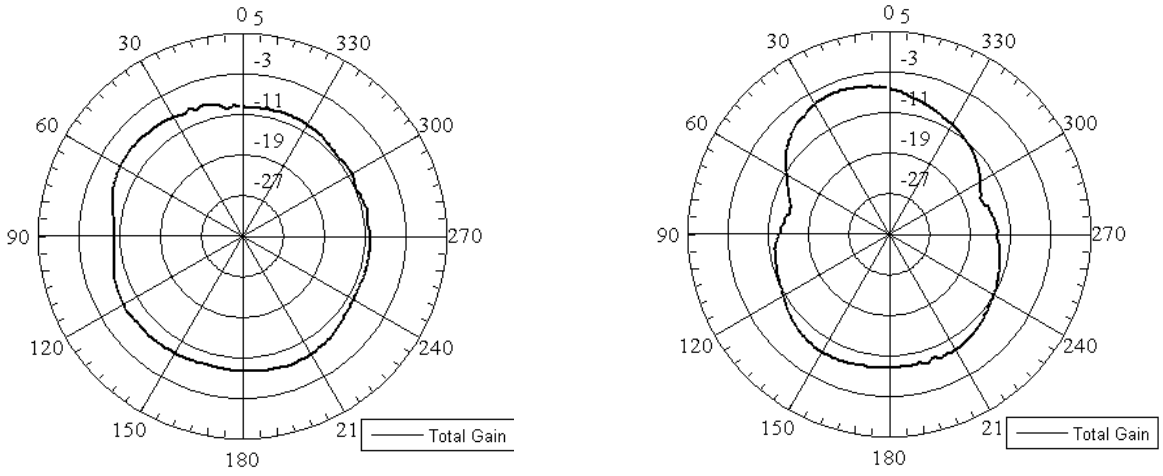

Figure 5-40 Elevation (x-z) plane Gain Pattern of Antenna elements 1 and 2 at 800 MHz

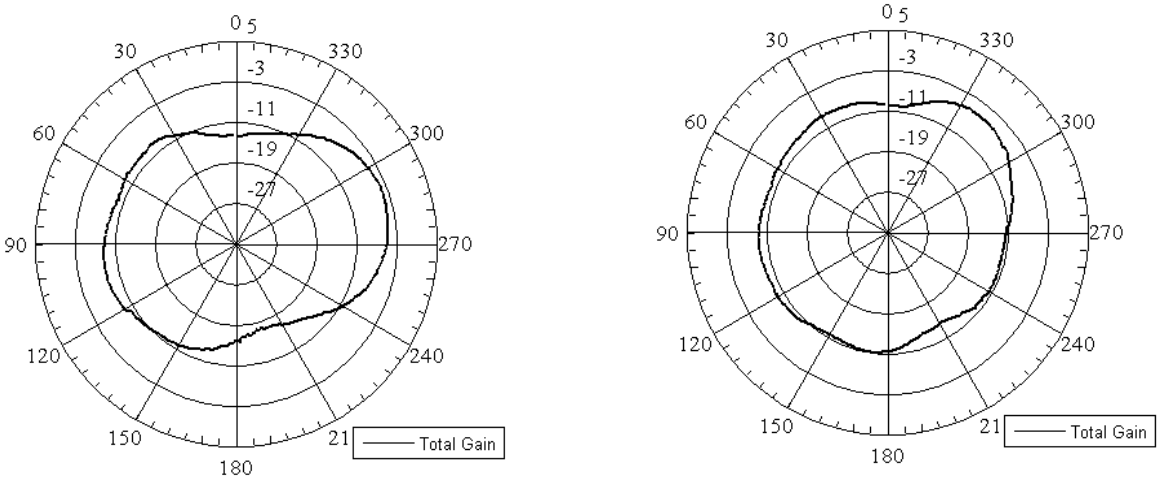

Figure 5-41 Azimuth (x-y) plane Gain pattern of antenna elements 1 and 2 at 800 MHz

5.8 2x1 MIMO Antenna: Model D1T

Model D1T is the same as model D1 but the substrate thickness has been increased from 0.8 mm to 1.56 mm. The fabricated model is shown in Fig. 5-42. Increasing substrate thickness has the effect of reducing the resonance frequency as well as improving the impedance matching as shown in the reflection coefficient plots shown in Fig. 5-43 and Fig. 5-44 for the low band and high band respectively. Dual resonance is observed at the low band with center frequencies of 750 MHz and 850 MHz. The -6 dB BW at these two resonance frequencies is 50 MHz and 60 MHz while the -10 dB BW is 25 MHz and 35 MHz, respectively.

The isolation is slightly improved at the lower band while it remains the same at the higher band compared to model D1 as shown in Fig. 5-45. The correlation Coefficient curves are shown in Fig. 5-46 for the low and high frequency bands. It is evident that this design will satisfy the LTE requirements with a good margin. The gain patterns are shown in Fig. 5-47 for the elevation plane and Fig. 5-48 for the azimuth plane with a maximum gain of -4 dB and -5 dB respectively.

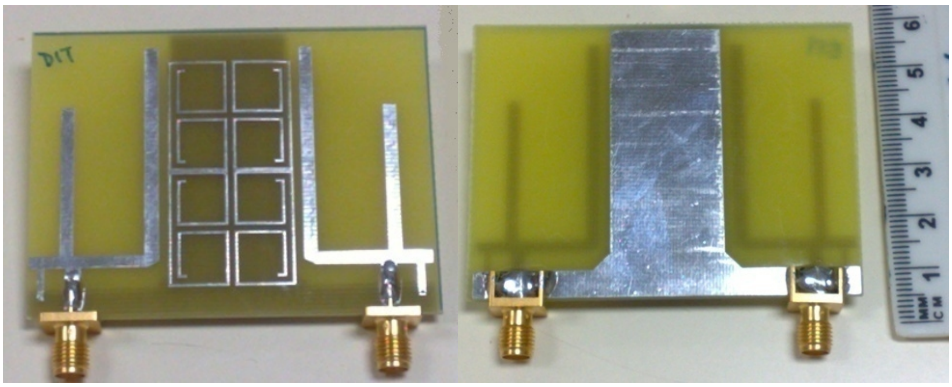

Figure 5-42 Front and back view of fabricated antenna model D1T

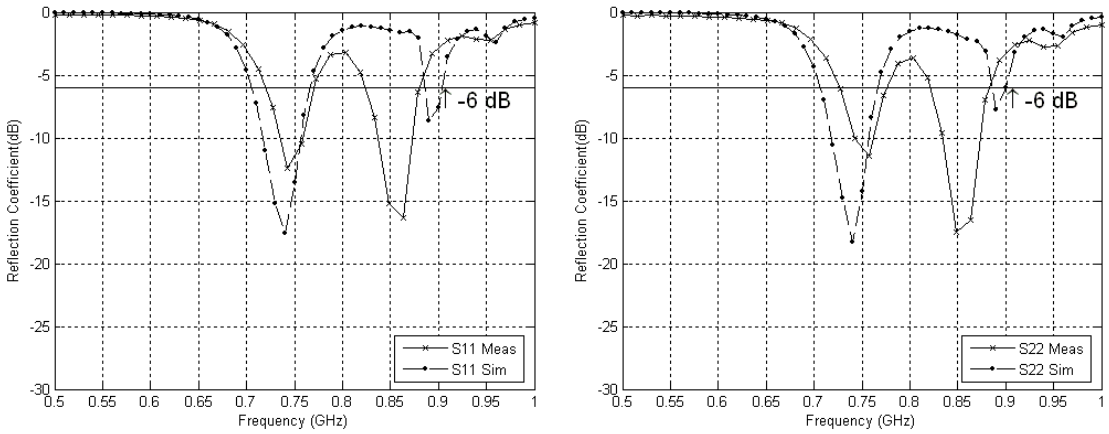

Figure 5-43 Simulated and Measured Reflection Coefficients (S_{11}, S_{22}) at low band

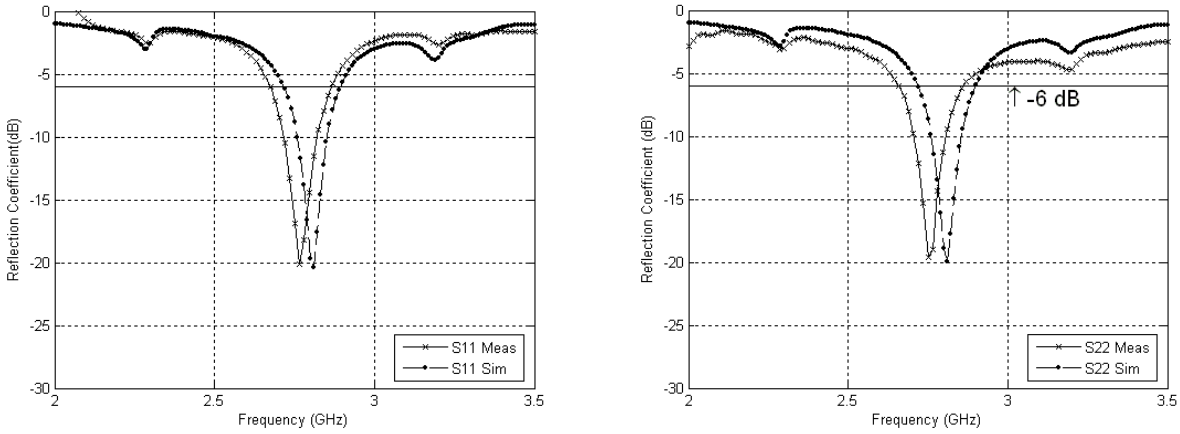

Figure 5-44 Simulated and Measured Reflection Coefficients (S_{11}, S_{22}) at high band

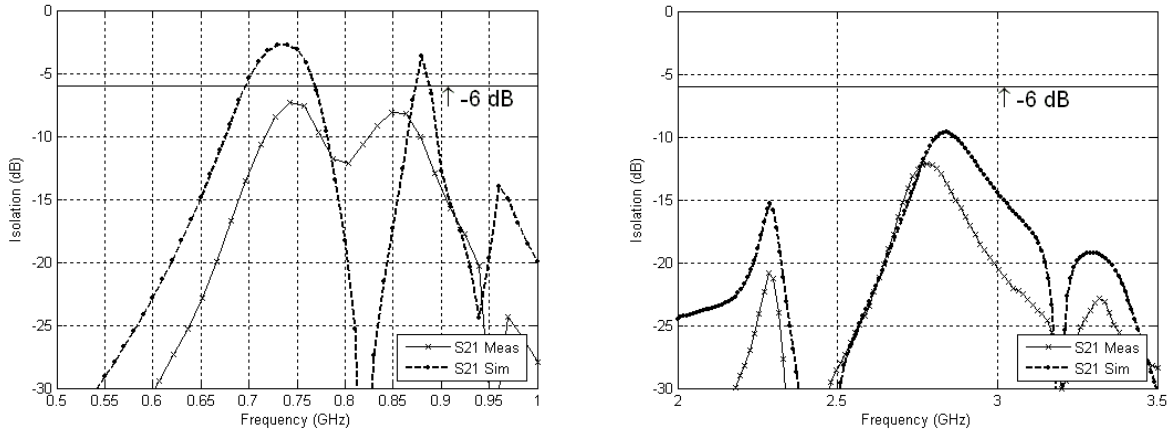

Figure 5-45 Simulated and Measured Isolation at low and high band

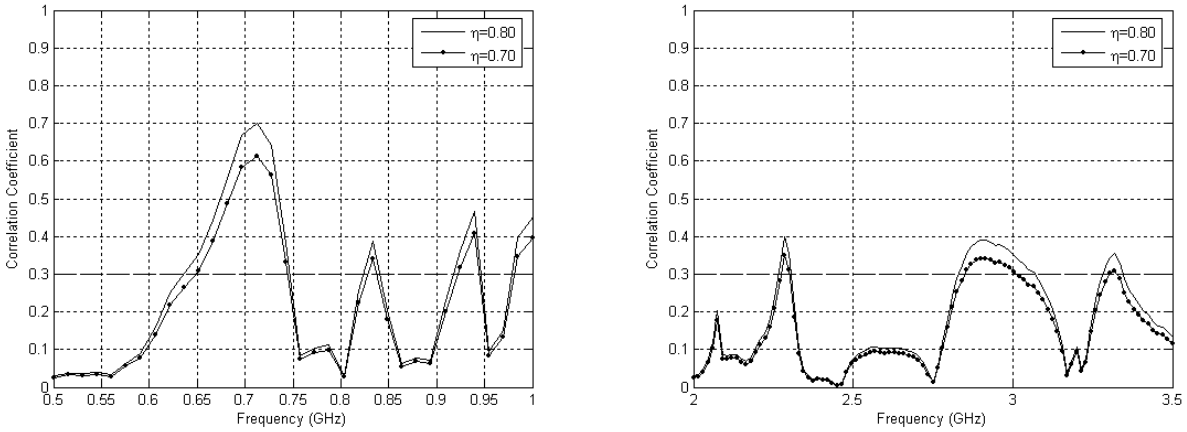

Figure 5-46 Correlation Coefficient for the antenna system at 70% and 80 % efficiency

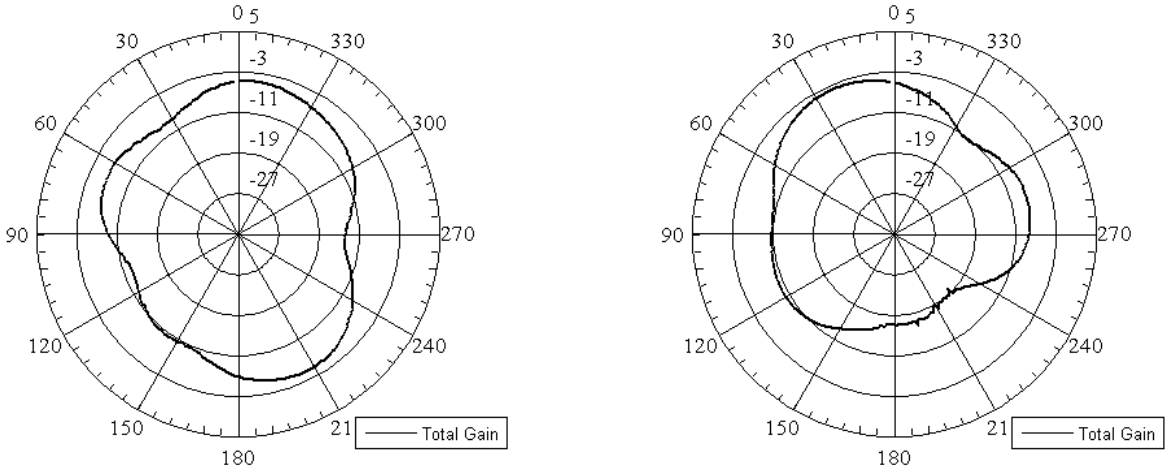

Figure 5-47 Elevation (x-z) plane Gain Pattern of Antenna elements 1 and 2 at 850 MHz

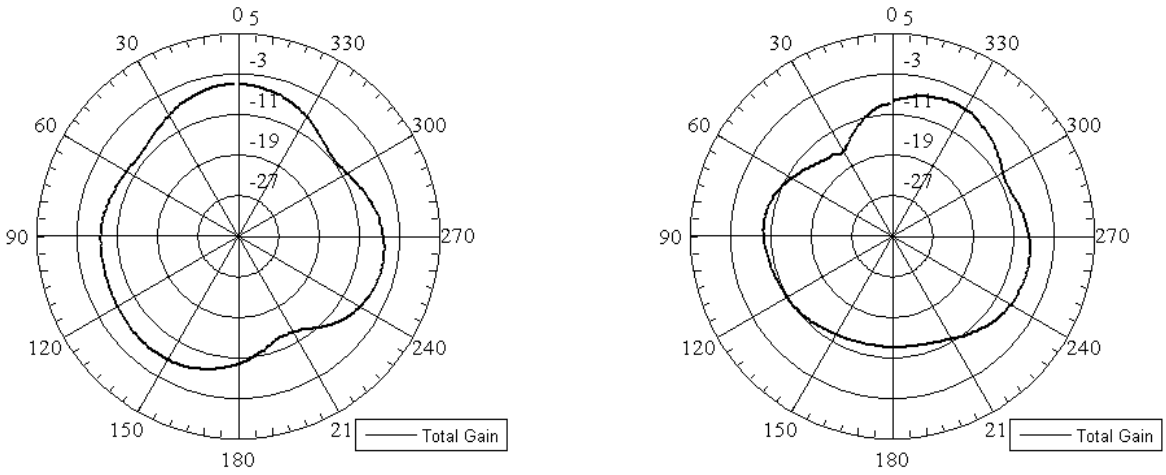

Figure 5-48 Azimuth (x-y) plane Gain pattern of antenna elements 1 and 2 at 850 MHz

Table 5-4 summarizes the measurement results for all fabricated MIMO antenna systems. While Model D1T shows better reflection coefficient and isolation performance, model E1T has much better efficiency with a compromise of -2 dB lower isolation.

Table 5-4 : Measurement Results for all the 2-Element Models

Model / Parameter	Band	Antenna Element	BW (-6dB)	BW (-10dB)	S_{xx}	S_{21}	f1 (-6dB)	f2 (-6dB)
Model A	Low	1	95	62	-15	-2	840	935
		2	96	64	-16		837	933
	High	1	340	193	-25	-3.5	2885	3225
		2	386	201	-23		2853	3239
Model D1	Low	1	93	12	-11	-7	845	938
		2	65	15	-11		830	895
	High	1	324	157	-30	-12	2950	3274
		2	248	136	-24		2972	3220
Model E1	Low	1	54	0	-8	-6.5	865	919
		2	59	0	-8		845	904
	High	1	345	147	-16	-12.5	2936	3281
		2	271	136	-17		2962	3233
Model D1T	Low	1	52	24	-12	-7.5	719	771
		2	50	20	-12		727	777
	High	1	191	104	-20	-12	2675	2866
		2	200	100	-19		2660	2860
Model E1T	Low	1	59	0	-9	-6.5	786	845
		2	60	0	-9		780	840
	High	1	239	112	-16	-10.5	2630	2869
		2	216	115	-18		2642	2858

Table 5-4 : Measurement Results for all the 2-Element Models (continued from previous page)

Model / Parameter	Band	Antenna Element	f1 (-10dB)	f2 (-10dB)	Efficiency (Simulation)	Max Gain (Measured)
Model A	Low	1	858	920	41.5	-1 dB
		2	854	918		
	High	1	2955	3148	69.9	
		2	2929	3130		
Model D1	Low	1	916	928	16.5	-2 dB
		2	856	871		
	High	1	2998	3155	61.4	
		2	3026	3162		
Model E1	Low	1	-	-	64.4	-2 dB
		2	-	-		
	High	1	3006	3153	77.9	
		2	3031	3167		
Model D1T	Low	1	735	759	4.9	-4 dB
		2	742	762		
	High	1	2717	2821	69.3	
		2	2705	2805		
Model E1T	Low	1	-	-	63.1	-4 dB
		2	-	-		
	High	1	2690	2802	77.3	
		2	2696	2811		

Table 5-5 shows a comparison between the measurement results of the 2x1 4-shaped MIMO antenna models D1T and E1T compared to the latest models that appeared in literature. It is evident that our models are among the few that cover a low band 700/800 MHz and a high band 2600/2800 MHz. Also our antenna systems occupy at least 35% less area compared to most models except [41, 64], providing comparable -6dB BW at the lower band of 700/800 MHz with a maximum gain of about -4 dB. The gain values are in line with those in [64, 65]. The lower size came at the expense of reduced isolation. Compared to [64], our design provides a planar compact structure instead of a 3D structure and thus it provides better integration capabilities and lower fabrication costs.

Table 5-5 Comparison with Related Work in 700 MHz band

Parameter/ Reference	Frequency band (MHz)	Single/ Multiband	Isolation (dB)	-10 dB BW (MHz)	Gain (dBi)	Single Element Size (mm)	Substrate Size (mm)
[41]	760 – 886	Single	-15	146	2.2	40x25 x1.56	40x50 x1.56
[46]	705-720	Single	-25	15	2.4	22x50	50x110 x1
[48]	755-787	Single	-15	32*	<0	48x12 x6	48x108 x0.8
[61]	746-796	Single	-10	100*	<0	38x9.5 x1	50x120 x1
[64]	735-810 GPS/PCS/ UMTS	Multiband	-15	70*	-3.42	40x20 x5	40x80 x1
[65]	746-794	Single	-35	100	-1.5~ -3.5	30x10x5	45x120
Model D1T	727-771 2675-2860	Multiband	-7.5 (L) -12 (H)	50* (L) 191* (H)	-4 dB	50x33.5 x1.56	50x67 x1.56
Model E1T	786-840 2642-2858	Multiband	-6.5 (L) -10.5 (H)	59* (L) 216* (H)	-4 dB	50x33.5 x1.56	50x67 x1.56

* -6 dB Bandwidth L= Low Band H= High Band

5.9 Conclusion

In this chapter, we have presented a novel 4-shaped antenna geometry that is the basic element in all proposed MIMO antenna systems in this work. A 2x1 MIMO antenna structure has been proposed and different models were designed and fabricated to improve isolation and resonance features. Model E1T gave the best combination of results and covered the 786 – 845 MHz band and the 2642 -2858 MHz band with more than 63% efficiency. The correlation coefficient was less than 0.7 at the low band and less than 0.3 at the high band. Table 5-4 was compiled to give a better insight of the performance of all the fabricated models while Table 5-5 gives a comparison of models D1T and E1T with the related work in the 700 MHz band that has appeared in literature. Our 2x1 supports dual band operation and is about 35 % smaller that most of the models that appeared in literature. Also it is a compact printed antenna unlike the planar counterparts that occupy larger volumes and appear as elevated 3D structures in the mobile handset.

CHAPTER 6

2x2 MIMO ANTENNA SYSTEM DESIGN

The 4-shaped dual band antenna element discussed in the previous chapter is used to design a 2x2 MIMO antenna system. The basic design is shown in Figure 6-1 and consists of four antenna elements placed in the four quadrants with a cross shaped ground plane. The size of each antenna element is 29x55 mm^2 and the total size of the 2x2 MIMO antenna system is 58x110 mm^2. All the antenna elements have the same dimensions and Table 6-1 shows the values for the different parameters for the model which were optimized for best bandwidth and isolation performance.

This basic design 2x2 MIMO antenna model was fabricated on an FR-4 substrate with two thicknesses, 0.8 mm and 1.56 mm. Different isolation enhancement techniques were investigated by considering three different models which are discussed in this chapter and their simulated and measurement results are presented. The measurement and simulation results agree well, the discrepancy is due to various factors such as the dielectric constant of the substrate has a different value than that assumed in the simulations, antenna

connectors are used in the fabricated models and were not included in the simulations, soldering of connectors and also the calibration did not include the extra connectors used to connect the antenna port to the network analyzer (thus not including the losses due to these coaxial connectors).

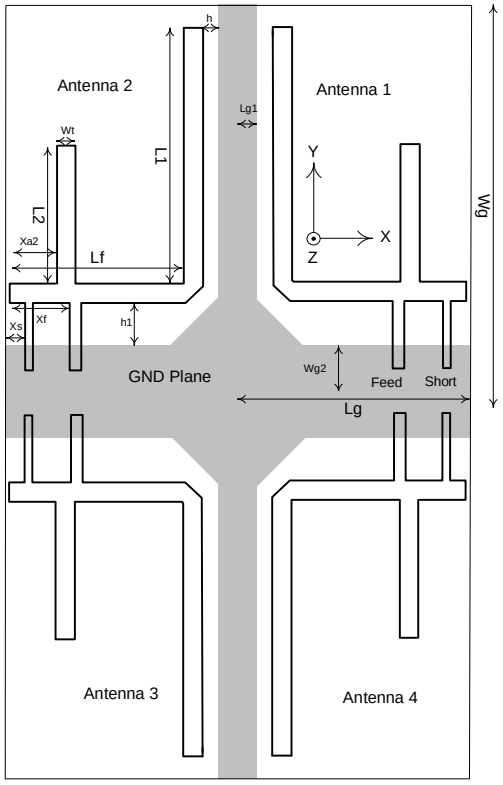

Figure 6-1 Basic design of 2x2 MIMO Antenna System

Table 6-1 Parameter values for Antenna element for 2x2 MIMO Antenna

Parameter	Value	Parameter	Value
Wg	55 mm	Xf	5 mm
Lg	29 mm	Xs	1.5 mm
Wg2	7 mm	Wt	2.6 mm
Lg1	5 mm	h1	3 mm
L1	43 mm	H	2 mm
L2	11 mm	D	1.56 mm
Lf	19.6 mm	Ws	1 mm
Xa2	2.5 mm	Wf	2.2 mm

6.1 2x2 MIMO Antenna: Basic Model

The 2x2 MIMO antenna basic model shown in Fig. 6-1 was fabricated on an FR-4 substrate of thickness 0.8 mm and 1.56 mm. The following sections will present the measurement and simulation results for these two models.

6.1.1 2x2 MIMO Antenna: Basic Model (0.8 mm substrate)

This section will present the results for the 2x2 MIMO Antenna Basic Model fabricated on 0.8 mm substrate. The simulated and measured reflection coefficients for this model are shown in Fig. 6-2 and Fig. 6-3 for the low band and the high band, respectively. At the low band, the -6dB bandwidth for each antenna element is about 50MHz. At the high band, the antenna measurements did not give results comparable

with simulations. The isolation curves are shown in Fig. 6-4. The worst case isolation between the antenna elements is -6 dB and occurred between antenna 1 and antenna 4 at the low band. This is due to the fact that the feed points for these antenna elements are very close to each other and the ground plane current results in strong coupling between the antenna elements. The radiation patterns for antenna 1 and 2 are shown in Fig. 6-5 for the elevation plane and in Fig. 6-6 for the azimuth plane. Due to unavailability of reference antenna below 1GHz, only the radiation patterns are presented for the antennas with resonant frequencies in the 700-800 MHz range. Please note that this is the best that could be measured using the Microwave Lab capabilities.

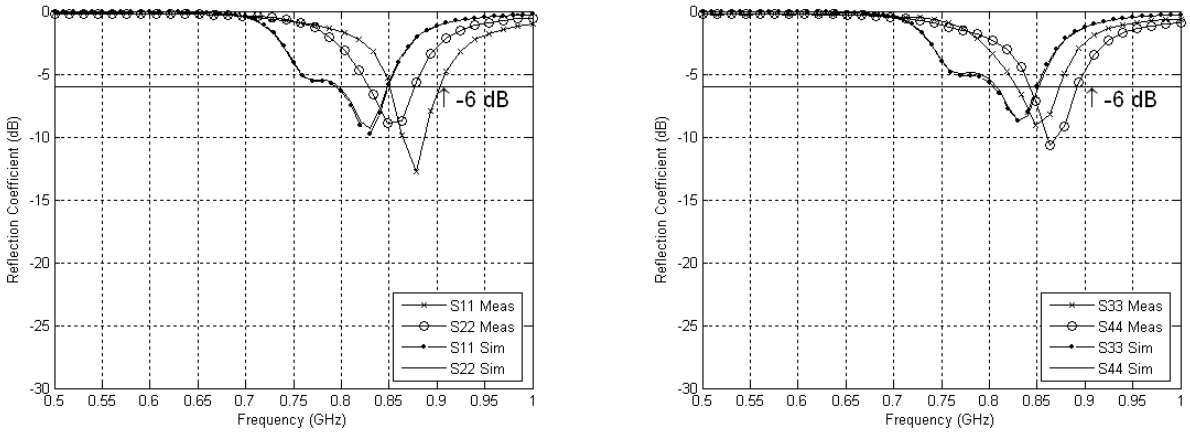

Figure 6-2 Simulated and Measured Reflection Coefficients (S_{11}, S_{22}, S_{33}, S_{44}) at lower band

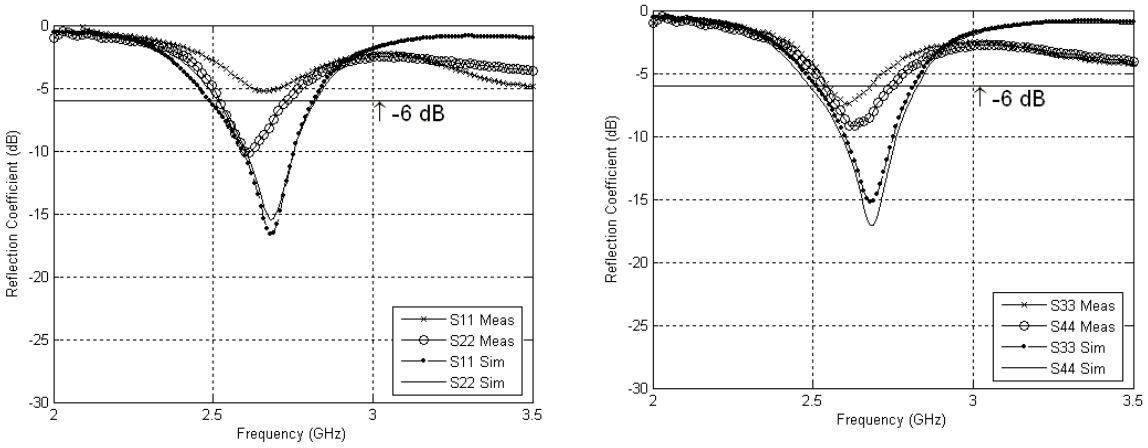

Figure 6-4 Simulated and Measured Reflection Coefficients (S_{11}, S_{22}, S_{33}, S_{44}) at higher band

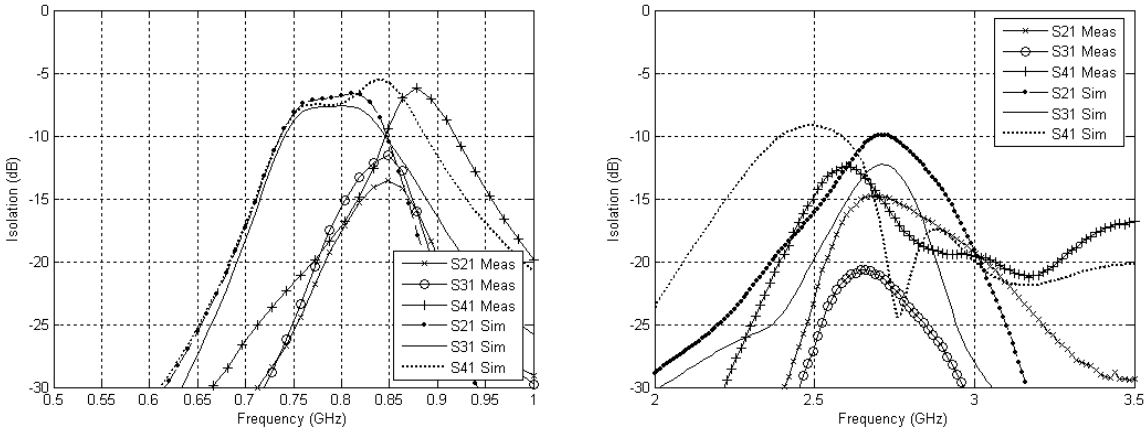

Figure 6-3 Simulated and Measured Isolation (S_{21}, S_{31}, S_{41}) at lower and higher bands

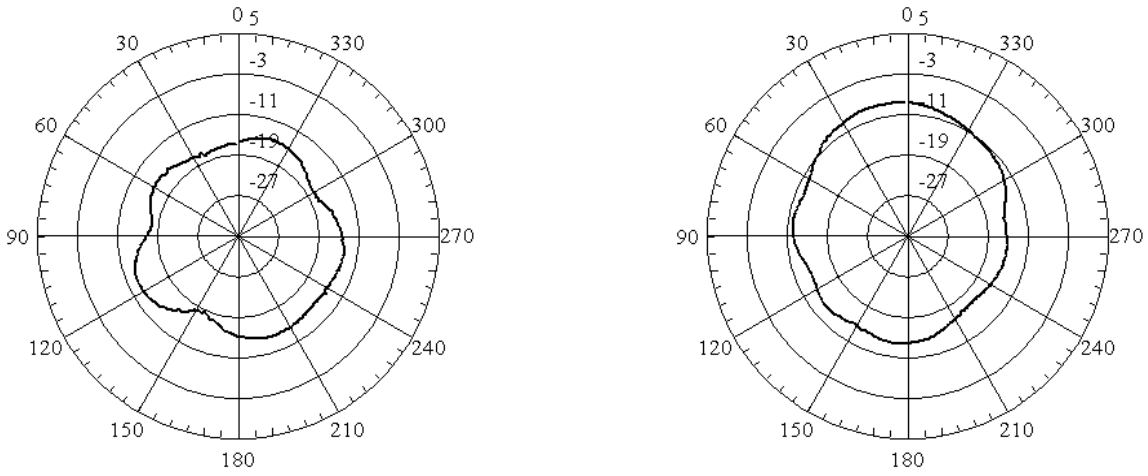

Figure 6-5 Elevation (x-z) plane radiation pattern of antenna 1 and 2 at 800 MHz

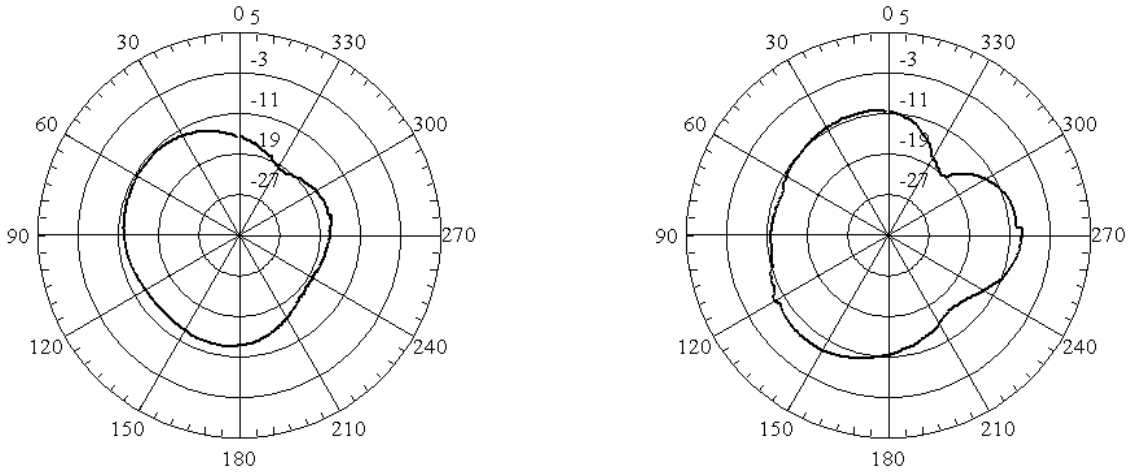

Figure 6-6 Azimuth (x-y) plane radiation pattern of antenna 1 and 2 at 800 MHz

6.1.2 2x2 MIMO Antenna Basic Model (1.56 mm substrate)

This section will present the results for the basic model fabricated using 1.56 mm substrate. As shown in the reflection coefficient plotted in Fig. 6-7, the lower band covered is from 760 to 810 MHz at -6dB value of reflection coefficient. The -6dB bandwidth for each antenna element is about 50MHz (6.35%). The -10dB bandwidth has a small value of about 10 MHz. The worst case isolation between the antenna elements as shown by the S_{41} plot of Fig. 6-9 is -6 dB between antenna 1 and antenna 4. This is due to the fact that the feed points for these antenna elements are very close to each other and the ground plane current result in strong coupling between the antenna elements. As shown in the correlation coefficient plots of Fig. 6-10, the correlation coefficient value is less than 0.3 for antennas 1 and 2 (3 and 4 by symmetry) and antennas 1 and 3 (2 and 4 by symmetry) which predict acceptable MIMO performance for these antenna pairs. However, for antennas 1 and 4 (and also 2 and 3), the value of correlation coefficient as shown in Fig. 6-11 is 0.7. However, this value is actually an upper bound according to equation (4.5) and in most part of the covered band, the correlation value is less than this.

The reflection coefficients at the high band are plotted in Fig. 6-8. The -6dB BW is about 135 MHz although it is 95 MHz for antenna element 1. These results are better than the ones obtained using the 0.8 mm substrate. The isolation curves at the high band are shown in Fig. 6-9 with S_{21} and S_{41} values of about -12 dB while S_{31} value of about -17dB.

The correlation coefficients at the high band are plotted in Fig. 6-12 and Fig. 6-13. The value of the correlation remains less than 0.3 in the band of interest.

The radiation patterns for the elevation and azimuth plane at 800 MHz are shown in Fig. 6-14 and Fig. 6-15, respectively. The maximum received power of about -9dB is measured, while the radiation pattern is almost omni-directional.

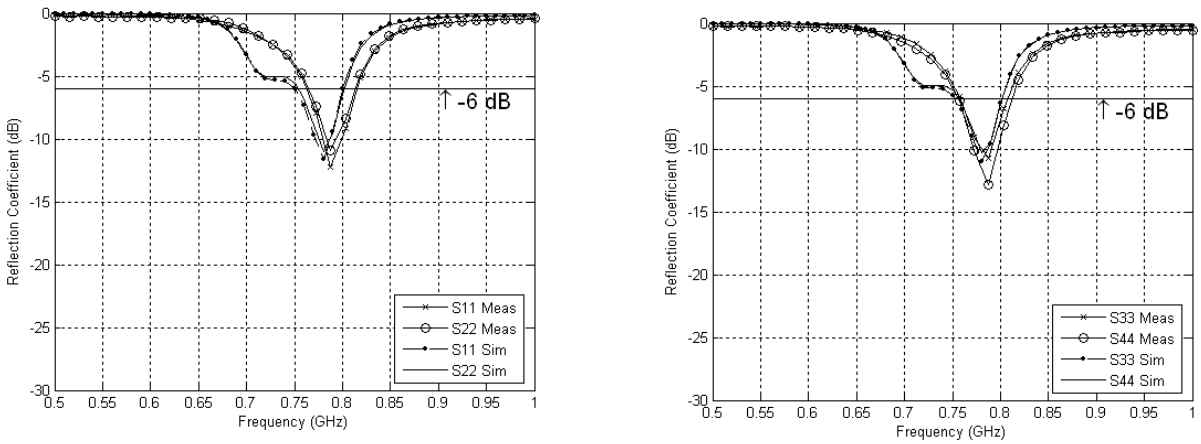

Figure 6-7 Simulated and Measured reflection Coefficient (S_{11}, S_{22}, S_{33}, S_{44}) for antennas at the lower band

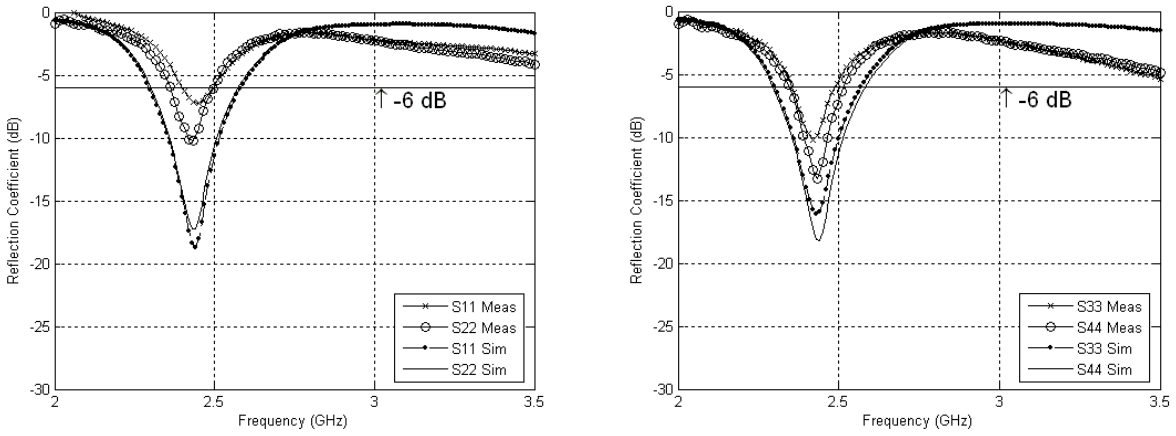

Figure 6-8 Simulated and Measured reflection coefficients (S_{11}, S_{22}, S_{33}, S_{44}) for the antennas at the higher band

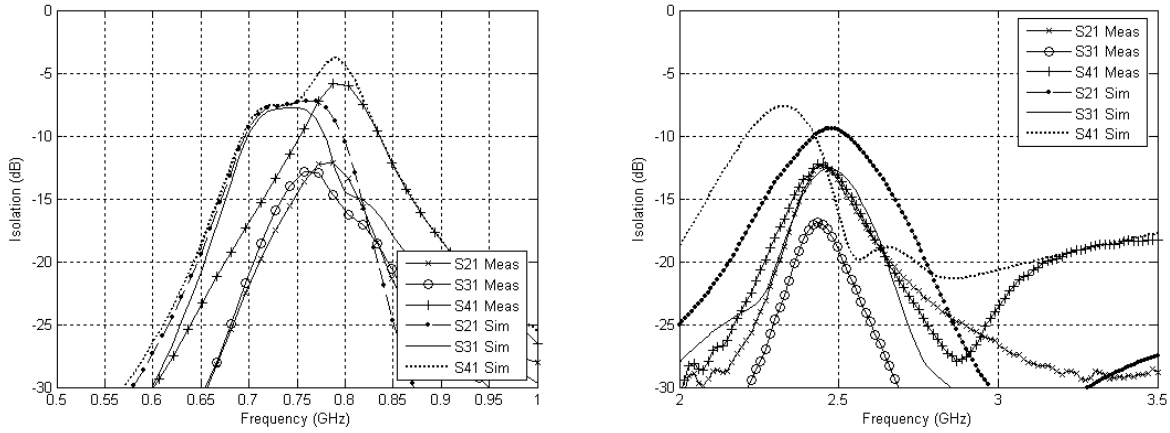

Figure 6-9 Simulated and Measured Isolation between antenna elements at low and high bands

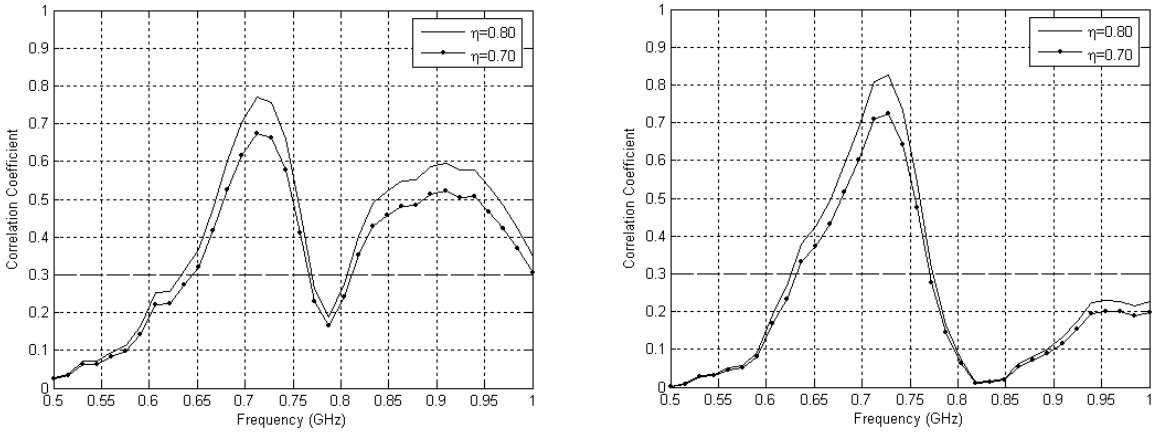

Figure 6-10 Correlation Coefficient between antenna 1 and 2 and 1 and 3 at low band

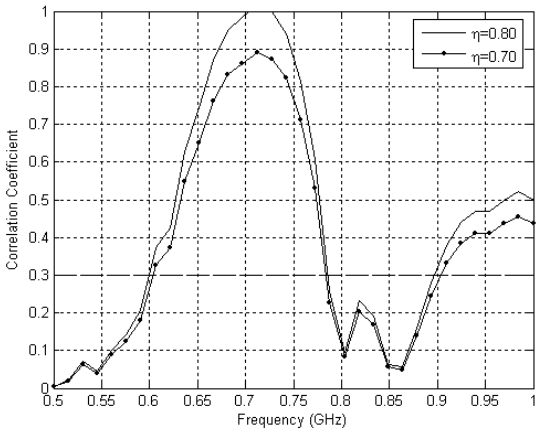

Figure 6-11 Correlation coefficient for antenna 1 and 4 at low band

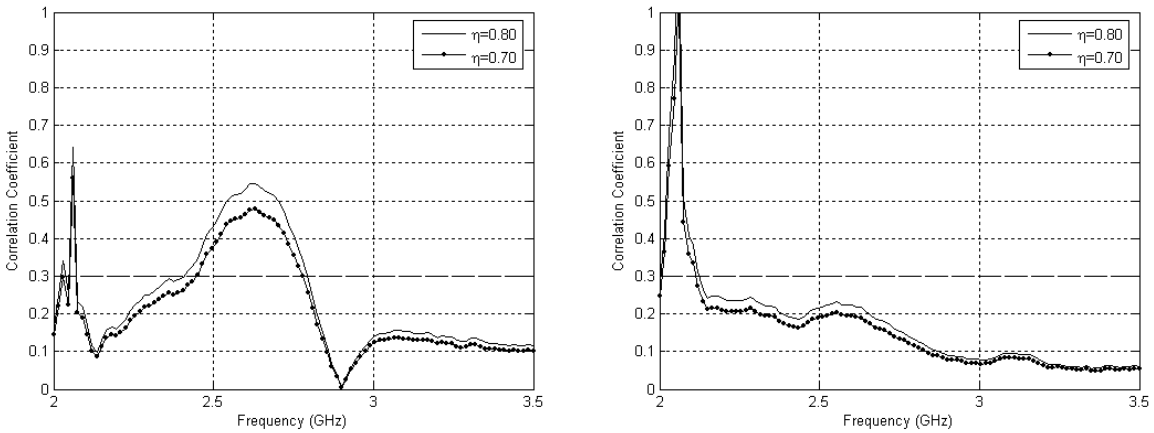

Figure 6-12 Correlation coefficient for antennas 1 and 2 and 1 and 3 at the higher band

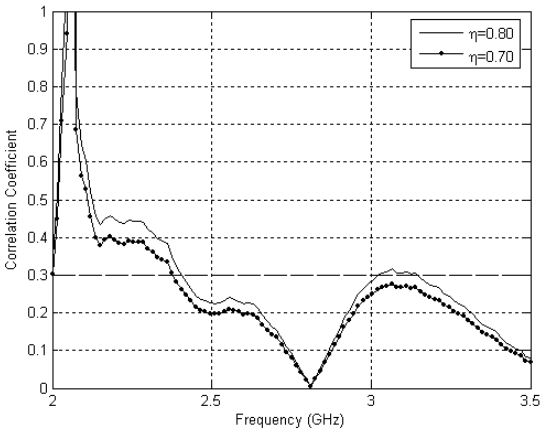

Figure 6-13 Correlation coeffient for antenna 1 and 4 at the higher band

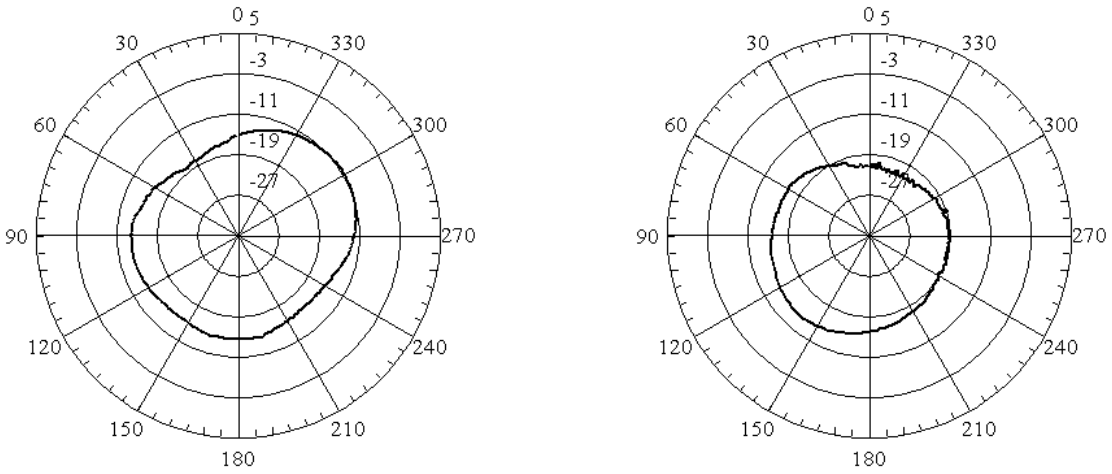

Figure 6-14 Elevation (x-z) plane Radiation pattern for antenna 1 and 2 at 800 MHz

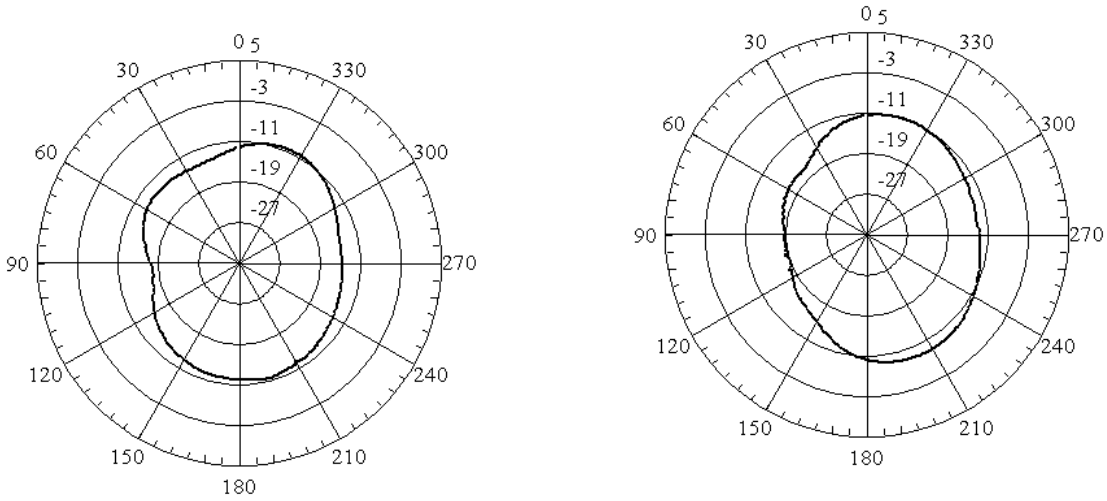

Figure 6-15 Azimuth (x-y) plane radiation pattern of antenna 1 and 2 at 800 MHz

6.2 2x2 MIMO Antenna: Model B

The 2x2 MIMO antenna model B is obtained by modifying the ground plane of the basic model as shown in Fig. 6-16 and was fabricated on FR-4 substrate of thickness 0.8 mm and 1.56 mm. As can be seen, three vertical slits (6x1.2 mm^2) separated by 1.8 mm have been etched from the horizontal ground plane of each antenna element. These slits were meant to modify the current distribution on the ground plane and hence improve the isolation between the antenna elements. The fabricated model is shown in Fig. 6-17. The following sections will present the measurement and simulation results for these two models.

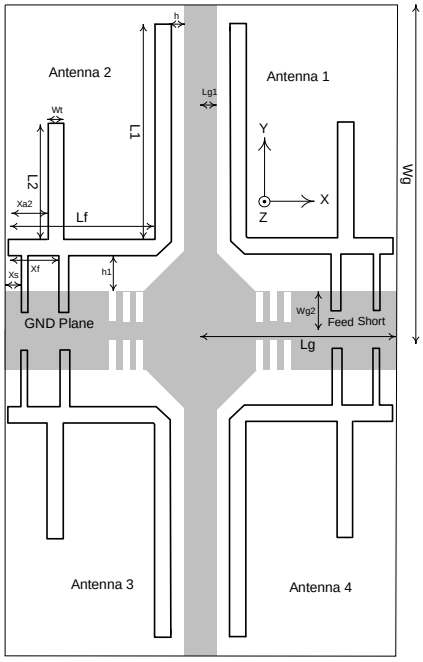

Figure 6-16 Model B with modified ground plane

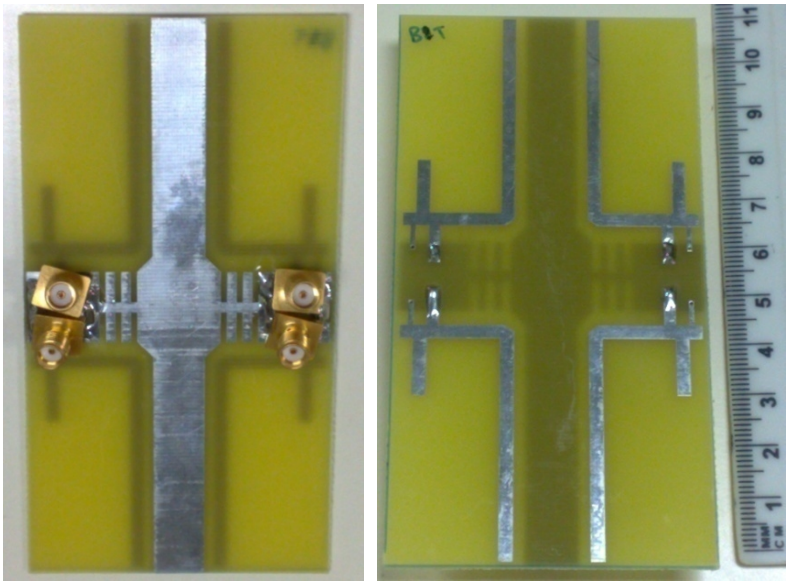

Figure 6-17 Fabricated 2x2 MIMO Antenna Model B1T

6.2.1 2x2 MIMO Antenna Model B1 (0.8 mm substrate)

The simulated and measured S-parameters are shown in Fig. 6-18 and Fig. 6-19 for the low band and the high band, respectively. Compared with the Basic Model (0.8 mm substrate), we see that there is a reduction in the resonant frequencies and there is improvement in the reflection coefficients and bandwidth at both the low and the high bands. At the low band, the -6 dB BW is about 60 MHz while the -10 dB BW is 26 MHz. At the higher band, the -6 dB BW is more than 186 MHz. However, there is rather deterioration in the isolation between some antenna elements as shown in the isolation plots for the lower (S_{21}) and higher bands (S_{41}) shown in Fig. 6-20. Also the simulated

radiation efficiency is very low (1%) compared with 64.9% for the Basic Model. The radiation patterns for this model are shown in Fig. 6-21 and Fig. 6-22.

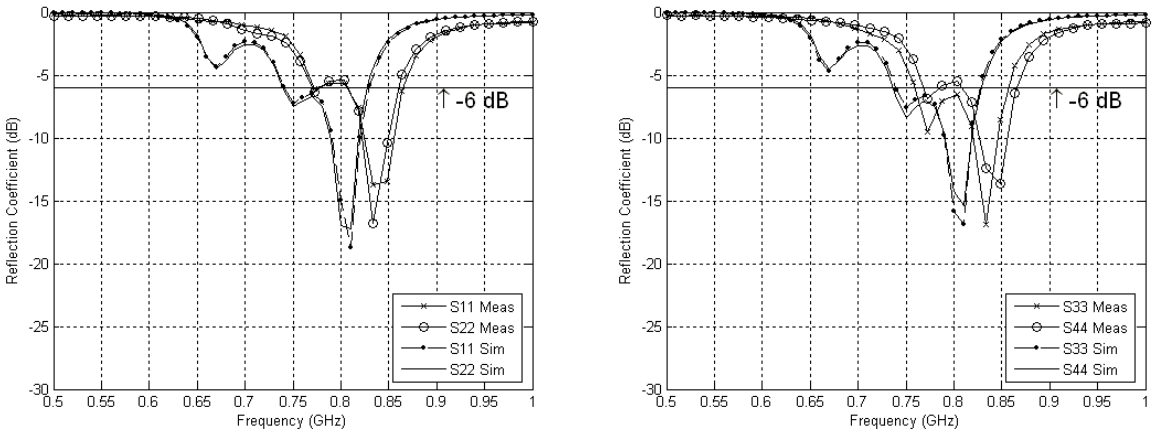

Figure 6-18 Simulated and Measured reflection Coefficients (S_{11}, S_{22}, S_{33}, S_{44}) for antennas at the lower band

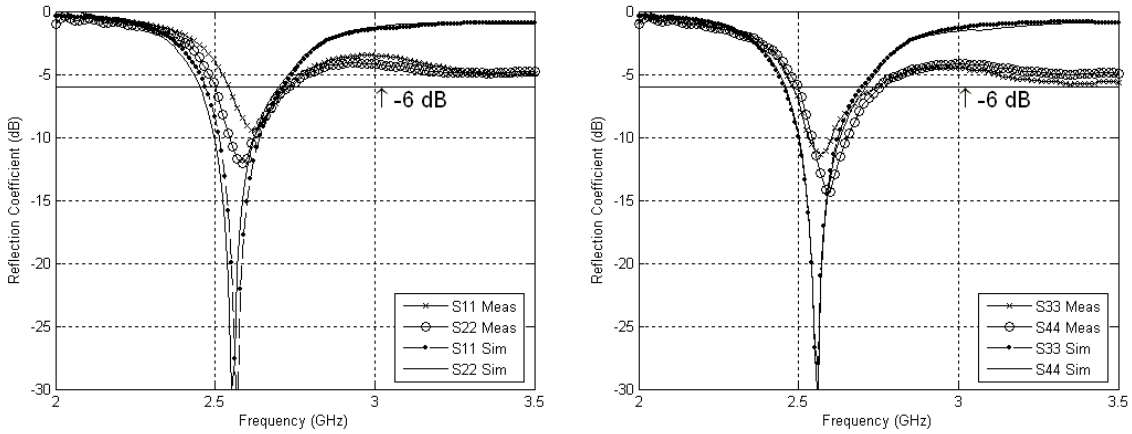

Figure 6-19 Simulated and Measured reflection Coefficient (S_{11}, S_{22}, S_{33}, S_{44}) for antennas at the higher band

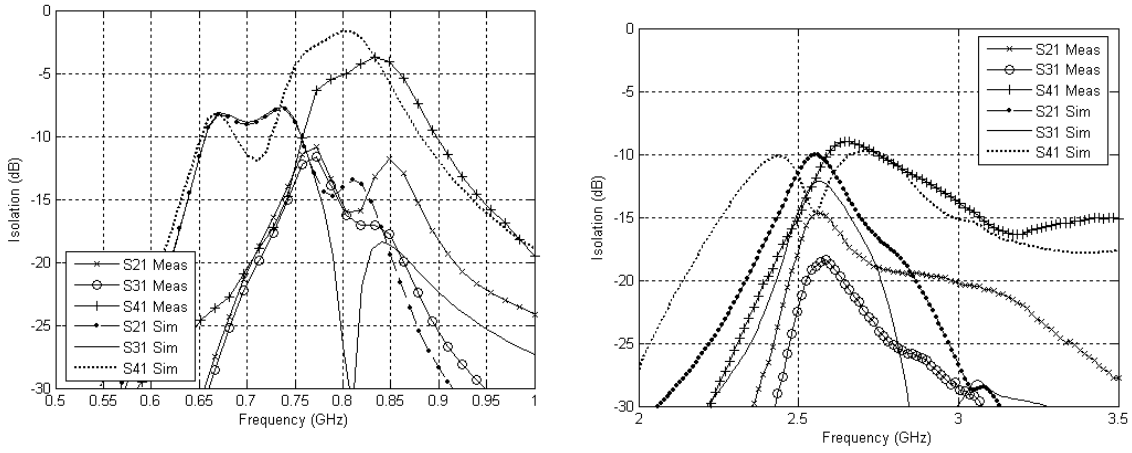

Figure 6-20 Simulated and Measured Isolation between antenna elements at lower and high bands

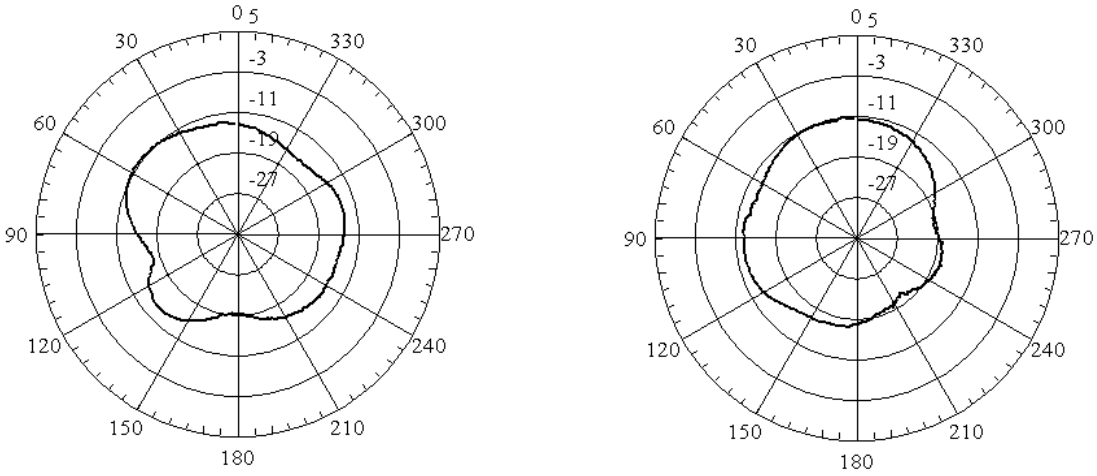

Figure 6-21 Elevation (x-z) plane Radiation pattern for antenna 1 and 2 at 800 MHz

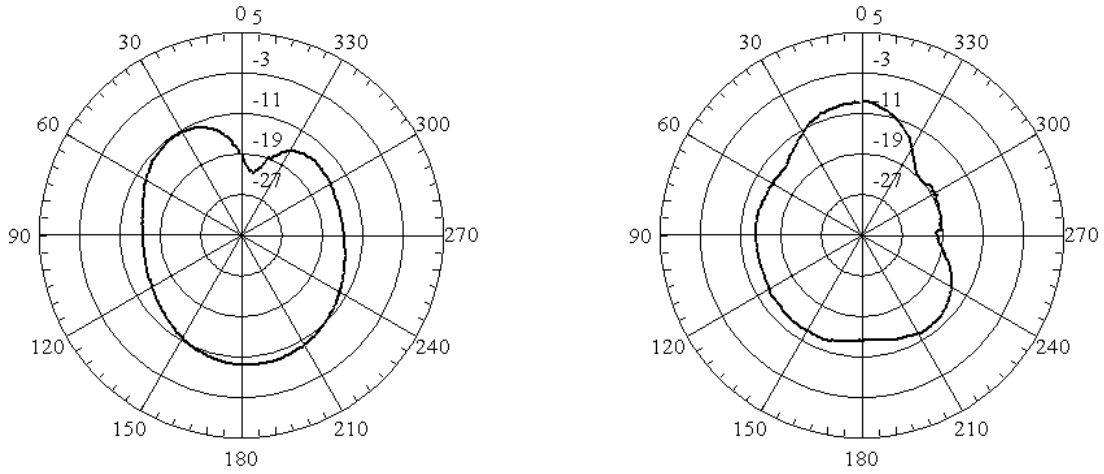

Figure 6-22 Azimuth (x-y) plane radiation pattern of antenna 1 and 2 at 800 MHz

6.2.2 2x2 MIMO Antenna Model: B1T (1.56 mm substrate)

The simulated and measured S-parameters for the Model B1T (1.56 mm substrate) are shown in Fig. 6-23 and Fig. 6-24 for the low band and the high band respectively. Compared with the Basic Model (1.56 mm substrate), we see that there is a reduction in the resonant frequencies and improvement in the reflection coefficients and bandwidth at both the low and the high bands. The -6dB BW at the lower band is about 100 MHz (except for antenna element 4 for which the value is 62 MHz) covering the band 694-794 MHz. The -10dB BW is about 30 MHz. At the high band, the -6 dB BW is more than 163 MHz covering the band 2312-2475 MHz while the -10 dB BW is more than 92 MHz.

The isolation at both the low and high bands is deteriorated as shown in the isolation plots in Fig. 6-25. It is to be noted that the simulation and measurement results are very close as the simulation in this case was done with ε_r=4 instead of ε_r =4.4 for the 0.8 mm substrate models. Plots of the correlation coefficient for the low band and high band are shown in Fig. 6-26 to 6-29. At the low band, the correlation coefficient is less than about 0.3 except for the antennas 1 & 4 where the value is higher due to the low isolation. At the high band, the correlation coefficient value is less than 0.3. Also the simulated radiation efficiency at low band is reduced to 22.3 % compared with 46.5% for the Basic Model. The elevation and azimuth plane radiation patterns for this model at 770 MHz are shown in Fig. 6-30 and Fig. 6-31 respectively. A maximum received power of -7 dB was observed.

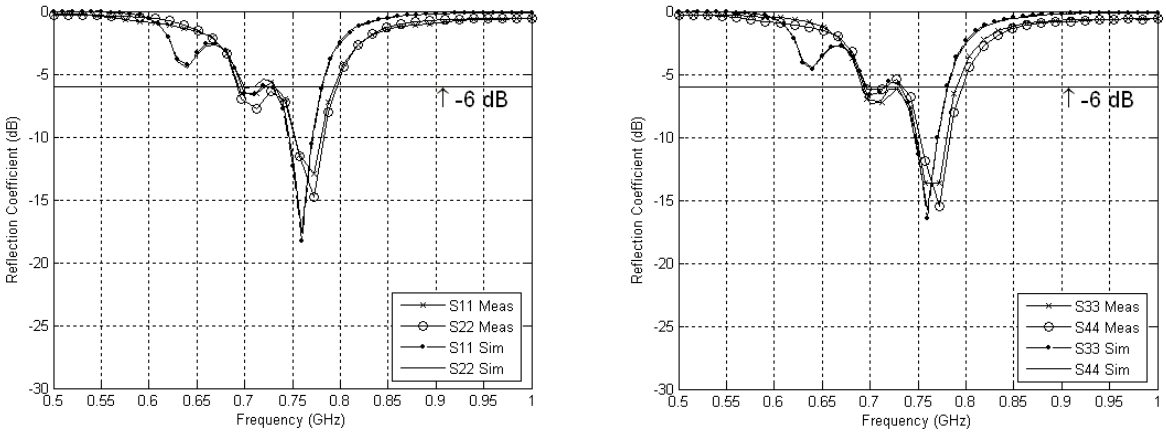

Figure 6-23 Simulated and Measured reflection Coefficients (S_{11}, S_{22}, S_{33}, S_{44}) for antennas at the higher band

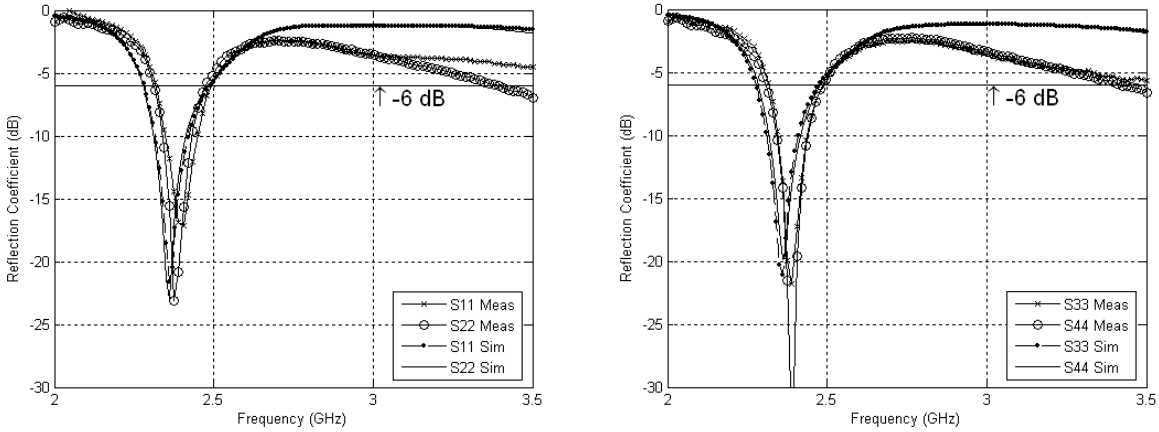

Figure 6-24 Simulated and Measured reflection Coefficients (S_{11}, S_{22}, S_{33}, S_{44}) for antennas at the lower band

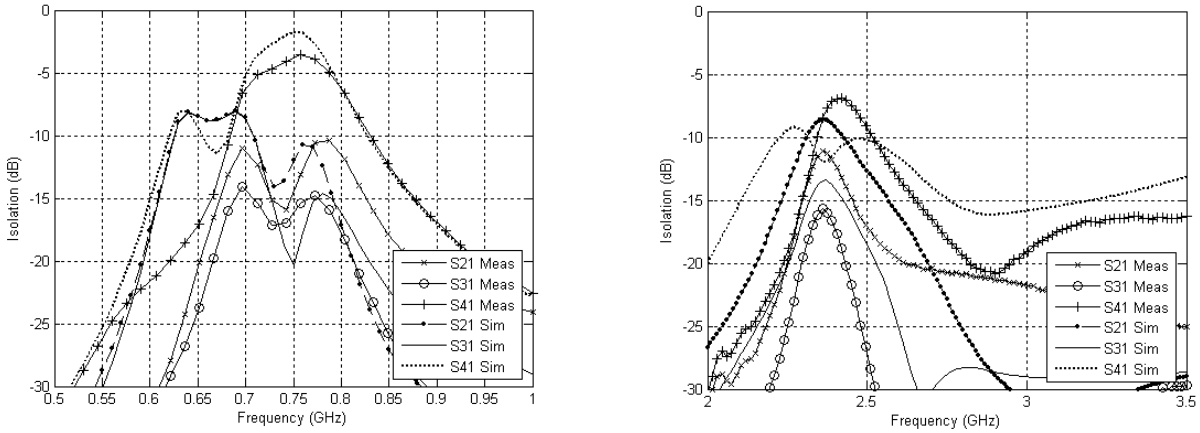

Figure 6-25 Simulated and Measured Isolation between antenna elements at lower and high bands

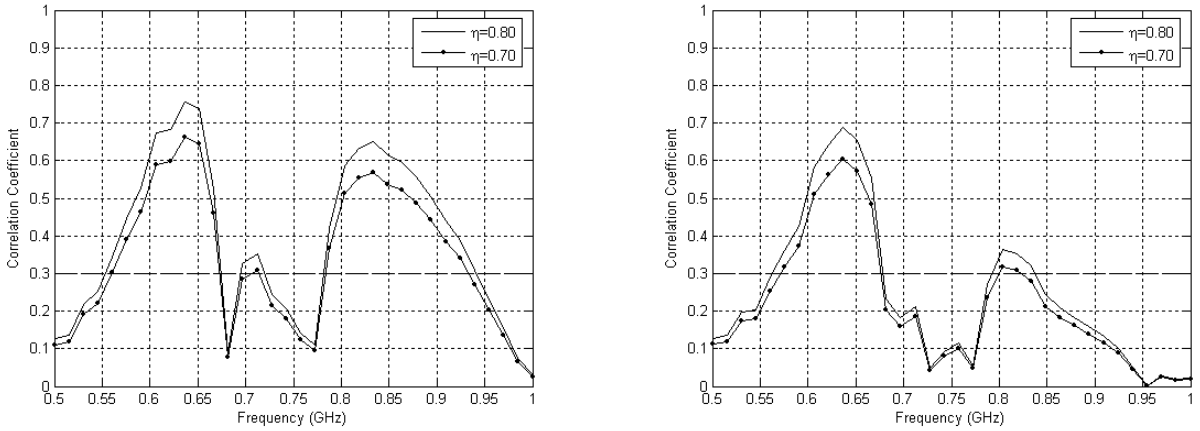

Figure 6-26 Correlation Coefficient between antennas 1 and 2 and 1 and 3 at low band

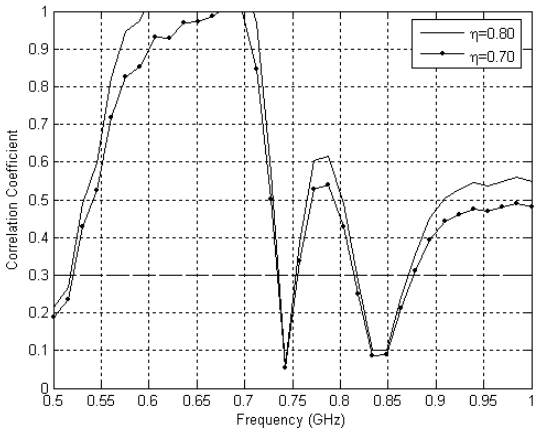

Figure 6-27 Correlation Coefficient between antennas 1 and 4 at low band

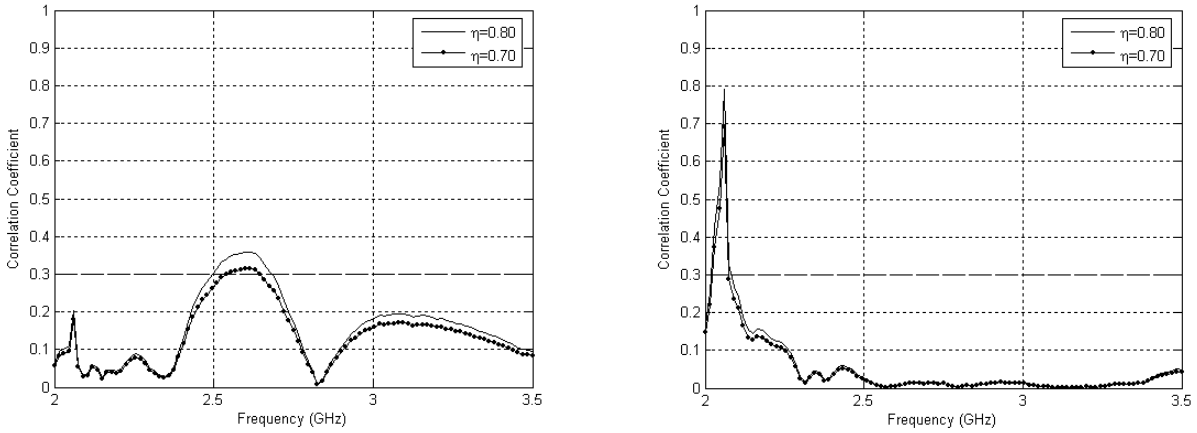

Figure 6-28 Correlation Coefficient between antenna 1 and 2 and 1 and 3 at higher band

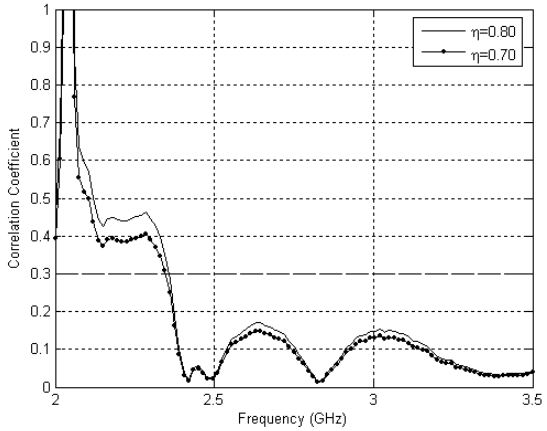

Figure 6-29 Correlation Coefficient between antenna 1 and 4 at high band

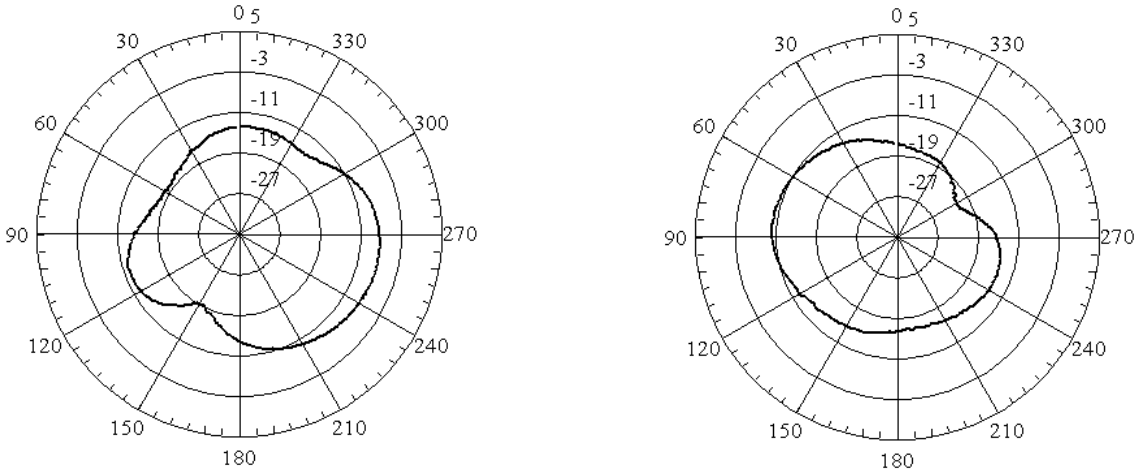

Figure 6-30 Elevation (x-z) plane Radiation pattern for antenna 1 and 2 at 770 MHz

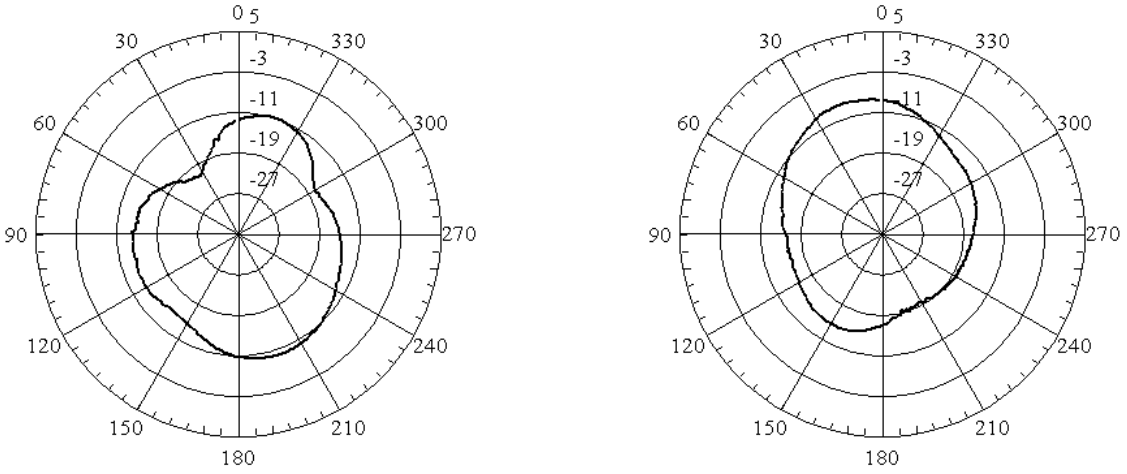

Figure 6-31 Azimuth (x-y) plane radiation pattern of antenna 1 and 2 at 770 MHz

6.3 2x2 MIMO Antenna: Model C

The 2x2 MIMO antenna model C is obtained by modifying the ground plane of the basic model as shown in Fig. 6-32 and was fabricated on FR-4 substrate of thickness 0.8 mm and 1.56 mm. As can be seen, a defected ground structure (DGS) has been used in the form of four circles of radius 2.5 mm etched from the ground plane. The purpose of these circles was to alter the current distribution on the ground plane and hence improve the isolation between the antenna elements. The fabricated model is shown in Fig. 6-33. The following section will present the measurement and simulation results for the model C1T only which was fabricated on 1.56 mm substrate.

6.3.1 2x2 MIMO Antenna Model C1T (1.56 mm substrate)

The measured and simulated reflection coefficients for this model fabricated on FR-4 substrate of 1.56 mm thickness are shown in Fig. 6-34 and Fig. 6-35 while Fig. 6-36 shows the isolation curves. Compared with the Basic Model (1.56 mm), there is no change in the reflection coefficients or isolation as shown in Table 6-2 which summarizes all the results obtained. Figures 6-37 to 6-40 show the correlation coefficients at the low band and high band. Fig. 6-41 and Fig. 6-42 show the elevation and azimuth plane radiation pattern of antenna 1 and 2 for this model. A maximum received power level of about -8 dB was observed.

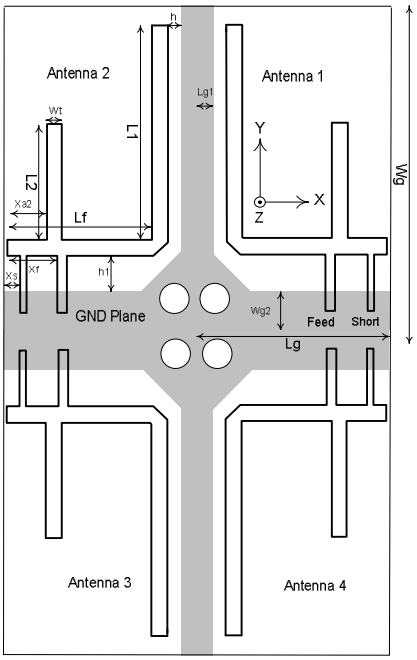

Figure 6-32 MIMO Antenna Model C

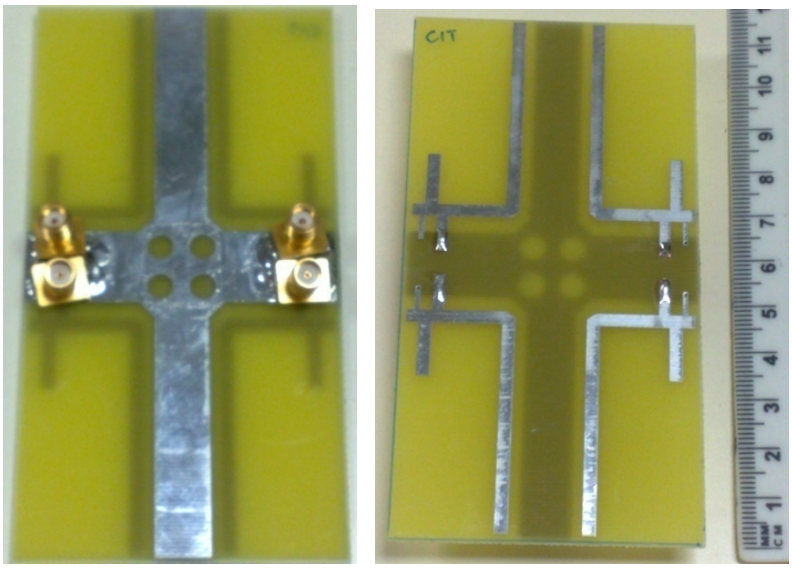

Figure 6-33 Fabricated 2x2 MIMO antenna model C

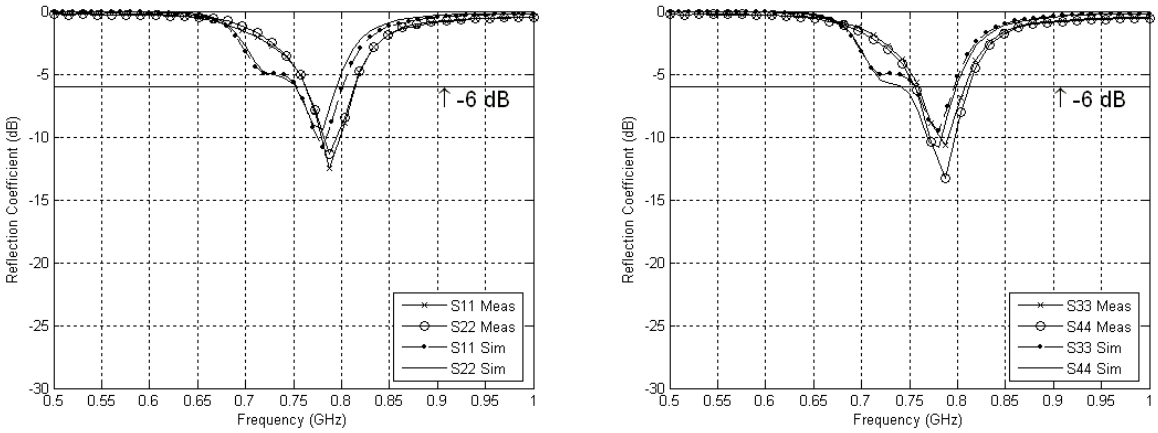

Figure 6-34 Simulated and Measured reflection Coefficient (S_{11}, S_{22}, S_{33}, S_{44}) for antennas at the low band

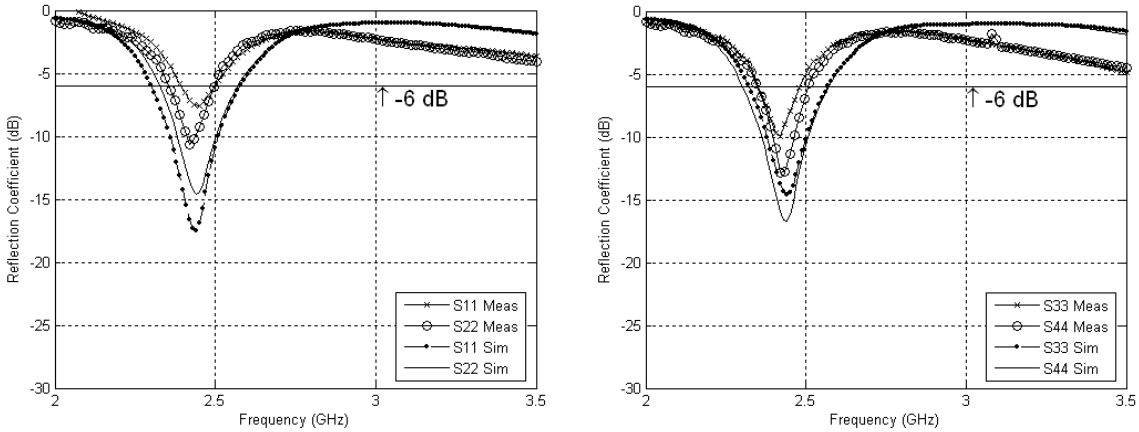

Figure 6-35 Simulated and Measured reflection Coefficient (S_{11}, S_{22}, S_{33}, S_{44}) for antennas at the high band

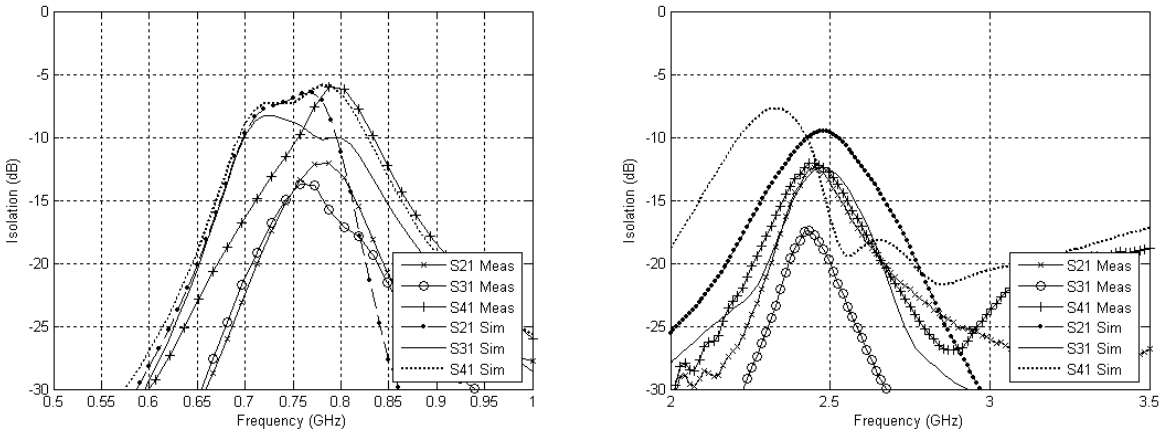

Figure 6-36 Simulated and Measured Isolation between antenna elements at low and high bands

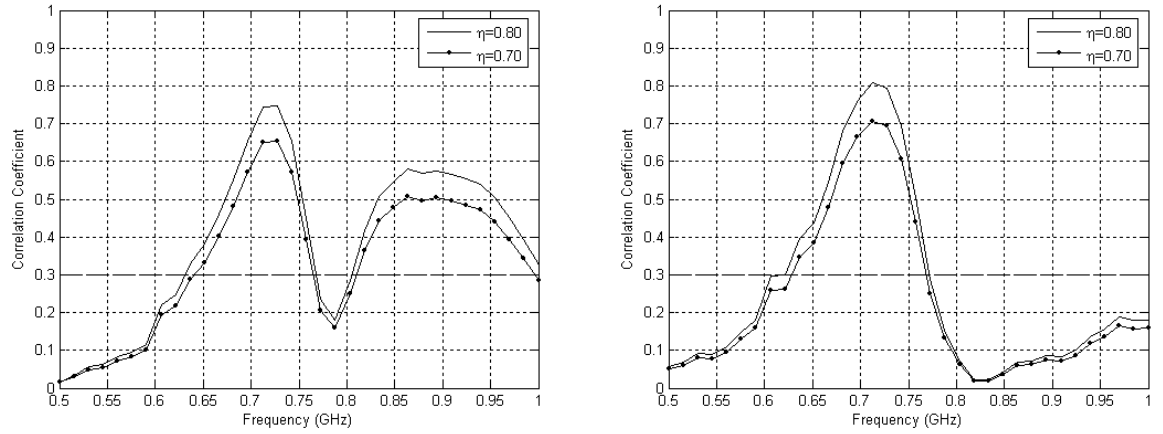

Figure 6-37 Correlation Coefficient for antennas 1 and 2 and 1 and 3 at low band

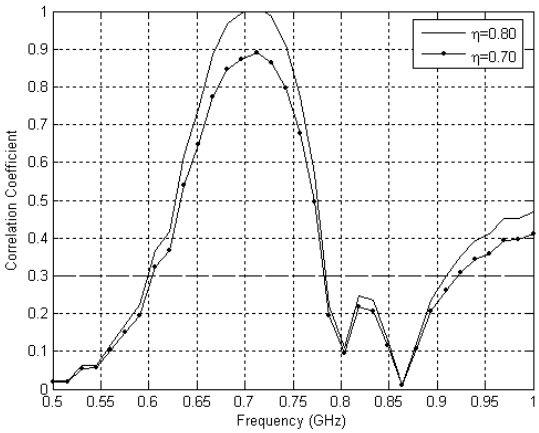

Figure 6-38 Correlation Coefficient for antennas 1 and 4 at low band

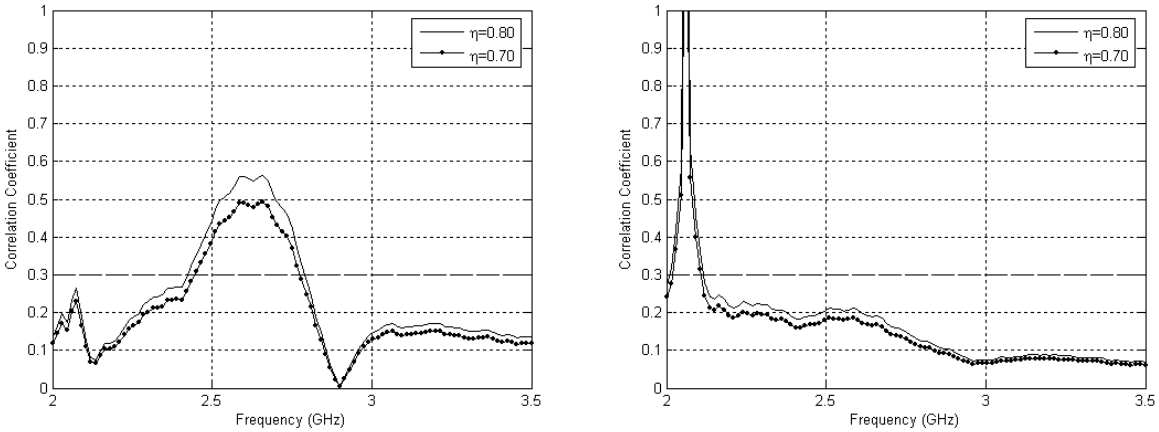

Figure 6-39 Correlation Coefficient for antennas 1 and 2 and 1 and 3 at high band

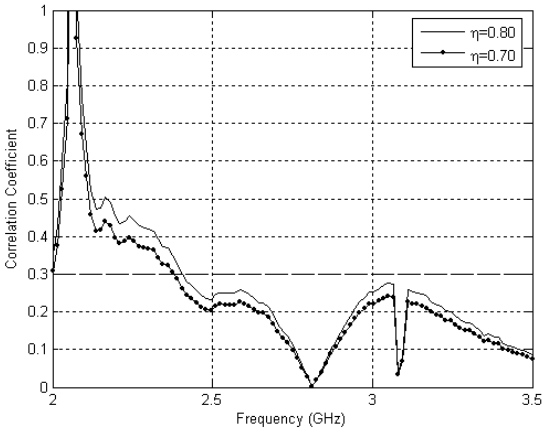

Figure 6-40 Correlation Coefficient for antennas 1 and 4 at high band

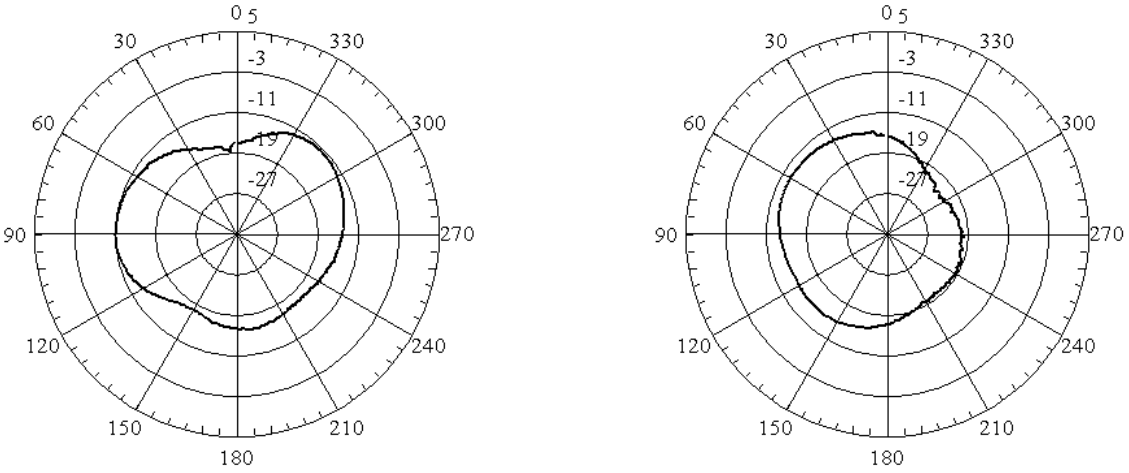

Figure 6-41 Elevation (x-z) plane Radiation pattern for antenna 1 and 2 at 800 MHz

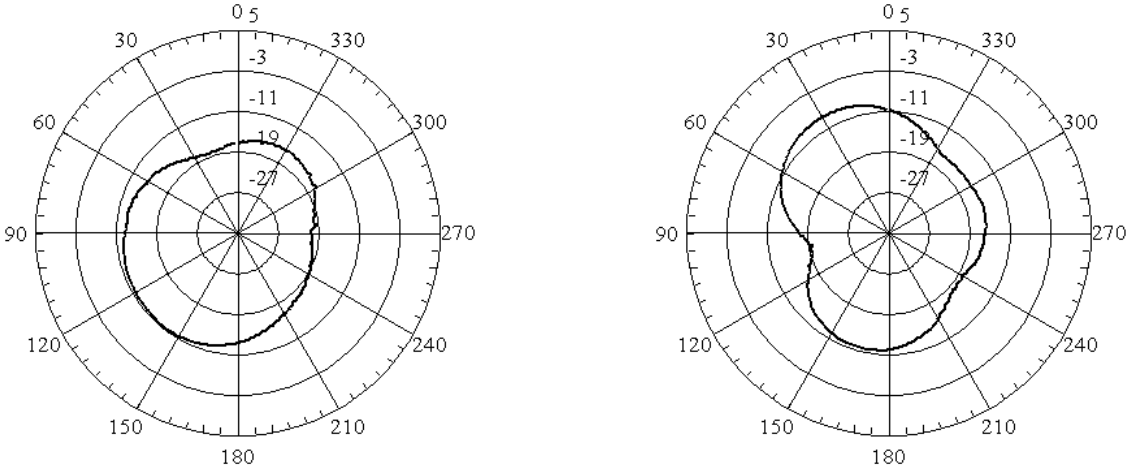

Figure 6-42 Azimuth (x-y) plane radiation pattern of antenna 1 and 2 at 800 MHz

6.4 2x2 MIMO Antenna: Model A

The 2x2 MIMO antenna model A is obtained by combining the two techniques described in the previous two models (B and C) with a cross shaped slit between the grounds added as shown in Fig. 6-43. Model A was fabricated on FR-4 substrate of thickness 0.8 mm and 1.56 mm. As can be seen, a horizontal (1x16 mm^2) and vertical (1x48 mm^2) slit has been etched in the ground plane (cross shape). These slits are meant to modify the current distribution on the ground plane and hence improve the isolation between the antenna elements. The fabricated model is shown in Fig. 6-44. The following section will present the measurement and simulation results for the model A1T only which uses the 1.56 mm thick substrate.

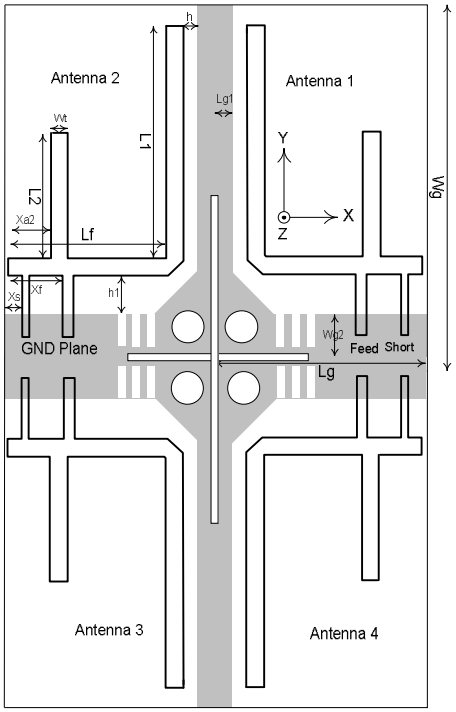

Figure 6-43 2x2 MIMO Antenna Model A

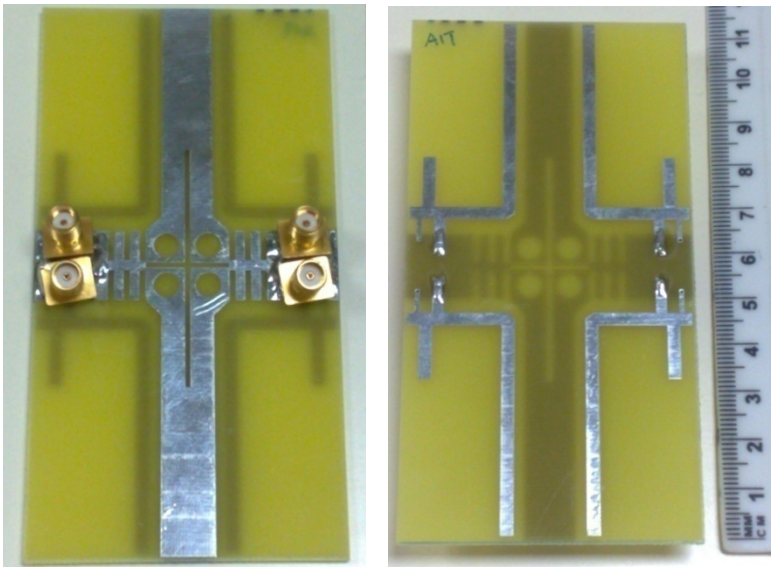

Figure 6-44 Fabricated 2x2 MIMO Antenna Model A

6.4.1 2x2 MIMO Antenna Model A1T (1.56 mm substrate)

The simulated and measured S-parameters for the Model A1T (1.56 mm substrate) are shown in Fig. 6-45 and Fig. 6-46 for the low band and the high band respectively. Compared with the Basic Model (1.56 mm substrate), we see that there is a reduction in the resonant frequencies and improvement in the reflection coefficients and bandwidth at both the low and the high bands. The -6dB BW at the lower band is about 60 MHz with a center frequency of 760 MHz. The -10dB BW is about 30 MHz. At the high band, the -6 dB BW is more than 135 MHz at a center frequency of 2380 MHz while the -10 dB BW is more than 80 MHz.

The isolation at both the low and high bands is deteriorated compared to the basic 2x2 model as shown in the isolation plots in Fig. 6-47. Plots of the correlation coefficient for the low band and high band are shown in Fig. 6-48 to Fig. 6-51. At the low band, the correlation coefficient is less than about 0.5 in the band of interest. At the higher band, the value is less than 0.3. Also the simulated radiation efficiency is reduced to 19.44 % compared with 46.5% for the Basic Model. This can be attributed to the fact that the ground plane acts as an integral part of the antenna and the circles and slits etched on the ground plane cause severe disturbance of the current on it. The elevation and azimuth plane radiation patterns for this model at 760 MHz are shown in Fig. 6-52 and Fig. 6-53 respectively. The maximum received power level was observed to be about -10 dB.

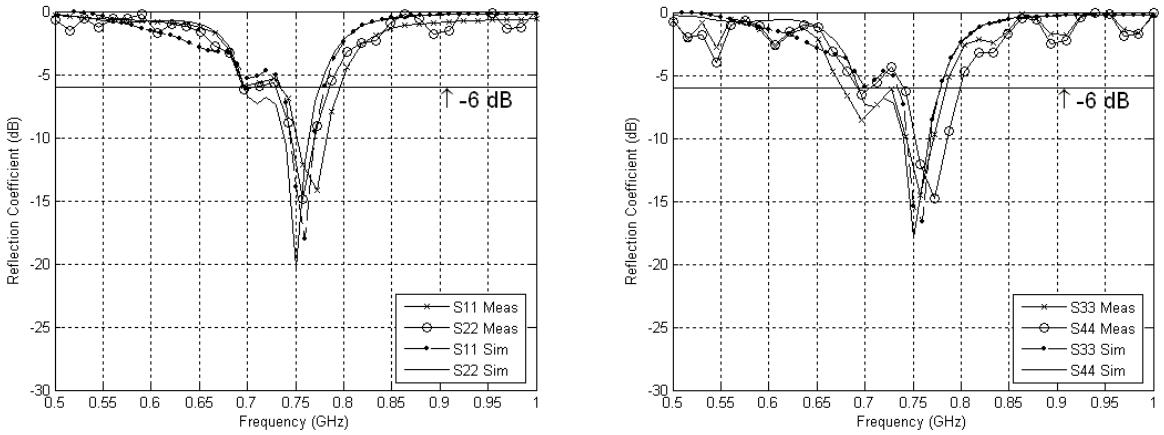

Figure 6-45 Simulated and Measured reflection Coefficient (S_{11}, S_{22}, S_{33}, S_{44}) for antennas at the low band

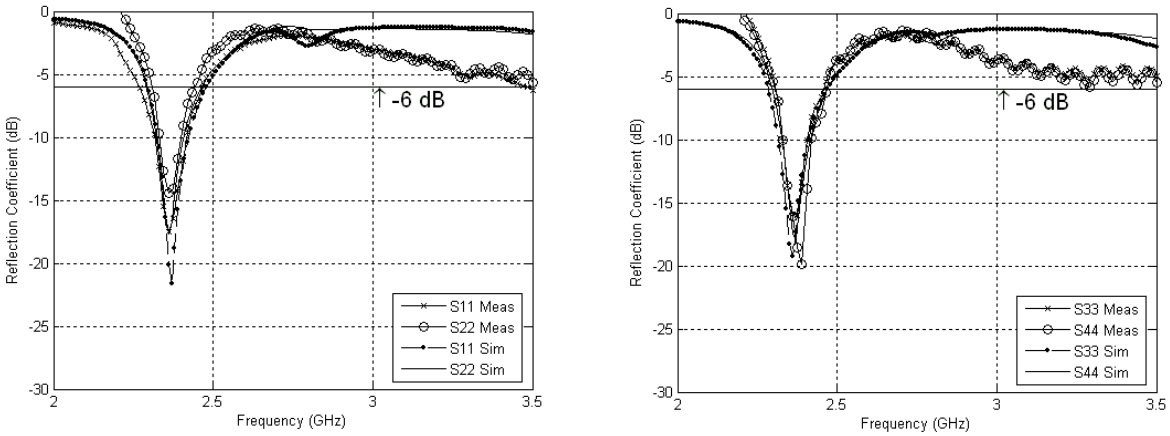

Figure 6-46 Simulated and Measured reflection Coefficient (S_{11}, S_{22}, S_{33}, S_{44}) for antennas at the high band

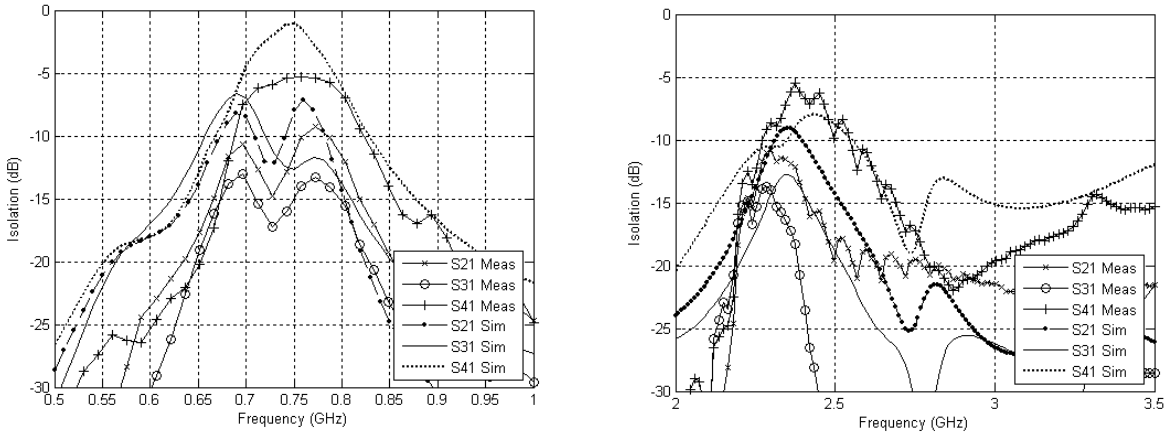

Figure 6-47 Simulated and Measured Isolation between antenna elements at low and high bands

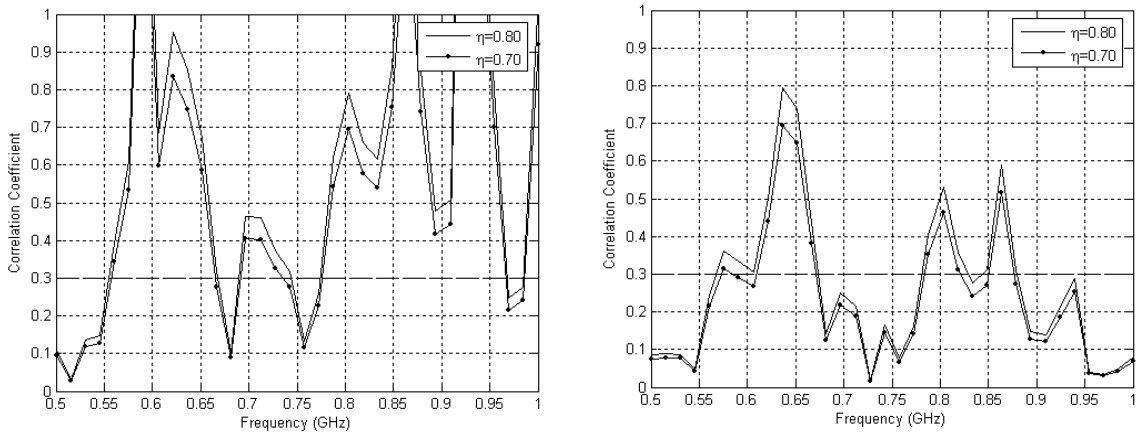

Figure 6-48 Correlation Coefficient for antennas 1 and 2 and 1 and 3 at low band

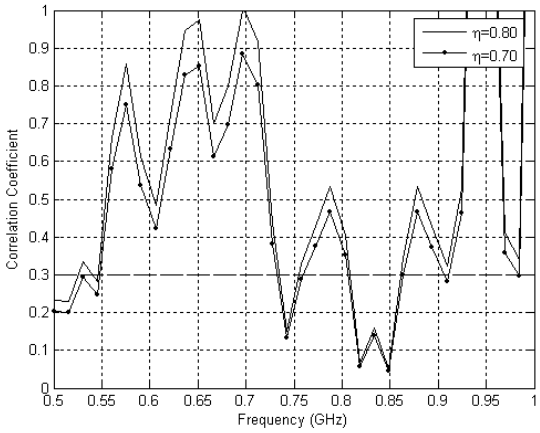

Figure 6-49 Correlation Coefficient for antennas 1 and 4 at low band

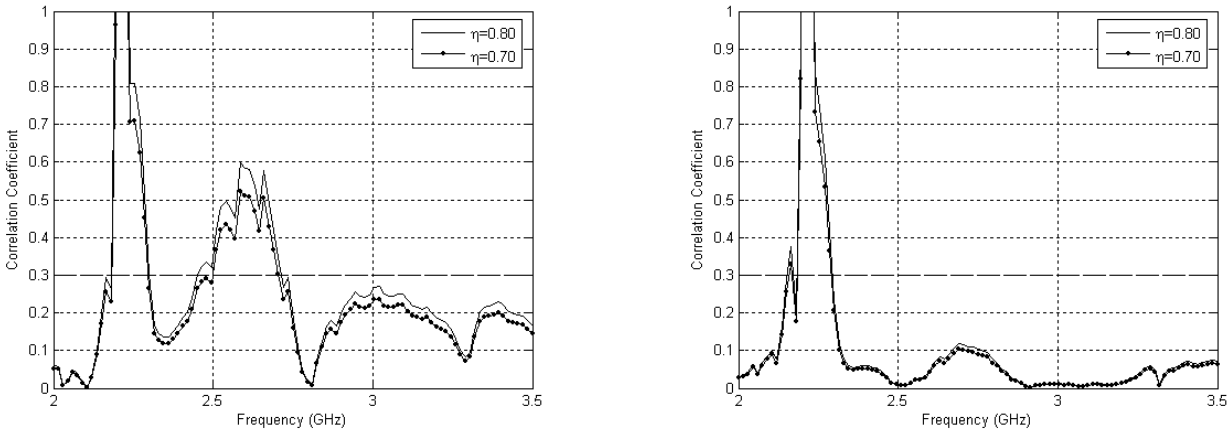

Figure 6-50 Correlation Coefficient for antennas 1 and 2 and 1 and 3 at high band

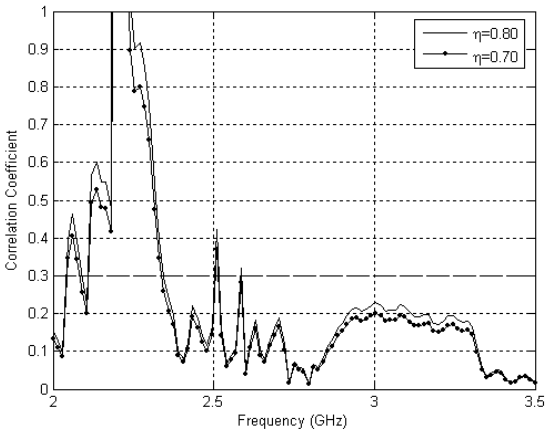

Figure 6-51 Correlation Coefficient for antennas 1 and 4 at high band

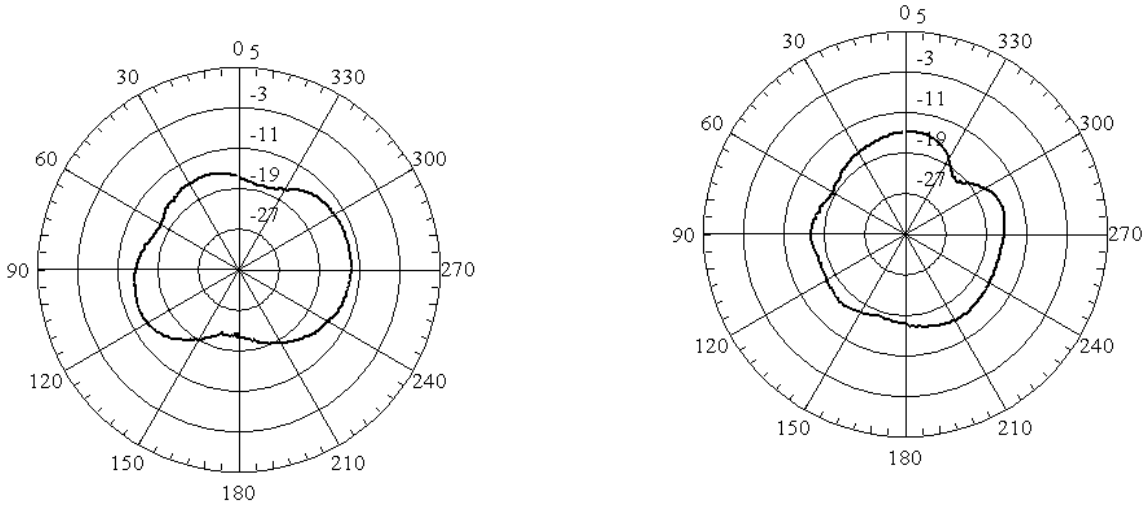

Figure 6-52 Elevation (x-z) plane Radiation pattern for antenna 1 and 2 at 760 MHz

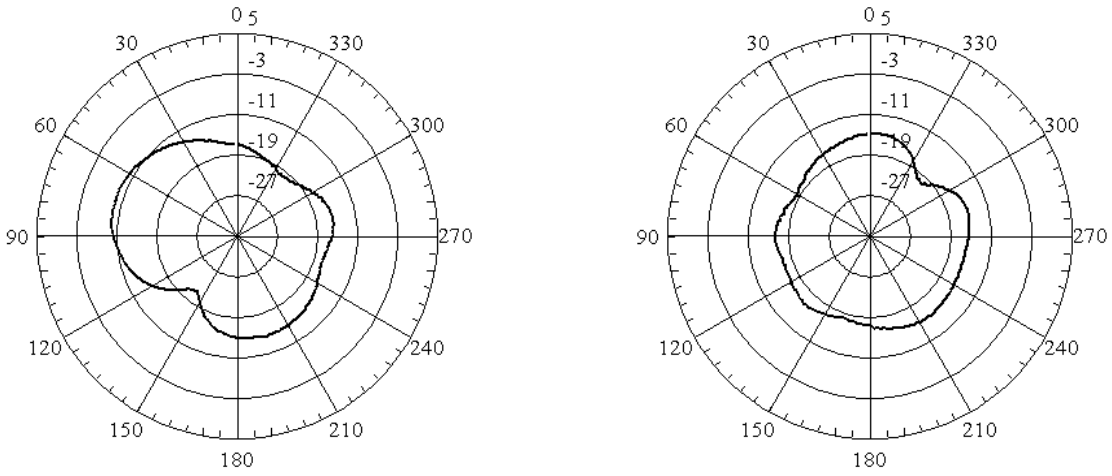

Figure 6-53 Azimuth (x-y) plane radiation pattern of antenna 1 and 2 at 760 MHz

Table 6-2 compares the results of all the 2x2 MIMO antenna system models with 1.56 mm substrate thickness. It is evident that the basic model with 1.56 mm substrate will give the best efficiency, while model B will give the largest BW of operation. The isolation performance of all the 4 models was close in general, with model A being the worst. Almost all models satisfy the correlation coefficient requirement of 0.3 in most of their operating bands. Figures 6-54 to 6-61 compare the 4 different models in terms of some of their parameters such as S-parameters and isolation for both the low and high bands. The basic model and Model C have similar characteristics which means the circles etched on the ground plane in Model C did not have effect on the performance of the antenna. The short vertical slits etched on the ground plane in models B and B1T resulted in improving the impedance matching at both the bands. However, these did not improve the isolation between the antenna elements. Models A and B also have similar

characteristics indicating that the cross shaped slot did not improve the isolation or other performance characteristics.

Table 6-2 : Measurement Results for all the 2x2 MIMO Antenna Models (1.56 mm substrate)

Parameter / Model	Band	Antenna Element	BW (-6dB)	BW (-10dB)	S_{xx}	S_{21}	S_{31}	S_{41}
Basic Model 1.56 mm	Low	1	52	19	-12	<-12	-13	-6
		2	49	9	-11			
		3	49	10	-11			
		4	56	6	-13			
	High	1	95	0	-7	<-12	<-17	<-12
		2	135	0	-10			
		3	135	0	-10			
		4	165	75	-13			
Model A1T 1.56 mm	Low	1	65	31	-13	<-9	<-13	-5
		2	59	31	-15			
		3	105	30	-14			
		4	55	34	-14			
	High	1	200	95	-17	<-11	<-13	<-6
		2	135	90	-14			
		3	150	80	-16			
		4	160	90	-19			
Model B1T 1.56 mm	Low	1	100	28	-13	-10	-15	-3.5
		2	103	32	-14.5			
		3	98	32	-13.5			
		4	62	32	-15.5			
	High	1	177	100	-17	-11	-15.5	-7
		2	163	92	-23			
		3	173	92	-22			
		4	180	98	-30			
Model C1T 1.56 mm	Low	1	51	19	-12.5	-12	-14	-6
		2	50	13	-11.5			
		3	48	9	-10.5			
		4	56	25	-13			
	High	1	105	0	-7.5	-12	-17	-12
		2	142	28	-10.5			
		3	131	0	-10			
		4	158	66	-13			

Table 6-2 : Measurement Results for all the 2x2 MIMO Antenna Models (1.56 mm substrate)…

continued from previous page

Parameter / Model	Band	Antenna Element	fc	Efficiency (Simulation)	Max Rx Power Measured (dB)
Basic Model 1.56 mm	Low	1	789	46.5	-9
		2	789		
		3	783		
		4	784		
	High	1	2448	64.2	-
		2	2428		
		3	2423		
		4	2433		
Model A1T 1.56 mm	Low	1	763	19.44	-10
		2	756		
		3	733		
		4	768		
	High	1	2370	53.2	-
		2	2378		
		3	2385		
		4	2390		
Model B1T 1.56 mm	Low	1	744	22.3	-7
		2	745		
		3	741		
		4	765		
	High	1	2406	54.3	-
		2	2394		
		3	2404		
		4	2397		
Model C1T 1.56 mm	Low	1	789	44.7	-8
		2	788		
		3	783		
		4	784		
	High	1	2447	63.6	-
		2	2426		
		3	2417		
		4	2428		

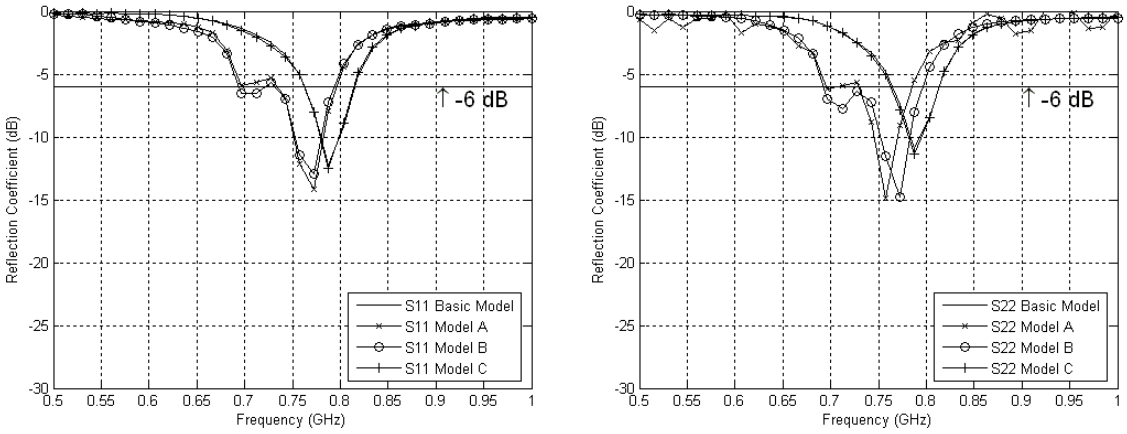

Figure 6-54 Comparison of low band S_{11}, S_{22} for the four fabricated models with 1.56mm substrate

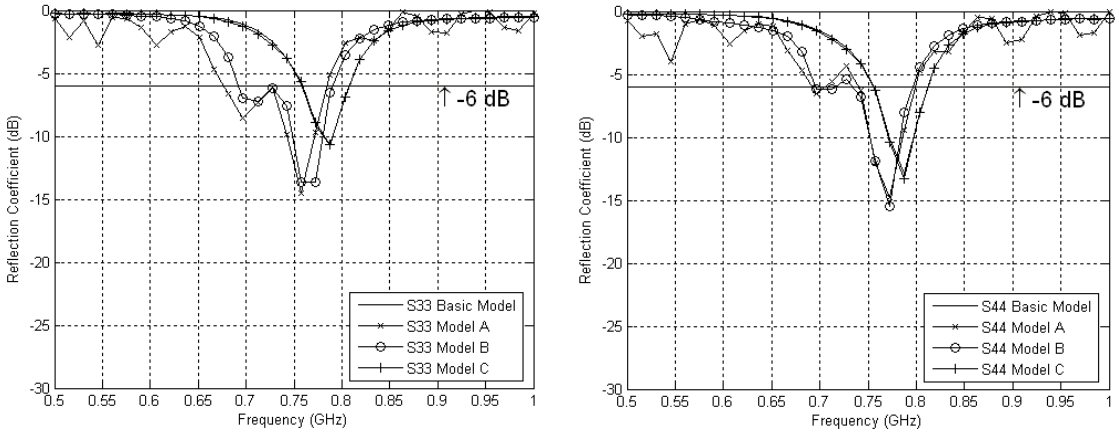

Figure 6-55 Comparison of low band S_{33}, S_{44} for the four fabricated models with 1.56mm substrate

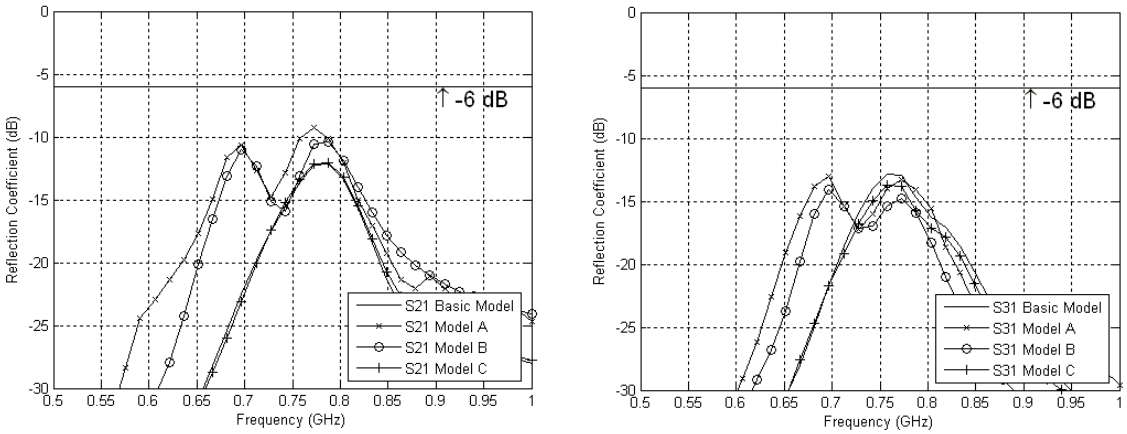

Figure 6-56 Comparison of low band S_{21}, S_{31} for the four fabricated models with 1.56mm substrate

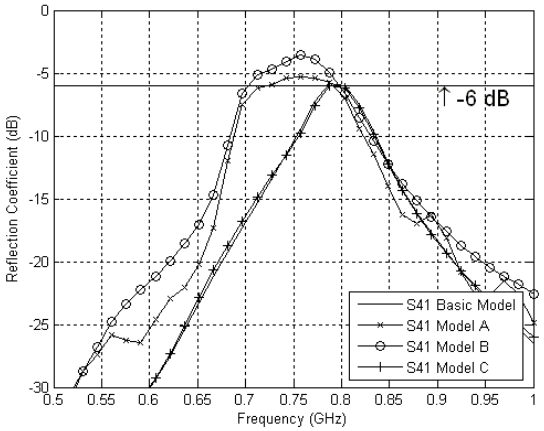

Figure 6-57 Comparison of low band S_{41} for the four fabricated models with 1.56mm substrate

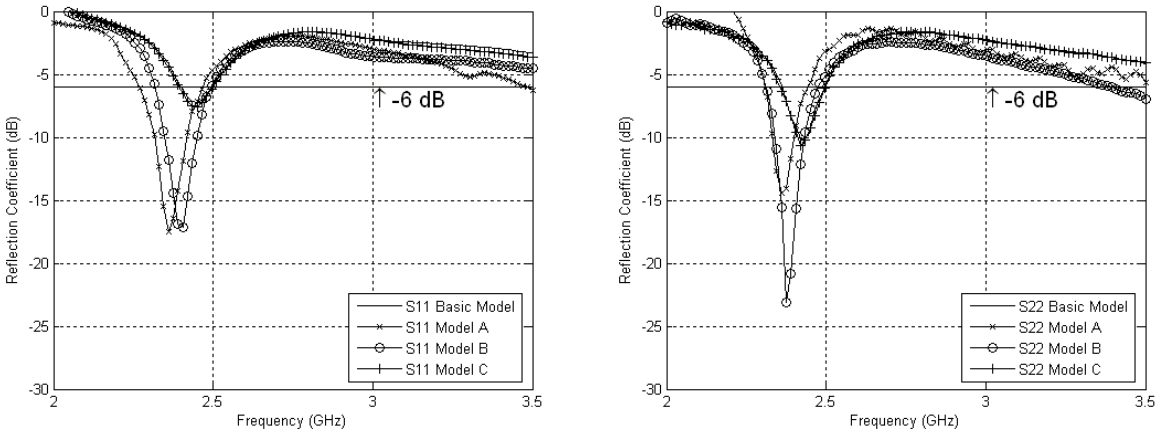

Figure 6-58 Comparison of high band S_{11}, S_{22} for the four fabricated models with 1.56mm substrate

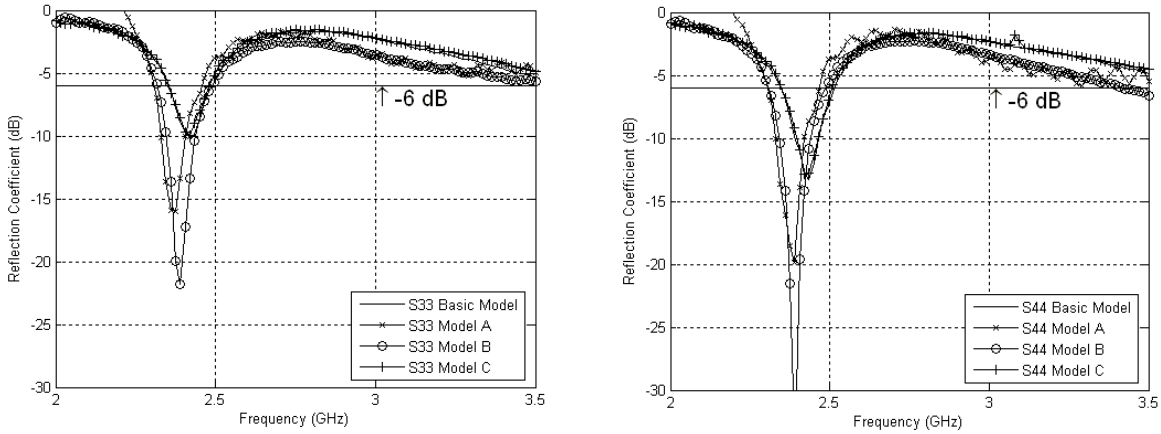

Figure 6-59 Comparison of high band S_{33}, S_{44} for the four fabricated models with 1.56mm substrate

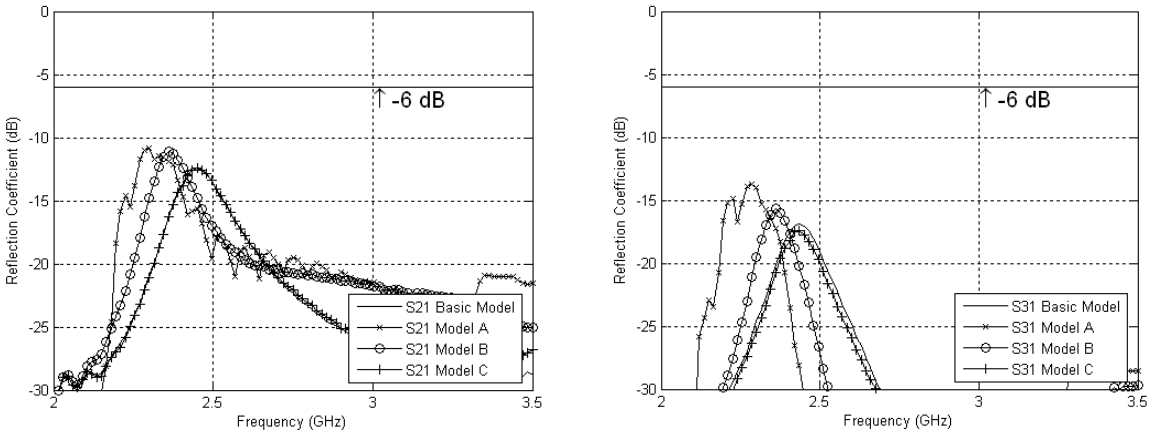

Figure 6-60 Comparison of high band S_{21}, S_{31} for the four fabricated models with 1.56mm substrate

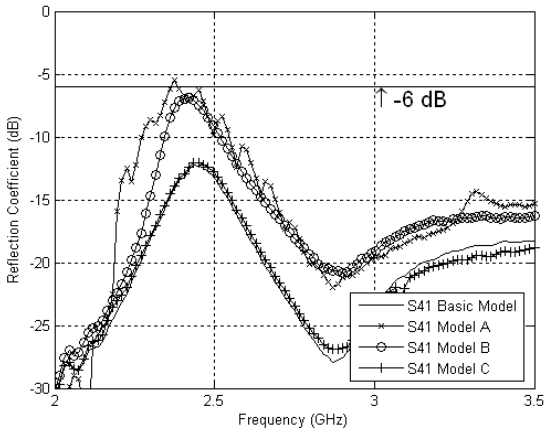

Figure 6-61 Comparison of high band S_{41} for the four fabricated models with 1.56mm substrate

Table 6-3 shows the measurement results of all the models fabricated with 0.8 mm substrate. Apart from the shift in the resonance frequencies at the low and high bands due to the smaller substrate thickness, it is evident that the isolation techniques did not provide better performance than the original design.

Table 6-4 shows a comparison of our models A1T and B1T with some 2x2 MIMO antenna systems that have appeared in literature. It is clear that the results are comparable. Up until the date of this work, no similar work that provides a 2x2 MIMO antenna system operating at 700 MHz band was available in literature which gives a higher value for this work.

Table 6-3 : Measurement Results for all the 2x2 MIMO Antenna Models (0.8 mm substrate)

Parameter / Model	Band	Antenna Element	BW (-6dB)	BW (-10dB)	S_{xx}	S_{21}	S_{31}	S_{41}
Basic Model 0.8 mm	Low	1	52	24	-13	-13.5	-11.5	-6
		2	49	0	-9			
		3	45	0	-9			
		4	50	0	-10.5			
	High	1	0	0	-5	-15	-20	-12
		2	212	0	-10			
		3	135	0	-7.5			
		4	216	0	-9			
Model A 0.8 mm	Low	1	54	25	-13.5	-10	-14	-4
		2	54	24	-15			
		3	55	22	-14			
		4	52	25	-12			
	High	1	290	117	-13	-14	-16.5	-7.5
		2	262	112	-12.5			
		3	251	66	-11			
		4	211	0	-9.5			
Model B 0.8 mm	Low	1	59	32	-14	-12	-16	-4
		2	54	28	-16			
		3	98	26	-17			
		4	58	30	-13.5			
	High	1	186	0	-9.5	-18.5	-14.5	-9
		2	232	78	-12			
		3	264	72	-11			
		4	254	112	-14			
Model C 0.8 mm	Low	1	47	17	-11	-12.5	-12	-6
		2	52	0	-9.5			
		3	40	0	-8			
		4	53	16	-11.5			
	High	1	0	0	-5.5	-15	-20	-12
		2	201	0	-9.5			
		3	133	0	-7			
		4	210	0	-9			

Table 6-3 : Measurement Results for all the 2x2 MIMO Antenna Models (0.8 mm substrate) continued from previous page

Parameter / Model	Band	Antenna Element	f_c	Efficiency (Simulation)	Max Rx Power Measured (dB))
Basic Model 0.8 mm	Low	1	877	64.9	-9
		2	853		
		3	851		
		4	867		
	High	1		70.8	-
		2	2626		
		3	2613		
		4	2640		
Model A 0.8 mm	Low	1	835	1	-9
		2	833		
		3	831		
		4	838		
	High	1	2615	70.9	-
		2	2631		
		3	2637		
		4	2617		
Model B 0.8 mm	Low	1	836	1	-8
		2	833		
		3	809		
		4	837		
	High	1	2635	72.1	-
		2	2616		
		3	2614		
		4	2625		
Model C 0.8 mm	Low	1	874	64.3	-8
		2	850		
		3	854		
		4	866		
	High	1		59.4	-
		2	2626		
		3	2612		
		4	2640		

Table 6-4 : Comparison of our 2x2 MIMO Antenna models with the 2x2 MIMO antennas that appeared in Literature

Reference / Parameter	Frequency band (MHz)	Single/ Multiband	Isolation (dB)	-10 dB BW (MHz)	Gain (dBi)	Single Element Size (mm)	Substrate Size (mm)
[73]	2400 / 5200	Dual	S_{21}=-7.4 S_{31} =-26 S_{41}=-21 S_{23}=-8.8 S_{24}=-25 S_{34}=-9.3	250 * 800 *	-3.5	-	45x32
[74]	2480	Single	S_{21}=-13 S_{31} =-8.5 S_{41}=-14 S_{34}=-15	130	2.4/2.1	-	40x40
[75]	4000	Single	-15	-	-	7x6x4m	90x150
[76]	2400	Single	All S_{ij} < -25	100	2.8	25x37.7	60X80
[77]	1840	Single	All S_{ij} < -24	420	2.72	-	80x80
Model A1T	740-785 2310-2445	Dual	S_{21}=-9 (L) S_{31}=-13 (L) S_{41}=-5 (L) S_{21}=-11(H) S_{31}=-13(H) S_{41}=-6 (H)	30, 55* (L) 80, 135* (H)	-0.6 (L) 6.43 (H)	29x55	58x110
Model B1T	734-790 2307-2475	Dual	S_{21}=-10 (L) S_{31}=-15 (L) S_{41}=-3.5(L) S_{21}=-11 (H) S_{31}=-15.5 (H) S_{41}=-7 (H)	28, 62* (L) 92, 163* (H)	-0.03 (L) 6.29 (H)	29x55	58x110

L Low band, H Highband, * -6 dB BW

6.5 Conclusions

In this chapter, we have presented the measured and simulated results for different 2x2 MIMO Antenna models based on the novel 4-shaped antenna element. Tables 6-2 and 6-3 summarize the measurement results for all 2x2 MIMO antenna models fabricated on FR-4 substrate of thickness 1.56 mm and 0.8 mm, respectively while table 6-4 gives a comparison of Models A1T and B1T with some 2x2 MIMO antenna systems that appeared in literature. The models that appeared in literature operated at higher frequency bands as the author could not find a 2x2 MIMO antenna system operating in the 700 MHz band for comparison. The models with 1.56 mm substrate gave better performance in terms of the bands covered and reflection coefficient. It is observed that the circles etched on the ground plane in model C do not offer any improvement in terms of isolation or reflection coefficient. Model A and B do not offer better isolation performance compared with the Basic Model, however, they have a noticeable improvement in the reflection coefficient and bandwidth. The 2x2 MIMO antenna system covered the 734-790 MHz LTE bands as well as the 2307-2475 MHz ISM band with a -6dB band width of 90 MHz at the low band and more than 165 MHz at the high band.

The 2x2 MIMO antenna system covering the 700 MHz band is the first to appear in literature. Its compact size and printed structure makes it an ideal candidate for future mobile terminals.

CHAPTER 7

CONCLUSION AND FUTURE WORK

In this work we designed and investigated a novel 4-shaped dual band antenna element which is then used to design and implement 2x1 and 2x2 MIMO antenna systems. The basic antenna geometry that we have come up with in this work was not straight forward, and it took us several months to close on the optimized 4-shaped geometry that fits very small antenna footprint and covers the bands of interest with good bandwidth.

The fabricated 2x1 dual band MIMO antenna system operated at 815 MHz and 2.75 GHz providing -6dB bandwidth of 60 MHz and more than 200 MHz at the two bands, respectively. Isolation of more than 6 dB at the low band and 11 dB at the high band was achieved despite the limited spatial separation between the two antennas of only $\lambda/16$. The 2x1 dual band MIMO antenna was fabricated on an FR-4 substrate of size 50x67x1.56 mm^3 which is at least 35% smaller than some models that appeared in literature. Capacitively loaded loops (CLLs) between the antenna elements were used to enhance

isolation. It was evident that isolation enhancement was limited but the CLLs shifted the resonance frequency downwards by about 50 MHz. The drawback was lower efficiency.

The dual band 2x2 MIMO antenna system operating at the 700/2400 MHz band is the first to appear in literature covering this low band and was fabricated on an FR-4 substrate of size 55x110x1.56 mm^3. It covered the 734-790 MHz band and the 2307-2475 MHz band with a -6dB band width of 90 MHz at the low band and more than 165 MHz at the high band. Thus it can be used in MIMO systems for the LTE 700 MHz band and other wireless standards in the 2400 MHz band such as WLAN, WiMAX, as well as higher LTE frequency bands. Isolation of more than 7 dB was achieved for most of the antenna elements indicating acceptable MIMO performance. Several isolation enhancement techniques were implemented and evaluated. It was found that improving isolation between such closely spaced antenna elements presents a challenge and conventional techniques may not prove very useful. The introduction of slits in the ground shifted the frequency of operation downward by about 35 MHz. Although the slits did not improve the isolation much, these improved the impedance matching significantly.

7.1 Future Work

The fact that the 4 elements occupy only 58x110x1.56 mm^3 poses a real challenge in isolation enhancement, especially at the low operating band of 700/800 MHz. While several isolation enhancement methods were utilized in this work, some future work can be performed to enhance the MIMO antenna system performance. Some future work can be:

1. Come up with new isolation enhancement methods such as using polarization diversity by arranging the antenna elements orthogonal to each other and test their behavior
2. Use other material substrates and investigate their effects on the antenna performance
3. Enhance the efficiency of the models by using multilayer structures

Bibliography

[1] Yue Gao, “Characterisation of Multiple Antennas and Channel for Small Mobile Terminals”, PhD thesis, Department of Electronic Engineering, Queen Mary, University of London, United Kingdom, June 2007

[2] Sundar G. Sankaran, “A brief overview of Wireless systems and standards” chapter in *Selected Readings on Telecommunications and Networking*, Jairo Gutierrez, Information Science Reference, 2008, pp. 1-7.

[3] “Recognizing the Promise of Mobile Broadband”, White Paper, the UMTS Forum, July 2010, pp.31.

[4] Choo Chiap Chiau, “Study of the Diversity Antenna Array for the MIMO Wireless Communication Systems”, PhD thesis, Department of Electronic Engineering, Queen Mary, University of London, United Kingdom, April 2006.

[5] “Evolution of Wireless Applications and Services”, white paper, Qualcomm Inc., December 2007.

[6] J. Winters, “On the capacity of radio communication system with diversity in a Rayleigh fading environment”, IEEE Journal on Selected Areas in Communications, vol. 5, no.5, pp.871-878, June 1987.

[7] G.J. Foschini,”Layered space-time Architecture for Wireless Communication in a Fading Environment when Using Multi-element Antennas”, Bell Labs Tech Journal, vol.1, no2, 1996.

[8] G.J. Foschini and M.J. Gans, “On Limits of Wireless Communications in a Fading Environment when Using Multiple Antennas”, Wireless Personal Communications, Vol 6, March 1998.

[9] I.E. Telatar, “Capacity of Multi-antenna Gaussian Channels”, European Transaction on Telecommunications, Vol. 10, No. 6, Nov/Dec 1999.

[10] V. K. Garg, *Wireless Communications and Networking*, Morgan Kaufmann, 2007.

[11] Mohammad S. Sharawi, "RF Planning and Optimization for LTE Networks" chapter in *Evolved Cellular Network Planning and Optimization for UMTS and LTE*, Lingyang Song Jia Shen, Ed.: CRC Press, 2010, pp. 399-432.

[12] S. Ajey, B.Srivalli and G.V.Rangaraj, "On Performance of MIMO-OFDM Based LTE Systems", *International Conference on Wireless Communication and Sensor Computing*, Chennai, India, 2-4 January 2010.

[13] OFDMA, online at www.semitechsemi.com/technologies/ofdma.php

[14] Harri Holma, Antti Toskala, *LTE for UMTS –OFDMA and SC-FDMA Based Radio Access*, 1st Edition, John Wiley, 2009.

[15] Constantine A. Balanis, *Modern Antenna Handbook*, John Wiley & Sons Inc., 2008.

[16] Yi Huang and Kevin Boyle, *Antennas: From theory to practice*, John Wiley & Sons Inc., 2008.

[17] IEEE Standard Definitions of Terms for Antennas, IEEE Std. 145-1993

[18] Constantine A. Balanis, *Antenna Theory: Analysis and Design*, Wiley-Interscience, 2005.

[19] Girish Kumar, K.P. Ray, *Broadband Microstrip Antennas*, Artech House, 2003.

[20] "S-Parameter Techniques, for Faster, More Accurate Network Design", Hewlett Packard Application Note 95-1, 1997.

[21] Zhi Ning Chen and Michael Y. W. Chia, *Broadband Planar Antennas: Design and Applications*, John Wiley & Sons, Ltd, 2006.

[22] Kai Fong Lee and Wei Chen, *Advances in Microstrip and Printed Antennas*, John Wiley and Sons, 1997.

[23] Debatosh Guha, Yahia M.M. Antar, *Microstrip and Printed Antennas, New Trends, Techniques and Applications*, John Wiley and Sons, 2011.

[24] Lal Chand Godara, *Handbook of Antennas in Wireless Communications*, CRC Press, 2002.

[25] Rod Waterhouse, *Printed Antennas for Wireless Communications*, John Wiley and Sons, 2007.

[26] M.C. T. Huynh. “A Numerical and Experimental Investigation of Planar Inverted-F Antennas for Wireless Communication Applications”. M.Sc. Thesis, Virginia Polytechnic Institute and State University, October 2000.

[27] Olivier Staub et al. “PCS Antenna Design: The Challenge of Miniaturization”, *Antennas and Propagation Society International Symposium*, Orlando, Florida, pp 548-551, Aug 1999.

[28] James S. McLean ”A Re-Examination of the Fundamental Limits on the Radiation Q of Electrically Small Antennas” *IEEE Transactions On Antennas and Propagation*, Vol. 44, No. 5, pp 672-676, May 1996.

[29] John L. Volakis, Chi-Chih Chen, Kyohei Fujimoto, *Small Antennas: Miniaturization Techniques & Applications*, McGraw Hill, 2010

[30] Roger F. Harrington, “Effect of Antenna Size on Gain, Bandwidth, and Efficiency”, *Journal of Research of the National Bureau of Standards-D. Radio Propagation*, Vol.64D, No. 1, January-February 1960.

[31] Randy Bancroft, “Fundamental Dimension Limits of Antennas Ensuring Proper Antenna Dimensions in Mobile Device Designs”, Centurion Wireless Technologies, Westminster, Colorado, USA.

[32] Andrew J. Compston et al., “A Fundamental Limit on Antenna Gain for Electrically Small Antennas”, IEEE 2008 Sarnoff Symposium,

[33] David Gesbert , Mansoor Shafi, Da-shan Shiu, Peter J. Smith and Ayman Naguib “From Theory to Practice: An overview of MIMO space-time coded wireless systems”, *IEEE Journal On Selected Areas In Communications*, VOL. 21, NO. 3, APRIL 2003

[34] Introduction to Multiple Antenna Systems: SIMO, MISO, MIMO, online at http://www.conniq.com/WiMAX/mimo-01.htm

[35] Shahab Sanayei and Aria Nosratinia, “Antenna Selection in MIMO Systems”, *IEEE Communications Magazine*, October 2004

[36] “MIMO Transmission Schemes for LTE and HSPA Networks”, White Paper, 3GAmericas, June 2009.

[37] Votis, Constantinos, "Envelope correlation parameter measurements in a MIMO antenna array configuration", *International Journal of Communications, Network and SystemSciences, April 1, 2010*

[38] Vanja Plicanic, Zhinong Ying, Thomas Bolin, Gerhard Kristensson,Anders Derneryd, "Antenna Diversity Evaluation For Mobile Terminals", *Proc. 'EuCAP 2006', Nice, France 6–10 November 2006*

[39] S. Blanch, J. Romeu, I Corbella, "Exact Representation of Antenna System Diversity Performance from Input Parameter Description", Electronics Letters, Vol. 39, No. 9, 1st May, 2003.

[40] Paul Hallbjörner, "The Significance of Radiation Efficiencies When Using S-Parameters to Calculate the Received Signal Correlation From Two Antennas", IEEE Antennas and Wireless Propagation Letters, Vol. 4, 2005.

[41] Mohammad S. Sharawi, Sheikh S. Iqbal, Yanal S. Faouri, "An 800 MHz 2x1 Compact MIMO Antenna System for LTE Handsets", *2011 German Microwave Conference (GeMIC)*, Darmstadt, 14-16 March 2011.

[42] F. Y. Zulki°i, E. T. Rahardjo, and D. Hartanto, "Mutual Coupling Reduction Using Dumbbell Defected Ground Structure for Multiband Microstrip Antenna Array", *Progress In Electromagnetics Research Letters, Vol. 13, 29{40, 2010*

[43] H. –T Chou et al., "Investigations of Isolation Improvement Techniques for Multiple Input Multiple Output (MIMO) WLAN Portable Terminal Applications", *Progress In Electromagnetics Research*, PIER 85, pp. 349–366, 2008

[44] Atif Jamil, Mohd Zuki Yusoff, Noorhana Yahya, "Current Issues and Challenges of MIMO Antenna Designs", *2010 International Conference on Intelligent and Advanced Systems (ICIAS)*, 15-17 June 2010.

[45] Chi-Yuk Chiu, Chi-Ho Cheng, Ross D. Murch and Corbett R. Rowell, "Reduction of Mutual Coupling Between Closely-Packed Antenna Elements", IEEE Transactions On Antennas and Propagation, Vol. 55, NO. 6, June 2007

[46] Rashid Ahmad Bhatti, Soongyu Yi, and Seong-Ook Park, "Compact Antenna Array With Port Decoupling for LTE-Standardized Mobile Phones", *IEEE Antennas and Wireless Propagation Letters*, VOL. 8, pp. 1430-1433, 2009.

[47] Anissa Chebihi et al., “A Novel Isolation Technique for Closely Spaced PIFAs for UMTS Mobile Phones”, *IEEE ANTENNAS AND WIRELESS PROPAGATION LETTERS*, VOL. 7, pp. 665-668, 2008

[48] Min-Seok Han and Jaehoon Choi, “MIMO Antenna Using a Decoupling Network for Next Generation Mobile Application” , *9th International Symposium on Communications and Information Technology*, ISCIT2009, Icheon, South Korea, 28-30 September 2009.

[49] Jie-Bang Yan, Chi-Yuk Chiu and Ross D. Murch, “ Handset 4-Port MIMO Antenna Using Slit Separated PIFA and Quarterwave-Slot Antenna Pair**”,** *Antennas and Propagation Society International Symposium 2008*, 5-11 July 2008.

[50] Kyeong-Sik Min, Dong Jin Kim, and Young-Min Moon, “ Improved MIMO Antenna by Mutual Coupling Suppression between Elements”, *The European Conference on Wireless Technology 2005*, 3-4 Oct. 2005.

[51] H. Chih-Chun, L. Ken-Huang, S. Hsin-Lung, L. Hung-Hsuan, and W. Chin-Yih, "Design of MIMO antennas with strong isolation for portable applications," in Antennas and Propagation Society International Symposium, 2009. APSURSI '09. IEEE, 2009, pp. 1-4.

[52] A. Rennings et al., “A Novel Low-Profile Triple-Band Antenna for Mobile Communications”, *International ITG Conference on Antennas*, Berlin, 17-19 Septermber, 2003.

[53] J. Cho, C.W. Jung and K. Kim, “Frequency-reconfigurable two-port antenna for mobile phone operating over multiple service bands”, *ELECTRONICS LETTERS*, Vol. 45, No. 20, pp. 1009-1011, 24th September 2009.

[54] Wei-Yu Li, Chun-Yih Wu, Kin-Lu Wong and Ming-Fang Tu, “Internal Small-Size PIFA for LTE/GSM/UMTS Operation in the Mobile Phone”, *IEEE Antennas and Propagation Society International Symposium (APSURSI), Toronto*, 11-17 July 2010.

[55] D. Misman, M. A. Abd. Aziz, M. N. Husain, P.J Soh, “Design of Planar Meander Line Antenna”, *Third European Conference on Antennas and Propagation ‘EuCAP 2009’*, Berlin, Germany, 23–27 March 2009.

[56] W. Swelam et al., “Compact Dual-Band Microstrip Patch Array Antenna for MIMO 4G Communication Systems”, IEEE Antennas and Propagation Society International Symposium (APSURSI), Toronto, 11-17 July 2010.

[57] Saraereh, O.; Jayawardene, M.; McEvoy, P.; Vardaxoglou, J.C.; , "Quad-band handset antenna operation for GSM900/DCS1800/PCS1900/UMTS," *Wideband and Multi-band Antennas and Arrays, 2005. IEE (Ref. No. 2005/11059)*, pp. 129- 133, 7 Sept. 2005

[58] A.A.H. Azremi et al., “ Five-Element Inverted-F Antenna Array for MIMO Communications and Radio Direction Finding on Mobile Terminal”, *Loughborough Antennas & Propagation Conference LAPC 2009*, Loughborough, UK, 16-17 November 2009.

[59] Qinjiang Rao and Dong Wang, “A Compact Dual-Port Diversity Antenna for Long-Term Evolution Handheld Devices”, *IEEE Transactions on Vehicular Technology*, VOL. 59, NO. 3, pp. 1319-1329, MARCH-2010.

[60] Mohammad S. Sharawi, Yanal S. Faouri, Sheikh S. Iqbal, “Design Of An Electrically Small Meander Antenna for LTE Mobile Terminals in the 800 MHz Band”, *IEEE GCC conference and Exhibition*, Dubai, 19-22 Feb. 2011.

[61] Norberto Lopez, Cheng-Jung Lee, Ajay Gummalla and Maha Achour, “Compact Metamaterial Antenna Array for Long Term Evolution (LTE) Handset Application”, *IEEE International Workshop on Antenna Techcnology*, iWAT 2009, Santa Monica, California, 2-4 March 2009.

[62] Sand-jin Eom et al., “Broadband Internal Antenna for 700 MHz LTE Application with Distributed Feeder”, *Asia Pacific Microwave Conference APMC 2009*, Singapore, 7-10 December 2009.

[63] Jeongsam Cho and Kangwook Kim, “A Frequency-reconfigurable Multi-port Antenna Operating over LTE, GSM, DCS, and PCS Bands”, *IEEE Antennas and Propagation Society International Symposium (APSURSI’09)*, Charleston, SC, 1-5 June 2009.

[64] Gyubok Park et al., “The Compact Quad-band Mobile Handset Antenna for the LTE700 MIMO Application”, *IEEE Antennas and Propagation Society International Symposium (APSURSI’09)*, Charleston, SC, 1-5 June 2009.

[65] Yeonsik Yu et al., “A Compact Hybrid Internal MIMO Antenna for LTE Application”, *Fourth European Conference on Antennas and Propagation EuCAP 2010*, Barcelona, Spain, 12-16 April 2010.

[66] Fang-Hsien Chu and Kin-Lu Wong, “Planar Printed Strip Monopole With a Closely-Coupled Parasitic Shorted Strip for Eight-Band LTE/GSM/UMTS Mobile Phone”, *IEEE Transactions On Antennas and Propagation*, VOL. 58, NO. 10, pp. 3426-3432, October 2010.

[67] R. Kuonanoja, “Low Correlation Handset Antenna Configuration for LTE MIMO Applications”, *IEEE Antennas and Propagation Society International Symposium (APSURSI), Toronto,* 11-17 July 2010.

[68] J.S. McLean, “The Radiative Properties of Electrically-Small Antennas”, *IEEE International Symposium on Electromagnetic Compatibility*, Chicago, IL, USA, pp.320-324, 22-26 August 194.

[69] Gary A. Thiele et al., “On the Lower Bound of the Radiation Q for Electrically Small Antennas”, *IEEE Transactions on Antennas and Propagation*, Vol. 51, No. 6, June 2003.

[70] Ibra Dioum et al., “Compact Dual-Band Monopole Antenna for LTE Mobile Phones”, *2010 Loughborough Antennas & Propagation Conference*, Loughborough, UK, 8-9 November 2010.

[71] H. Y. David Yang, “Miniaturized Printed Wire Antenna for Wireless Communications”, IEEE Antennas and Wireless Propagation Letters, VOL. 4, 2005

[72] Y. Gao et al., “A Modified PIFA with a Small Ground Plane”, 2005 IEEE Antennas and Propagation Society International Symposium, pp.515 – 518, vol. 2B, 3-8 July 2005.

[73] Shohei Fujio et al., “Small Dual Band Modified Meander Antenna with Multiple Elements”, 2005 IEEE Antennas and Propagation Society International Symposium, Vol. 2A, pages 351-354, 2005.

[74] Chi-Yuk Chiu et al., “Compact Four-Port Antenna Suitable for Portable MIMO Devices”, IEEE Antennas and Wireless Propagation Letters, Vol. 7, 2008.

[75] Rashid A. Bhatti et al., “Design and Evaluation of a PIFA Array for MIMO-Enabled Portable Wireless Communication Devices”, IEEE Antennas and Wireless Propagation Letters, Vol. 8, 2009.

[76] Hui Li et al., “A Compact Planar MIMO Antenna System of Four Elements with Similar Radiation Characteristics and Isolation Structure”, IEEE Antennas and Wireless Propagation Letters, Vol. 8, 2009.

[77] S. Zhang et al., “Printed MIMO antenna system of four closely-spaced elements with large bandwidth and high isolation”, Electronics Letters, 22nd July 2010, Vol. 46 No. 15.

Vitae

NAME:	Mohammad Azam Jan
BIRTH:	1st of April 1971, Charsadda, PAKISTAN
NATIONALITY:	Pakistani
EDUCATION:	BACHELOR OF SCIENCE (BSc) in Electrical Engineering, 1994, NWFP University of Engineering & Technology, Peshawar, PAKISTAN MASTER OF SCIENCE (MSc) in Telecommunication Engineering, 2011 , Department of Electrical Engineering King Fahd University of Petroleum & Minerals Dhahran, K.S.A.
Present Address:	Khobar, Eastern Region, Saudi Arabia
Permanent Address:	Hayatabad, Peshawar, Pakistan.
Mobile Number:	966 509055605
E-mail Address:	azamjan@yahoo.com